

Development of Decision Supporting Methods for Emergency Teams in Case of Severe Accidents in Nuclear Power Plants

Zur Erlangung des akademischen Grades einer
Doktorin der Ingenieurwissenschaften (Dr.-Ing.)
von der KIT-Fakultät für Maschinenbau des
Karlsruher Instituts für Technologie (KIT)

angenommene

Dissertation

von

M. Sc. Anastasia Stakhanova

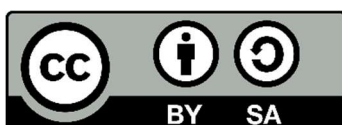
geboren in Balashiha (Russische Föderation)

Tag der mündlichen Prüfung: 14.12.2023

Hauptreferent: Prof. Dr.-Ing. Robert Stieglitz
Karlsruher Institut für Technologie

Korreferent: Prof. Cesar Queral
Universidad Politécnica de Madrid

2024



This document is licensed under a Creative Commons Attribution-ShareAlike 4.0 International License (CC BY-SA 4.0): <https://creativecommons.org/licenses/by-sa/4.0/deed.en>

Acknowledgements

First and foremost, I have to thank Prof. Dr. Robert Stieglitz – the head of the Institute for Neutron Physics and Reactor Technology (INR) – for opportunity to work here on my thesis and supervising.

I am deeply grateful to Dr.-Ing. Victor Hugo Sanchez-Espinoza – my technical advisor and Reactor Physics and Dynamic (RPD) group leader – for his constant support during these three years, discussions and advice, which helped me to focus on the most important parts of the research.

My very special thanks to Dr.-Ing. Fabrizio Gabrielli – deputy RPD group leader. He provided the ASTEC inputs for all presented simulations, without his help it would not be possible to finish the work in time. Furthermore, I was always able to discuss with him new results, current status of the work and ask for advice. For that and constant moral support I want to thank him.

I would also like to show gratitude to other members of RPD group – staff members and PhD students – for advice, discussions and questions during the group meetings, which helped me to formulate my thoughts and present results better, and friendly atmosphere.

I wish to extend my special thanks to the secretariat – Klug Petra, Birgit Zagolla and Ingeborg Schwartz – for they support with any bureaucratic issue and help with integrating into the team and society here.

This work was made in cooperation with Framatome GmbH, and I want to thank Dr. Axel Hoefler (Senior Expert & Senior Advisor) and Eva-Maria Pauli (Technical Advisor) for their constant work with us on the project, discussing results during the regular meetings and, of course, for providing mathematical description of the prediction algorithm.

The work through the thesis would not be possible without my husband Felix Schneider and his everyday support and deep and constant belief in me.

Karlsruhe, May 2024

Anastasia Stakhanova

Abstract

In case of a severe accident (SA) in a nuclear power plant (NPP) the main information needed for the emergency team and the authorities is the type, quantity, temporal and spatial behavior of the fission products (FPs) released into the environment – the source term (ST). Therefore, modelling of how this release will spread out is important in order to evaluate the severity of the consequences for the population and environment.

The great challenge in case of SA is that information about FP release is to be delivered as fast as possible i.e. in minutes and be reliable at the same time. This information can be provided with detailed simulations using integral severe accident codes, like ASTEC, MAAP, MELCOR, etc. within hours but not minutes. These codes have been developed to simulate the SA progression and the fission product transport from the vessel to the environment. Due to the nature of the physical/chemical models implemented in such codes to describe mathematically key-phenomena in a NPP during SA, they are usually time-consuming. Therefore, faster alternative approaches are required for the emergency teams as basis for timely decisions. For example, the RASTEP code is based on the Bayesian Belief Networks (BBN) approach that allows choosing one of the pre-calculated release values very fast, using information about current plant status. Known drawbacks of this approach is the fact that the pre-calculated ST values represent the results of SA simulation with some best estimated input parameters values, and results cannot be changed in any way according to the current situation at the plant.

In this context a first-of-its-kind computational framework is developed, which allows a fast ST prediction based on both a training database of the results of SA code simulations and the data from plant detectors. Monte Carlo-based Bayesian inference approach (MOCABA) developed by Framatome has been chosen as prediction algorithm. To construct the prediction of ST measured data (in our case, it was dose rate values) and database filled with SA simulation results are used. MOCABA is a general approach, which can be used for any kind of the physical process and predict any parameter of the interest. Results of simulations stored in database allows to calculate the mean values for all parameters of interest (predicted and measured) as well as correlations between them. It can be used in combination with actual measurements to predict the trend of parameter of interest in the future, when no more measurements are available anymore.

The European reference code ASTEC is used to perform the severe accident analysis of selected accidental sequences – Medium Break Loss-of-Coolant Accident (MBLOCA); MBLOCA + Station Black-Out (SBO) – for the pressurized water reactor (PWR) KONVOI plant.

For the generation of the data base, a Python-based tool, Fast Source Term Calculation (FSTC), has been developed that allows to automatically perform a large number of SA

simulations as it usually done in the framework of uncertainty and sensitivity (U&S) quantifications.

The training database contains results of multiple simulations for a given scenario performed with different values of chosen input parameters. That allows to cover the range of possible scenario progression variants. To do so the most important parameters influencing on the ST need to be identified. Starting with the broad list of potentially important parameters, using U&S analysis methods implemented in FSTC tool, this list has been reduced and later on used in producing many (in our case, hundreds) ASTEC simulations stored in the data base.

MOCABA prediction approach is fully implemented in the FSTC tool. The prediction capability of the FSTC tool is benchmarked against an in-house proprietary code provided by Framatome on QUENCH-08 simulation results, and then applied both to the QUENCH-08 and to the PWR KONVOI severe accident sequences. The algorithm appears to be quite sensitive, for example, to the similarity between prepared and measured data curve shapes, which imposes some limitations on its usage. The investigation of limitations of the MOCABA algorithm helps to identify areas for improvements when the algorithm is applied to predict the radiological ST.

The developed methodology for the fast prediction of the radiological ST after SA in NPPs, which central element are the methods implemented in FSTC tool, can be implemented by utilities, where measured data of radiation dose may exist if a severe accident happens. In addition, the FSTC tool was used to perform U&S analysis of the SA sequences at KONVOI NPP in the frame of the Management and Uncertainties of Severe Accidents (MUSA) project, and obtained results were compared to the ones produced with other U&S tools such as URANIE. For more convenient and wider use of the FSTC tool, and especially its part for U&S analysis, at KIT an implementation of a Graphical User Interface (GUI) and additional features, like coupling with other codes, was started at KIT.

This thesis has been made in the frame of the WAME project and was funded by the German Federal Ministry for Economic Affairs and Climate Action (BMWi), funding code FZK 1501582.

Kurzfassung

Im Falle eines schweren Unfalls (SU) in einem Kernkraftwerk (KKW) sind die wichtigsten Informationen für Hilfskräfte und Behörden die Art, Menge und das zeitliche und räumliche Verhalten der in die Umgebung freigesetzten Spaltprodukte (SP) – der Quellterm. Daher ist es wichtig zu modellieren, wie sich diese Freisetzung verhält, um die Schwere der Konsequenzen für die Bevölkerung und die Umwelt abschätzen zu können.

Die große Herausforderung im Fall eines SU ist, dass Informationen über SP Freisetzung so schnell wie möglich, d.h. innerhalb von Minuten, vorliegen und gleichzeitig zuverlässig sein müssen. Diese Informationen lassen sich mithilfe detaillierter Simulatoren wie z.B. ASTEC, MAAP, MELCOR etc. berechnen in mehreren Stunden, nicht Minuten. Diese Programme wurden entwickelt, um den Fortschritt des SU und den Transport der SP aus dem Reaktorbehälter in die Umgebung zu simulieren. Aufgrund der Komplexität der physikalisch/chemischen Modelle, die in diesen Programmen implementiert werden, um mathematisch wichtige Phänomene in einem KKW während eines SA zu beschreiben, sind sie üblicherweise sehr zeitaufwändig. Daher sind schnellere, alternative Ansätze nötig, um Rettungskräften eine Basis für zeitkritische Entscheidungen zu bieten. Zum Beispiel basiert RASTEP auf Bayessche Netze (BN), die erlauben, schnell aus mehreren vorberechneten Werten für die Freisetzung zu wählen, unter Berücksichtigung von aktuellen Informationen über den Zustand des Kraftwerks. Ein bekannter Nachteil dieses Ansatzes ist, dass die vorberechneten Quellterm Werte die Ergebnisse einer SU Simulation mit den besten Schätzungen der Werte der Eingabeparameter darstellen, und dass sie sich nicht mit der aktuellen Situation des Kraftwerks verändern können.

In diesem Kontext wird ein neuartiges Konzept für die Berechnung entwickelt, welches eine schnelle Vorhersage des Quellterms erlaubt auf der Basis einer Datenbank von Ergebnissen von SU Simulatoren und Daten von Detektoren aus dem Kraftwerk. Der auf Monte-Carlo Bayessches Inferenz basierende Ansatz (MOCABA), entwickelt von Framatome, wurde als Algorithmus gewählt. Um die Vorhersage des Quellterms zu entwickeln, werden Messdaten (in unserem Fall Dosisleistung) und eine Datenbank mit SA Simulationen verwendet. MOCABA ist ein genereller Ansatz, der für jede Art von physikalischen Prozess benutzt werden kann und jeden Parameter von Interesse vorhersagen kann. Die Ergebnisse der Simulationen aus der Datenbank erlauben es, den Durchschnitt aller Parameter von Interesse zu bestimmen (sowohl die Vorhergesagten als auch die Gemessenen) und Korrelationen zwischen ihnen zu bestimmen. Er kann in Kombination mit echten Messdaten genutzt werden, um den Trend eines Parameters von Interesse in der Zukunft vorherzusagen, für die keine Messdaten mehr vorliegen.

Der europäische Referenzcode ASTEC wird verwendet um die Analyse verschiedener Unfallszenarien für den Druckwasserreaktor KONVOI durchzuführen: Unfall des mittleren Lecks; Unfall des mittleren Lecks + kompletter Ausfall der Stromversorgung.

Zum Erzeugen der Datenbank wurde ein Python-basiertes Tool, *Fast Source Term Calculation* (FSTC) entwickelt, das es erlaubt, viele SU Simulationen automatisch durchzuführen, wie es bei Unsicherheits- und Sensitivitätsanalyse üblich ist.

Die Trainingsdatenbank besteht aus den Ergebnissen mehrerer Simulationen für dasselbe Szenario mit unterschiedlichen Werten ausgewählter Eingabeparameter. So kann die Spanne möglicher Unfallverläufe abgedeckt werden. Um das zu tun, müssen die wichtigsten Parameter für den Quellterm bestimmt werden. Ausgehend von der breiten Liste potenziell wichtiger Parameter, mit den Unsicherheits- und Sensitivitätsanalysemethoden aus FSTC, wurde diese Liste verkleinert und später dazu verwendet, hunderte ASTEC Simulationen für die Datenbank anzulegen.

MOCABA ist vollständig in FSTC implementiert. Die Qualität der Vorhersagen von FSTC werden getestet gegen einen proprietären in-house Code von Framatome auf QUENCH-08 Simulationsergebnissen und danach angewendet auf die QUENCH-08 und KONVOI Unfallszenarien. Der Algorithmus scheint zum Beispiel empfindlich auf Unterschiede zwischen der Form der vorbereiteten und gemessenen Verläufen zu sein, was seine Verwendung einschränkt. Eine Untersuchung der Einschränkungen des MOCABA Algorithmus hilft uns, Bereiche zu identifizieren, in denen der Algorithmus verbessert werden kann, um den radiologischen Quellterm besser vorhersagen zu können.

Die entwickelte Methode zur schnellen Vorhersage des radiologischen Quellterms nach SU in KKW, deren zentrale Elemente in FSTC implementiert sind, kann in Situationen verwendet werden, in denen Messwerte der Strahlensdosis nach einem SU existieren. Darüber hinaus wurde FSTC verwendet, um U&S Analysen der SU Sequenzen in KONVOI im Rahmen des *Management and Uncertainties of Severe Accidents* (MUSA) Projekts durchzuführen. Die Ergebnisse wurden mit denen anderer Unsicherheits- und Sensitivitätswerkzeuge wie URANIE verglichen. Um die Bedienung und breitere Verwendung von FSTC zu erleichtern, besonders des Teils für Unsicherheits- und Sensitivitätsanalyse, wurde die Implementierung einer Grafischen Nutzeroberflächen und weitere Features, wie die Einbindung anderer Simulatoren, am KIT begonnen.

Diese Arbeit wurde im Rahmen des WAME Projekts durchgeführt und wurde gefördert durch das Bundesministerium für Wirtschaft und Klimaschutz, Förderkennzeichen 1501582.

Publications related to this thesis

As first author:

Stakhanova, A., Gabrielli, F., Sanchez-Espinoza, V.H., Hoefler, A. and Pauli, E., 2022. Uncertainty and sensitivity analysis of the QUENCH-08 experiment using the FSTC tool. *Annals of Nuclear Energy*, 169, (2022), p.108968. DOI: <https://doi.org/10.1016/j.anucene.2022.108968>

Stakhanova, A., Gabrielli, F., Sanchez-Espinoza, V.H., Pauli, E., Hoefler, A., Uncertainty and sensitivity analysis of the ASTEC simulations results of a MBLOCA scenario in a generic KONVOI plant using the FSTC tool. In *Proceedings of 10th European Review Meeting on Severe Accident Research (ERMSAR-2022)*, 2022, pp.861-872.

Stakhanova, A., Gabrielli, F., Sanchez-Espinoza, V.H., Hoefler, A. and Pauli, E., Application of the MOCABA algorithm and the FSTC tool for source term predictions during severe accident scenarios. *Annals of Nuclear Energy*, 184, (2023), p.109703. DOI: <https://doi.org/10.1016/j.anucene.2023.109703>

Stakhanova, A., Gabrielli, F., Sanchez-Espinoza, V.H., Pauli, E., Hoefler, A., Uncertainty and sensitivity analysis of the ASTEC simulations results of a MBLOCA scenario in a generic KONVOI plant using the FSTC tool. *Annals of Nuclear Energy*, 192, (2023), p.109964. DOI: <https://doi.org/10.1016/j.anucene.2023.109964>

In the list of authors:

Gabrielli, F., Sanchez-Espinoza, V.H., Stakhanova, A., Hoefler, A., Pauli, E., Feldmann, H., Source Term Evaluation Following MBLOCA and SBLOCA Scenarios in a Generic KONVOI-1300 NPP by Means of the ASTEC Code. *Eurosafe 2021*, Paris, November 22-23 (2021).

Gabrielli F., Stakhanova, A., Sanchez-Espinoza, V.H., Pauli, E., Hoefler, A., Feldmann, H., Impact of Realistic Fuel Inventories on the Radiological Consequences of a Severe Accident Scenario in a Generic KONVOI Plant by Means of the ASTEC Code. In *Proceedings of KERNTECHNIK 2022*, June 21-22, Leipzig, Germany.

Pauli, E., Hoefler, A., Gabrielli, F., Stakhanova, A. and Sanchez-Espinoza, V.H., Prediction of the radiological consequences of a severe accident scenario in a generic KONVOI nuclear power plant. In *Proceedings of 10th European Review Meeting on Severe Accident Research (ERMSAR-2022)*, 2022, pp. 338-350.

Sanchez-Espinoza, V. H., Gabrielli, F., Imke, U., Zhang, K., Mercatali, L., Huaccho, G., et. al., KIT reactor safety research for LWRs: Research lines, numerical tools and prospects. *Nuclear engineering and design*, 414, (2023), p. 112573. DOI: <https://doi.org/10.1016/j.nucengdes.2023.112573>

Contents

| | |
|--|-----------|
| Acknowledgements..... | 3 |
| Abstract..... | 5 |
| Kurzfassung..... | 7 |
| Publications related to this thesis..... | 9 |
| List of Acronyms | 13 |
| 1 Introduction..... | 15 |
| 1.1 Motivation..... | 15 |
| 1.2 Main thesis objectives..... | 17 |
| 1.3 Structure of the thesis | 18 |
| 2 Phenomenology and emergency management at severe accidents for pressurized water reactors (PWR)..... | 20 |
| 2.1 Phenomenology of severe accidents in a Pressurized Water Reactor..... | 20 |
| 2.2 Emergency management in case of severe accidents in Nuclear Power Plants..... | 24 |
| 2.3 Radiological source term prediction by ASTEC severe accident code | 28 |
| 2.4 Radiological source term prediction by fast running tools | 30 |
| 3 Mathematical description of the Monte Carlo based Bayesian approach (MOCABA) for the fast source term calculation | 34 |
| 3.1 Mathematical formulation of the ‘prior’ part of the prediction algorithm..... | 34 |
| 3.2 Mathematical formulation of the ‘posterior’ part of the prediction algorithm | 36 |
| 4 Tool for the fast source term calculation (FSTC) | 39 |
| 4.1 Database generation for the source term prediction task using the FSTC tool..... | 41 |
| 4.1.1 Sampling | 41 |
| 4.1.2 Run multiple simulations | 41 |
| 4.1.3 Find samples to exclude..... | 42 |
| 4.1.4 Collect data..... | 43 |
| 4.1.5 Filter data | 43 |
| 4.1.6 Uncertainty and sensitivity analysis..... | 44 |
| 4.2 Fast Source Term Calculation Module for the Bayesian prediction algorithm | 45 |
| 4.2.1 Prior part | 45 |
| 4.2.2 Posterior part | 46 |
| 4.2.3 Automated prediction algorithm run on the sets of data | 46 |
| 5 Integral validation of the FSTC-MOCABA approach by the QUENCH-08 experiment..... | 48 |

| | | |
|----------|---|------------|
| 5.1 | QUENCH-08 experiment and its ASTEC model | 48 |
| 5.2 | Uncertain input parameters for QUENCH-08 simulations | 53 |
| 5.3 | Results of U&S analysis | 56 |
| 5.4 | Results of applying MOCABA algorithm for hydrogen source term prediction..... | 64 |
| 5.4.1 | Predictions using simulation data as measurements..... | 65 |
| 5.4.2 | Predictions using real experimental data as measurements..... | 69 |
| 6 | Integral validation of the FSTC-MOCABA approach by the KONVOI-1300 pressurized water reactor | 72 |
| 6.1 | KONVOI NPP and its ASTEC model | 72 |
| 6.2 | Uncertain input parameters for considered scenarios | 74 |
| 6.3 | Description of the MBLOCA SA Scenario | 77 |
| 6.4 | Results of U&S analysis | 78 |
| 6.5 | Results of applying the MOCABA algorithm for the source term prediction in MBLOCA SA scenario..... | 82 |
| 7 | Conclusions and future work..... | 86 |
| | References..... | 89 |
| | Appendix A: U&S analysis and existing tools. | 99 |
| A.1 | Uncertainty and sensitivity analysis applied to severe accidents..... | 99 |
| A.2. | Existing tools for U&S analysis..... | 102 |
| | Appendix B: FSTC tool | 105 |
| B.1. | Preparing documentation for the FSTC tool..... | 105 |
| B.2. | Unit testing | 107 |
| B.3. | Performance testing..... | 108 |
| B.4. | Comparison of the ‘U&S analysis’ module of the FSTC tool with the URANIE platform..... | 111 |
| B.5. | Validation of the MOCABA algorithm implementation..... | 112 |
| | Appendix C: Application of the FSTC-tool for the generation of the data base for PWR MBLOCA + SBO SA Scenario..... | 114 |
| C.1 | Results of U&S analysis..... | 114 |
| C.2 | Applying the MOCABA algorithm to the MBLOCA+SBO simulations..... | 118 |
| | Appendix D: Constraints and limitations of the MOCABA algorithm presented on the simple ‘toy’ example | 122 |
| | Appendix E: List of publications | 130 |

List of Acronyms

| English | German | Description |
|------------|--------|---|
| AC | | Alternating Current |
| ACCUs | | Passive Accumulators |
| ANN | | Artificial Neural Network |
| ASTECC | | Accident Source Term Evaluation Code |
| BBN | BN | Bayesian Belief Network / Bayessche Netze |
| BEPU | | Best Estimate plus Uncertainty |
| BMWi | | Bundesministeriums für Wirtschaft und Klimaschutz / German Federal Ministry for Economic Affairs and Climate Action |
| CEA | | Commissariat à l'énergie atomique et aux énergies alternatives (French Alternative Energies and Atomic Energy Commission) |
| DA | | Data Assimilation |
| DCH | | Direct containment heating |
| DSA | | Deterministic safety analysis |
| EBS | | Extra Borating System |
| ECCS | | Emergency Core Cooling System |
| EFWS | | Emergency Feed Water System |
| EPA | | Environmental Protection Agency |
| ERO | | Emergency response organization |
| EURATOM | | European Atomic Energy Community |
| FaSTPro | | Fast Source Term Prognosis |
| FoM / FoMs | | Figure(s) of Merit |
| FP / FPs | SP | Fission Product(s) / Spaltprodukt |
| FP5 | | Fifth framework programme |
| FSTC | | Fast Source Term Calculation tool |
| FW | | Feed water |
| FWP /FWPs | | Feed Water Pump(s) |
| GE | | General Emergency |
| GLLS | | Generalized Linear Least Squares |
| GRS | | Gesellschaft für Anlagen- und Reaktorsicherheit |
| GUI | | Graphical User Interface |
| HPIS | | High Pressure Injection System |
| INR | | Institute for Neutron Physics and Reactor Technology |
| JRODOS | | Java based Real-time on-line decision support system |
| KATUSA | | KArlsruhe Tool for Uncertainty and Sensitivity Analysis |
| KWU | | Kraftwerk Union company |
| LHS | | Latin Hypercube Sampling |
| LHVF | | Lower Head Vessel Failure |
| LP | | Lower Plenum |
| LPIS | | Low Pressure Injection System |
| MAAP | | Modular Accident Analysis Program |
| MBLOCA | | Medium Break Loss-of-Coolant Accident |
| MCCI | | Molten corium concrete interaction |
| MCP /MCPs | | Main Coolant Pump(s) |
| MCR | | Main Control Room |
| MIC | | Maximal Information Coefficient |
| MOCABA | | Monte Carlo-based Bayesian inference model |
| MSL | | Main Steam Line |
| MUSA | | Management and Uncertainties of Severe Accidents project |
| NOUE | | Notification of Unusual Event |
| NPP | KKW | Nuclear power plant / Kernkraftwerk |
| OS | | Operating system |
| PAG | | Protective action guide |
| PDF /PDFs | | Probability Density Function(s) |
| PIRT | | Phenomena Identification and Ranking Technique |
| PSA | | Probabilistic Safety Analyses |

| | | |
|----------|----|---|
| PWR | | Pressurized Water Reactor |
| RASTEP | | RApid Source TErm Prediction |
| RPS | | Reactor Protection System |
| RCS | | Reactor Coolant System |
| RPD | | Reactor Physics and Dynamic group |
| RPV | | Reactor Pressure Vessel |
| SA | SU | Severe accident / schwere Unfall |
| SAE | | Site Area Emergency |
| SAM | | Severe Accident Management |
| SAMGs | | Severe Accident Management Guidelines |
| SBO | | Station Black-Out |
| SG / SGs | | Steam Generator(s) |
| SOCRAT | | System Of Codes for Realistic Assessment of severe accidentTs |
| SRS | | Simple Random Sampling |
| ST | | Source Term |
| TDD | | Test-driven Development |
| TSC | | Technical Support Center |
| U&S | | Uncertainty & Sensitivity analysis |
| Zry | | Zircaloy |

1 Introduction

1.1 Motivation

Severe accidents (SA) in a nuclear power plant (NPP) may lead to dramatic consequences for the population and the environment due to contamination caused by fission products (FPs) release. The concept of defense in depth [\[INSAG, 1996\]](#), at least its first three levels, focuses on preventing release of radioactive materials into the environment. If all these measures fail, the technical support center (TSC) is obliged to provide to the emergency response organization (ERO) information about release (amount, composition, time characteristic), which is called the source term (ST). The ERO must take prompt decisions e.g. about evacuation, distribution of iodine tablets, etc. in order to protect population against the radiological hazard. Hence, reliable information is urgently needed by the ERO about the radiological ST as soon as possible after a severe accident with core damage to take adequate decisions about immediate countermeasures. That information is to be provided as fast as possible and it must be reliable, to initiate timely adequate measures.

The prediction of the radiological source term in case of hypothetical severe accidents with core meltdown are typically performed using integral severe accident codes such as MELCOR [\[Humphries et. al., 2015\]](#), ASTEC [\[Chailan et. al., 2019\]](#), SOCRAT [\[Kiselev, 2015\]](#), MAAP [\[Luxat et. al., 2016\]](#), AC2 [\[Wielenbeg et. al., 2019\]](#), which are able to model the key physical phenomena taking place in the reactor core, pressure vessel, primary and secondary circuits, and in containment of a NPP during a severe accident progression. The prediction accuracy of the numerical tools for severe accidents in NPPs are constantly being improved by extensive validation using experimental data [\[Gómez-García-Toraño et. al., 2022\]](#), [\[Chatelard et. al., 2022\]](#). Since the severe accident phenomenology (physics, chemistry, fluid mechanics, etc.) is very complex, integral severe accident codes need quite long time to predict the radiological source term. SA codes exhibit different degree of detail, e.g. codes use mechanistic models and quite coarse thermal hydraulic nodalization, affecting calculation time and accuracy.

Simulations of severe accident sequences with these codes can get quite time consuming – depending on the SA scenario and the SA code – varying from minutes (MAAP) up to hours (ASTEC, MELCOR) and even up to days, in case of using more detailed thermal hydraulic simulations. Consequently, the international community are exploring alternative computational approaches that allow a fast prediction (seconds) of the radiological source term as technical basis for the decisions of the ERO. One promising approach is the Bayesian Belief Networks (BBN) extracting information stored in precomputed database covering a wide-range of accidental conditions of a NPP and answers from the operator about current state of the plant systems. It is implemented in the commercial tools like RASTEP [\[Knochenhauer et. al., 2012\]](#) and FaSTPro

[\[Hage, 2018\]](#). Another approach to predict the radiological source term in real time is to use fast-running codes with simplified models of the SA processes [\[Dedda, 2013\]](#). In addition, the Artificial Neural Network (ANN) is also being considered as a promising methodology [\[Santhosh et. al., 2020\]](#).

The BBN-based approach implemented in commercial tools is currently the most widely used for the radiological ST prediction in real-time after a severe accident. Despite the BBN approach allows to obtain the information about ST very fast – in seconds – the input database used by such tools need to be prepared in advance and it represents subjective perception of the analyst about the accident progression. In real life, due to the complexity of the SA phenomena and the large uncertainties, there are many pathways for the progression of severe accidents in NPPs. As a result, the ST quantities may be quite different from what is expected. But in the BBN approach the chosen from precomputed database ST value cannot be corrected according to the real situation at the NPP, while it is crucial to provide to the emergency team the reliable ST value to adequately manage the radiological consequences of the SA.

To overcome that drawback, a new approach based on Bayesian inference approach – MOCABA [\[Hoefer et. al., 2015\]](#) – aims to combine the pre-generated data (e. g. about radiological source term) with the measured data (e. g. from NPP detectors measuring the dose rates). A main feature of this approach is, that the combination of the values stored in the database with actual measured values at the NPP allows to improve the prediction of parameters of interest when performing the Bayesian inference. In general, MOCABA has no limitations for the type of modelled physical process (in other words, it could be applied not only to predict source term in case of SA, but to very different tasks [\[Castro et.al., 2016\]](#)) and for the type of predicted parameter.

Implementation of the selected approach for ST prediction requires:

- A detailed mathematical description of the algorithm.
- Representative database. This database of radiological source terms must cover a wide range of hypothetical severe accident sequences for a specific NPP.
- Measured data from NPP detectors. For SA at NPP measurements can be substituted with simulation results imitating such data.

Representative database required for new Bayesian inference approach consists of large number of SA simulation results. The simulation scope covers the full chain of physical-chemical phenomena taking place during the in-vessel and ex-vessel phases of severe accidents, since these phenomena determine the release and transport of fission products from the core to the containment in a NPP and finally the amount of species and their temporal evolution i.e. the radiological source term that potentially can be released into the environment after a severe accident. For different accidental sequences the variation of a selected number of key-parameters

that may have a large impact on the source term prediction have to be considered. On this regard, Phenomena Identification and Ranking Table (PIRT) and engineering judgment are used to identify such key parameters, and sampling methods like Simple Random and Latin Hypercube – to generate the sets of key parameters values. Uncertainty and sensitivity (U&S) analysis helps to identify the parameters are mostly influencing on the ST and finally prepare the database for the prediction algorithm.

In this doctoral thesis, the novel approach shown in **Figure 1-1** is based on a representative database, measured data and a Bayesian predictive algorithm is developed and applied.

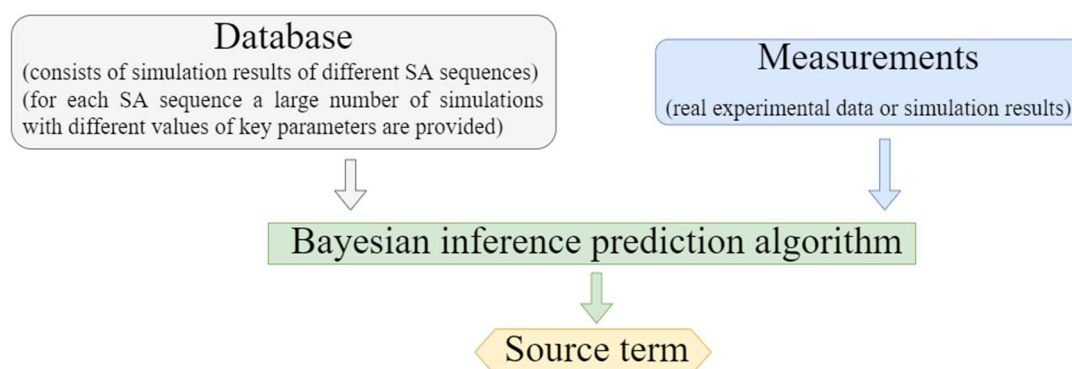


Figure 1-1 – Scheme of the Bayesian inference approach to predict the source term of a severe accident in NPP.

The main thesis objectives derived from the motivation are described in the next section.

1.2 Main thesis objectives

The main thesis objective is to develop, implement and apply a fast running novel approach allowing real-time radiological source term prediction based on Bayesian inference approach as shown in **Figure 1-1**.

Firstly, the database on radiological source terms is created covering a broad range of possible outcomes of considered accident scenarios. The progression of a SA can vary significantly due to influence from a wide range of uncertainties. Therefore, the most important uncertain parameters (for a given accident scenario) have to be identified using methods of U&S analysis. After that, the database for the prediction algorithm can be prepared – it consists of results of multiple simulations performed with varied values of these parameters. To address that part, in principle, any available tool for U&S analysis can be used, but the available tools like, for example, URANIE [Blanchard et. al., 2018] or DAKOTA [Dalbey et. al., 2022] are large frameworks for extensive functionality and too complicated to be adopted and used in the frame of this doctoral thesis. Hence, to address both U&S analysis and source term prediction tasks, a dedicated tool easy to use and with full access to the source code is needed.

Therefore, the first task is to develop the tool, which combines desired functionality for:

- Preparing the input database.
- Performing U&S analysis.
- Simulating the measured data if real measurements are not available.
- ST prediction.

Newly developed tool is to be first applied to the test case to prepare the input database for ST prediction and its U&S analysis functionality is validated against existing tools. Before performing the U&S analysis for the plant case (KONVOI-1300 NPP), the first application of U&S tool is executed for a simpler case, here the QUENCH-08 experiment. This experiment is complex enough to be relevant for a U&S analysis application [\[Gabrielli et. al., 2018\]](#) and the ASTEC simulations faster executed comparing to the SA simulation of a full KONVOI NPP. Among all existing tools for U&S analysis, URANIE [\[Blanchard et. al., 2018\]](#) is chosen for validation purpose.

When the database is prepared, it can be used to predict the ST value in real time. Because the suggested prediction algorithm can be in general applied to any physical process and predict any chosen parameter, for the QUENCH-08 simulations it is used to predict amount of hydrogen produced during the experiment. Moreover for, QUENCH-08 experimental data are available, and the prediction approach can be verified by real measurements.

To test the correctness of the prediction algorithm, its implementation is validated against the original implementation, being delivered by Framatome in form of a proprietary executable file. The validation is carried out using results of QUENCH-08 simulations.

After the verification and validation procedure for the QUENCH-08 experiment the approach is applied to an entire NPP. First, identifying the uncertain input parameters important for the accident simulations requires a lot of efforts (choice is made based on the knowledge about the SA phenomenology; experimental data and existing analysis results available in the literature; engineering judgement). After that, the database for prediction algorithm is prepared for selected accident scenarios. And finally, the prediction algorithm is applied. Obviously, no real data is available in this project for SA at NPP, and to imitate these measurements additional simulations are performed.

In the next section the objectives of the thesis are reflected in the thesis structure.

1.3 Structure of the thesis

Based on the motivation and thesis objectives the thesis is organized in following way:

[Chapter 2](#) is fully addressed to the literature review. Firstly, the phenomenology of the severe accident is briefly discussed. Then, the topics of nuclear reactor safety, safety management and emergency planning are introduced. After that, briefly described how the severe accident code calculates the source term. And finally, the fast-running approaches – mostly on tools using BBN – are presented.

[Chapter 3](#) is devoted to the mathematical description of the prediction algorithm.

The description of a newly developed Fast Source Term Prediction tool, its functionality for preparing the input database and U&S analysis are presented in [Chapter 4](#).

Testing the whole methodology on the results of the QUENCH-08 experiment simulations is discussed in [Chapter 5](#). At first a short description of the experiment is given, as well as the choice of uncertain input parameters for ASTEC simulations, the results of U&S analysis and applying the MOCABA algorithm for the prediction of the amount of released hydrogen using the temperature values are presented.

[Chapter 6](#) has a similar structure as the previous one, but it is devoted to KONVOI-1300 simulations. Results of U&S analysis and ST prediction are presented for the Medium Break Loss-of-Coolant Accident (MBLOCA) scenario.

In [Chapter 7](#) conclusions and recommendations for future works are discussed.

Appendixes contain information on:

- [Appendix A](#) – Brief introduction into U&S analysis and short description of the existing software.
- [Appendix B](#) – Preparing documentation for the FSTC tool; unit and performance testing; validation of U&S analysis part of the tool against the URANIE platform; validation of the MOCABA algorithm implementation against the proprietary code developed in Framatome.
- [Appendix C](#) – Integral validation of the FSTC-MOCABA approach on the results of the MBLOCA+SBO accident scenario simulations.
- [Appendix D](#) – Constraints and limitations of the MOCABA algorithm shown on the simple ‘toy’ model.
- [Appendix E](#) – The list of publications is provided.

2 Phenomenology and emergency management at severe accidents for pressurized water reactors (PWR)

The main objective of this thesis is to provide a fast running tool supporting the emergency team in a NPP to predict the source term value. To address that issue, knowledge from very different, but interconnected areas need to be used.

Firstly, the physics of severe accidents is a complex subject due to many processes being involved and due to the difficulties with performing experiments and creating the models. SA phenomenology cannot be described here in detail (only some processes are briefly addressed where needed), very detailed description of the current knowledge level may be taken from, for example [\[Sehgal, 2012\]](#). Here, brief description is provided in [Subchapter 2.1](#).

Then, safety at a NPP in general is discussed in [Subchapter 2.2](#). Scoping the safety culture and, what levels of safety exist at a NPP, and the accident management procedures. That section will help us to put the goal of the thesis in some frame and understand more clearly what could be done to improve severe accident management and help the emergency team.

Calculation of the source term with SA code ASTEC is briefly described in [Subchapter 2.3](#). Existing SA codes are very detailed, and thus computationally expensive. They can be used to prepare results of SA simulations in advance, but in case of a SA at a NPP, the situation needs to be analyzed very fast and the assessed source term value should be ready quickly. To address that issue, different approaches and tools have been developed – one of the most popular is to use BBN to choose the most appropriate source term value from several prepared beforehand. Currently existing approaches and tools for real-time source term prediction are addressed in [Subchapter 2.4](#).

2.1 Phenomenology of severe accidents in a Pressurized Water Reactor

A severe accident at a nuclear power plant is an incident involving the significant degradation of the reactor core, associated fission products release from degraded core, their transport to the primary system and containment and risk of containment failure with release of the fission product into the environment. The severe accident starts with the initiating event, and in this work the accidents starting with break in the cold leg and loss of offsite power are demonstrated. In this section the various processes happening during the severe accident are briefly described. They can be divided into in-vessel (early and late phase) and ex-vessel phenomena. Schematically, the main physical processes and involved safety systems are shown in **Figure 2-1**.

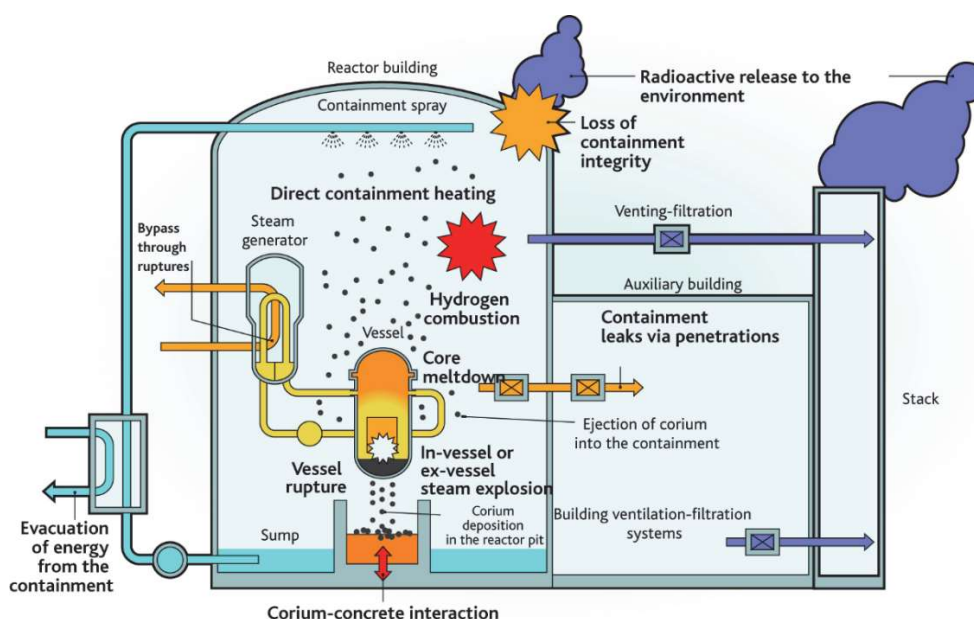


Figure 2-1 – Potential physical barriers failures and physical effects occurring during a SA. From [Van Dorsseleare, 2011].

The in-vessel phase includes everything starting from the cladding oxidation in the uncovered code and ends with the lower head vessel failure. The list of in-vessel phenomena is given in **Table 2-1**.

| <i>Early in-vessel phase</i> |
|---|
| Cladding oxidation – exothermal reaction with hydrogen production |
| Cladding ballooning and burst |
| Liquefaction and relocation of: <ul style="list-style-type: none"> - Control and structural materials; - Zircaloy cladding; |
| Eutectic interaction between molten material and solid structures e.g. cladding, UO ₂ -pellets |
| Liquefaction and slumping of the fuel. Molten pool formation. |
| <i>Late in-vessel phase</i> |
| Relocation of the molten pool into the lower plenum |
| Stratification of the materials in the lower plenum |
| Corium interaction with the vessel wall (leading to the lower head vessel failure) |
| Steam explosion |

Table 2-1 – Some potential in-vessel phenomena occurring at different phases of a SA.

The description of in-vessel phenomena starts with Zircaloy (Zry) oxidation of the cladding [Coryell, 1994], [Schanz et. al., 2004]. That physical phenomena happens in light-water reactors, when the reactor core is not covered by with water anymore, but with steam. This contact of steam with hot Zry cladding lead to three important effects – heat production, hydrogen production and Zry cladding oxidation – heat produced in that exothermal reaction will be an additional impact of heating and therefore further degradation the core structures; produced hydrogen can lead to a deflagration; physical properties of oxidized cladding differ from initial ones, and lead to a delayed destruction of the cladding covered by a protective oxide layer. Important factors for this oxidation process are – availability of the steam, amount of Zry present at that location at a given time, and how much oxygen can diffuse through the already oxidized layer of the cladding.

The other phenomena threatening the integrity of the fuel rods not from the outside like oxidation in the steam environment, but from the inside – is the cladding ballooning and burst [\[Minato et. al., 1991\]](#), [\[Gao et. al., 2022\]](#) due to the difference between internal pressure and the decreased, because of the loss-of-coolant, pressure outside of the cladding. A cladding burst lead to the release of the fission products and expose the fuel and inner layers of the cladding to the steam environment.

Liquefaction and further relocation [\[Barrachin et. al., 2013\]](#), [\[Veshchunov et. al., 2013\]](#) of control and structural materials happens between 1500 and 1700 K due to chemical interactions between, for example, Zry and Fe or Zry and B₄C; melting of Zry cladding – usually between 2000 and 2250 K. Oxide layer can prevent the cladding failure for some time, but it will allow the inner layer of the cladding to be in contact with the fuel and dissolve in it, forming the U-O-Zr mixture [\[Li et. al., 2017\]](#), [\[Itoh et. al., 2020\]](#).

When the temperature is becoming high enough, the fuel and rest of the cladding material starts to slump to the bottom of the core region, forming blockages and drastically changing the flow area. Formed molten pool is covered with crust and it will keep the fission products inside for some period of time. Formation of the molten pool [\[Bandini et. al., 1998\]](#), [\[Asmolov et. al., 2004\]](#) is considered as a relative boundary between the early and late in-vessel phases. Molten pool is melting through the existing structures inside vessel towards the LP, where it will contact with water. The interaction of molten corium and structure material with water causes instantaneous steam generation causing a pressure peak. Molten pool relocation into the LP, its behavior here and its interaction with water is a complicated process [\[Buck et. al., 2010\]](#). In that frame the following can be investigated:

- Slumping of a significant amount of materials into the LP;
- Interaction melt jets with water [\[Dinh et. al., 1999\]](#);
- Forming of debris particles and their re-melting;
- Corium stratification [\[Salay et. al., 2004\]](#) in the LP;
- Focusing effect – the metal layer of the stratified corium concentrates heat flux on the reactor vessel wall.

At this point of the accident progression the lower head vessel failure (LHVF) [\[Sehgal et. al., 1998\]](#), [\[Mao et. al., 2016\]](#) can happen. The integrity of the vessel is threatened due to different reasons, for example:

- Steam explosion, when corium comes into contact with water in the lower head.
- Contact with corium jets leading to the erosion of the vessel wall.
- Molten corium pool exchanging heat with the vessel wall and leading to its penetration due to the focusing effect.

After the LHVF the ex-vessel phase [\[Atkhen et. al., 2016\]](#) of the accident starts, and at this point containment integrity is preventing a massive FPs release into the environment. The ex-vessel phenomena are listed in **Table 2-2**.

| <i>Phenomena directly threatening containment integrity</i> |
|---|
| Direct containment heating |
| Hydrogen combustion |
| Steam explosion |
| Molten corium-concrete interaction |
| <i>Other phenomena</i> |
| FPs (in gas and aerosol forms) physics and chemistry |

Table 2-2 – Some potential ex-vessel phenomena occurring at different phases of a SA.

Direct containment heating (DCH) occurs in case of LHVF happening at a high-pressure, much higher, than in containment. In such conditions melt will be forcefully injected into the reactor cavity (could be dry or filled with water), fragmented and transported further. The risk to containment integrity in that case exists due to the intensive heat exchange between the containment atmosphere and the finely fragmented melt particles and due to the combustion of the hydrogen produced during this melt particles dispersion process.

Hydrogen – produced as a results of reaction between steam and zirconium, steel, boron carbide, fuel, corium, or in molten corium-concrete interaction – threatens the containment integrity due combustion [\[Meyer et. al., 2014\]](#). Special conditions (temperature, pressure, amount of hydrogen and oxidant) should be met to make combustion sustainable and, of course, the initiating event must happen. How big will be the area of hydrogen combustion, if it happens, and whether combustion will happen in the most severe form – detonation – these phenomena are difficult for modelling and not everything is fully understood yet from physical point of view [\[Liu et. al., 2021\]](#), [\[Zhang et. al., 2019\]](#). Possible options to prevent such event are – igniters, recombiners, inerting containment atmosphere or mixing containment atmosphere to avoid high local concentrations of hydrogen.

In case of a cavity filled with water, contact between molten corium and water can lead to a steam explosion [\[Meignen et. al., 2014\]](#) – the hot fuel pieces fragment into smaller and smaller particles, water evaporates around them, generated vapor film can collapse leading to higher pressurization and forming the propagating front, which will affect surrounding structures.

The molten corium-concrete interaction [\[Bonnet et. al., 2017\]](#) yields a release of steam, hydrogen and other gases, which increases the containment pressure and thus, risk of hydrogen combustion. Molten corium concrete interaction (MCCI) is also a source of aerosols for the source term, and in case of insufficient cooling melting through the basemat leads to the release of the FPs into the environment.

Behavior of aerosols in containment [\[Haste et. al., 2013\]](#), [\[Girault et. al., 2012\]](#) is a difficult task for modelling due to the long time scales (up to days); complexity of involved processes

happening in containment, like MCCI; and big volume of the containment itself; agglomeration, condensation of aerosols and aerosol chemistry are also included in the modelling task.

The correct modelling of all above-mentioned processes is crucial to predict the final release of the fission products into the environment in case of containment leaks or failure. The information about the release into the environment is the essential information for the ERO to plan measures for the population and environment protection.

2.2 Emergency management in case of severe accidents in Nuclear Power Plants

Nuclear reactor safety became an intensively discussed topic after Three Mile Island [Tolman et. al., 1988] and especially after the Chernobyl accident [Adamov et. al., 1996] and the concept of ‘defense in depth’ was gradually developed. The definition and a detailed description of that concept can be found in [INSAG Series, 1988], [INSAG Series, 1996]. This concept is proposing multiple independent layers of defense, which are trying to guarantee that even in case of any abnormal condition, external hazard, equipment failure and/or human error it is possible to control the situation at the NPP and prevent release into the environment. During its development, the ‘defense in depth’ concept was broadened to include also monitoring and diagnostic tools, for example [INSAG Series, 1996]. As a result, this concept is considered to be encompassing by incorporating physical barriers, accident management procedures, monitoring, etc. related to the safety of a NPP.

The five layer structure (based on description from [INSAG Series, 1996]) of ‘defense in depth’ is illustrated in **Figure 2-2**.

Five layers of 'defense in depth' concept

Maintain core structural integrity

Level 1: Prevent abnormal operation and system failures

Level 2: Control abnormal operation and detect failures

Level 3: Ensure performing of safety functions (activate safety systems). Keep operation within design basis

Level 4: Accident management. Limit accident progression.

Level 5: Off-site emergency response. Mitigate radiological consequences

Figure 2-2 – Different safety layers and their objective of the ‘defense in depth’ NPP safety concept.

The main goal of this thesis is to develop a computational tool and a methodology to provide a radiological source term value in real time, which is attributed to *Level 5*, when a regulatory body needs to know the level of release to the environment and its progression in time.

A better scenario in case of some abnormalities is to prevent any radioactive release into the environment completely. For that, firstly, physical barriers exist. It is worth mentioning that these barriers are designed in a conservative manner with margins between ‘normal’ state and ‘failure’. Firstly, fuel is confined in a fuel matrix which is considered the first barrier. Fuel tablets are surrounded by cladding, and only if it cracks or melts, radioactive materials can propagate further. The next barrier is the reactor pressure vessel (RPV) – molten core can fall into the lower plenum (LP) and leading finally to a RPV failure, releasing radioactive material to the containment. The primary cooling system is another barrier for the released materials and while it is intact, radioactive materials are confined. The containment itself is the other layer of defense, preventing radioactive materials from release into the environment. The containment has passive autocatalytic recombiners, which guarantee controlled hydrogen combustion and prevent an uncontrolled explosion, and a spray system, which helps to wash condensed radioactive material from the walls. The containment itself can be damaged, for example, due to the direct heating overpressure (from hydrogen burning or from a steam pressure wave arising from molten core falling into a water layer) or a hydrogen/steam explosion. But, even in the case of an explosion, it needs to be strong enough to damage the containment integrity. Another possibility for fission products to escape from an undamaged containment is a leakage, e.g. in form of a damaged isolation valve.

Active use of accident management has been mentioned as an ‘important recent development’ in [\[INSAG Series, 1987\]](#), and since then a lot of work and improvements were made in developing safety guidelines, analyzing safety procedures and measures, in automatic diagnostic systems, etc. Accident management is a set of actions that need to be taken in case of an accident to prevent a severe course or to mitigate the consequences if prevention is not successful: that part is named Severe Accident Management (SAM). As stated in [\[IAEA, 2009\]](#), an accident management concept can be described in the form of a work-flow started with ‘objectives’ – mainly, it is what is to be done, for example, to ‘prevent significant core damage’ or ‘maintain containment integrity’, followed with strategies and measures (for example, containment venting) and finalized by development of procedures and guidelines for the responsible personnel.

In very simple words, personnel must know what abnormalities are happening and what measures need to be taken to prevent further progression of the accident. To detect any kind of abnormalities, intelligent diagnostic systems [\[Saghafi et. al., 2016\]](#) provide important help complementing human monitoring. Such systems detect deviation from normal functioning of NPP systems, from normal values (of temperature, pressure, etc.), but also help to identify the type of the accident (using, for example, BBN), replacing manual analysis of fault/event trees.

Appropriate measures are described in Severe Accident Management Guidelines (SAMGs) present in any NPP are first initiated by main control room (MCR) staff until the TSC is ready to take responsibility. The TSC is estimating the possible source term and communicating with ERO. At this interface the possible application of the outcome of this thesis is located. A detailed description of accident management is outside of the scope of this work and all needed information about, for example, roles and hierarchy of personnel, practical usage of the SAMGs and development of the SAGMs can be found in official reports such as [\[IAEA, 2009\]](#). The scheme of the on-site part of ERO is presented on **Figure 2-3**.

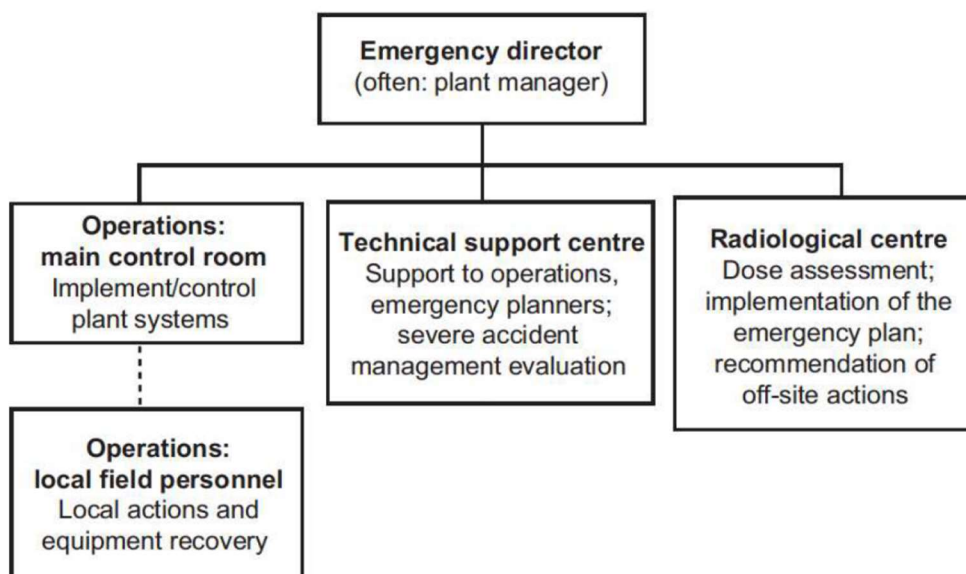


Figure 2-3 – Typical layout of the technical elements of the on-site emergency response organization, from [\[IAEA, 2009\]](#).

To classify the emergency situation, events or conditions are grouped according to:

- 1) Potential or actual effects or consequences.
- 2) Resulting onsite and offsite response actions, see e.g. [\[IAEA, 1997\]](#), [\[US EPA, 2022\]](#).

The emergency classification according to [\[NRC, 2022\]](#) consists of events, which are increasing in severity like:

- Notification of Unusual Event (NOUE) – A situation potentially degrading the plant's level of safety or indicating a security threat to the facility. Radioactive release, which requires offsite actions, is not expected yet unless further degradation of the safety systems.
- Alert – Situation can (or has already) seriously degrade the plant safety; threaten site personnel; damage to site equipment. Anyhow, offsite release is expected to be minimal (below limits defined in, i.e. Environmental Protection Agency's (EPA) protective action guides (PAGs) [\[US EPA, 2022\]](#). At that point personnel must be ready to perform

confirmatory radiation monitoring if required, and ensures that offsite authorities receive current information on plant status.

- Site Area Emergency (SAE) – That event causes (or likely will cause) major failures of plant functions protecting the public. The event can involve intentional damage or malicious acts that could lead to the likely failure of (or prevent effective access to) equipment required for the public protection. Offsite radioactive release is expected to stay below the exposure levels beyond the site boundary. In case of SAE, for example, personnel should evacuate nearby areas, if the situation becomes more serious. In addition, such a level includes government authorities providing updates to the public.
- General Emergency (GE) – Such type of event causes (or shortly will cause) substantial reactor core damage, with the potential for uncontrolled releases of radioactive material. It covers events that prevent plant staff physically to control the facility. Offsite release is expected to exceed the exposure levels beyond the plant site. The protective actions for the public include continuous dose monitoring, consultation with offsite authorities and providing updates to the public by government authorities.

Different public protective actions are employed in different phases of the accident. At all time, the protective actions are based on the classification of the accident (see Table B1 in [IAEA, 1997](#)). During the fission product release to the environment, actions are employed based on projections and in plume ambient dose rate measurements (see Table B2 in [IAEA, 1997](#)). After the plum passage, actions are performed based on deposition concentration and ambient dose rate measurements (see Table B3 in [IAEA, 1997](#)).

The real-time knowledge of the fission product release to the environment the source term is therefore, a fundamental information needed from ERO to activate the necessary protective measure to the population. On-line measurements in the plant, i.e. containment, and in the region surrounding the nuclear site provide the actual picture of the source term evolution. Nevertheless, the possibility to have reliable time-predictions of the source term may significantly improve the effectiveness of the protective measures. For this purpose, SA codes represent a valuable support to the decision maker, since they are able to simulate the time-evolution of the source term from the start of the accident up to the release into the environment. However, SA codes cannot be used for a real-time monitoring of the source term, because computational time required for such simulations is rather long. In addition to it, it is difficult to understand the initiators as well as the boundary conditions of the SA event. Consequently, the modelling of the on-going scenario is rather challenging. At the same time, severe accident codes are able to provide nowadays reference source term estimations, despite the still existing uncertainties of the physical models implemented for some selected phenomena.

The approach proposed in this work is to compute reliable source term predictions in real-time to improve the quality of the information needed by ERO as well as the effectiveness of the

protective measures during a SA scenario in a NPP. Concerning the reliability, the extensive employment of the ASTEC code in this work allows performing quite sophisticated source term evaluations, thanks to well validated physical models [\[Jones, et. al., 2003\]](#), [\[Van Dorsselaere et. al., 2010\]](#). Furthermore, the assessment of a training database for the Bayesian algorithm for source term predictions, allows having at once the results for a quite wide range of SA scenarios. Finally, the possibility to have an innovative platform of codes for realistic source term predictions further improves the quantitative performance of the results of the analyses of fission product dispersion in the environment. Such evaluations are performed by using codes like the JRODOS [\[Landman et. al., 2014\]](#), developed at KIT. Therefore, the approach described here has the potential to support both the ERO in the decision making process and the improvement of the performance of the protective actions during a severe accident.

2.3 Radiological source term prediction by ASTEC severe accident code

The European severe accident code ASTEC used in this thesis for the simulations is under development since 1997 [\[Peltier, 1999\]](#) in Institut de radioprotection et de sûreté nucléaire (IRSN) and recently the KIT became a co-developer. The ASTEC code has modular structure, in which each module is focused on particular group of phenomena, see **Figure 2-4**. All modules (except SYSINT and IODE) presented on **Figure 2-4** are used in the simulations. ELSA and ICARE modules simulate the whole in-vessel phase up to the LHVF, after that, RUPUICUV and MEDICIS simulate the corium behavior and its interaction with reactor structures. Gas combustion in containment is modelled by the CPA and COVI modules. Aerosol behavior in containment is calculated by CPA module, in circuits – with SOPHAEROS module. CESAR module computes thermohydraulics in all circuits through the whole SA progression, and in RPV up to the beginning of the core degradation processes. The dose rate in containment is computed by DOSE module. The detailed description of the ASTEC modules and implemented physical models can be found in the code manuals [\[Coindreau, O., 2017\]](#), and here only the brief description of the source term calculation is provided due to its importance for the whole topic of the thesis.

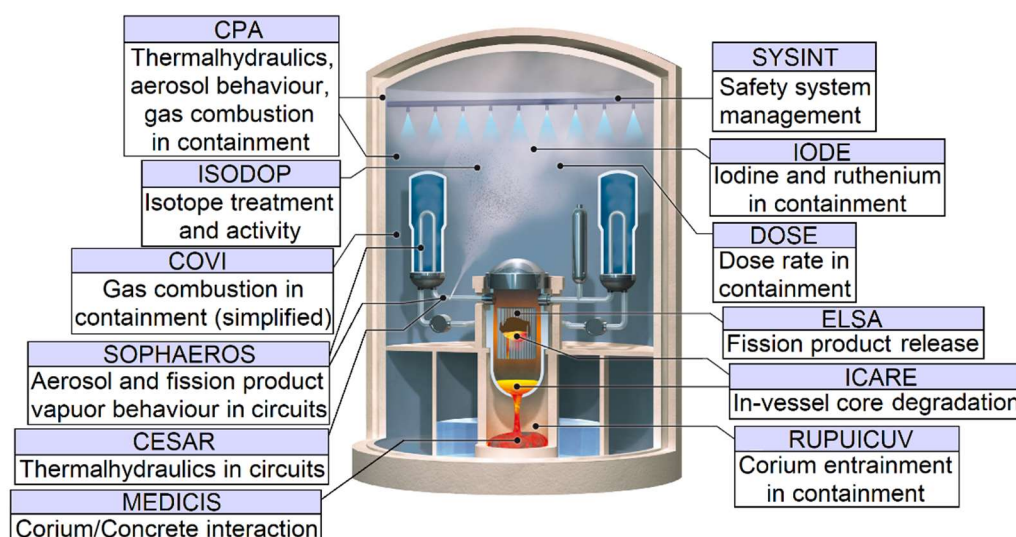


Figure 2-4 – Structure of the ASTEC code with its modules and related phenomena.
Based on [Chatelard et. al., 2014].

The FPs release starts in the intact reactor core. The ELSA module models the FPs release from the intact fuel and control rods. It divides the FPs into three categories by volatility:

- Highly volatile: Xe, Kr, I, Br, Cs, Rb, Cu, Se, Te, Sb, Ag.
- Semi-volatile: Ba, Ru, Sr, La, Eu, Ce, Mo.
- Low-volatile: Rh, Pd, Tc, Nb, Zr, Np, Pu, Nd, Pm, Gd, Tb, Dy, Ho, Er, Tm, Yb, Pr, Am, Cm, Sm, U, Zn, As, Cd, Sn, Ga, Ge, In, Y.

The FPs are released from the UO_2 fuel matrix grains divided into classes by size. For highly-volatile FPs the total release rate is integrated over all grains of all grain sizes. The semi-volatile FPs diffuse through the grain to its surface, and then released from it by evaporation process. For the release of the low-volatile FPs the main mechanism is the volatilization of UO_2 .

The cladding of the fuel rods is going through heating and oxidation, and finally cracks – these processes are computed by the ICARE module. Through these cracks the highly volatile FPs are finally released into the vessel domain. Remained volatile FPs will be released later from the fuel liquid fraction. The semi-volatile FPs will not be released during the fuel liquefaction, but only from the formed molten pool.

The degraded core and core structures are forming the molten pool, which gradually slumps to the lower plenum. The release from the molten pool is calculated also by the ELSA module. Up to this stage of the SA progression the FPs can exit the vessel only through the primary system, where their transport and behavior are calculated by SOPHAEROS module.

After the lower head vessel failure the mass of the degraded core will move to the cavity, where the process of MCCI starts, which is modelled by the MEDICIS module. The gaseous transfer of the FPs through the layers of the stratified corium into the atmosphere is modelled here. In addition to it, the RUPUICUV module calculates the addition of the FPs in the containment from the corium droplets.

The FPs released during the above mentioned processes are transported through the circuits modelled by the SOPHAEROS module. It works with the gas species, like Xenon and Krypton, and other volatile or non-volatile species in the condensed phase. Examples of the modelled processes are:

- Chemical interactions of species in gas and vapor forms.
- Aerosols coagulations.
- Aerosols deposition on the surfaces.
- Etc.

The FPs can reach the containment, for example, through the breaks in the circuits. In the containment the following modules are used to calculate the processes related to the FPs:

- SOPHAEROS calculates Iodine and Ruthenium chemistry.
- CPA module simulates the FPs transport; aerosols behavior in the containment volumes (transport, condensation, deposition on the walls); etc.

In parallel to all written above the ISODOP module computes isotopes and elements masses at each time step in five domains (core, primary and secondary circuits, containment, and environment).

Finally, the FPs from the containment can be released into the environment through the containment leakages.

2.4 Radiological source term prediction by fast running tools

Simulating SA with codes is time-consuming and cannot be performed during a SA. Thus, simpler approaches to assess the ST value are required. Around the time when the history of SA code starts, in [\[Manesse, et. al., 1988\]](#) has been mentioned that the potential release value can be calculated with “a set of assumptions” based on the plant measurements. Unfortunately, no more details were provided in that work, so it is not clear what method and assumptions were used. In [\[Chauliac et. al., 1992\]](#) the French approach for plant status diagnosis and ST prognosis is described. In that work, a group of different codes are mentioned, which are able to collect the available plant measurements and give an estimation about, for example, core residual power, containment leakage, etc. These data serve as an input for the PERSAN code, which can calculate the FP release. No detailed information about the PERSAN code was provided in that work and no additional information was found in other open publications and reports. In [\[IAEA, 1997\]](#) a simple approach for ST calculation is shown, which consists of one formula and all data for that formula is provided in tables in the same report. In 1998-2002 in the frame of the fifth framework programme (FP5) of the European Atomic Energy Community (EURATOM), development of the SPRINT [\[Grindon et., 2004\]](#) tool based on the Bayesian belief network and the short-running

code ASTRID [\[Herviou et. al., 2004\]](#), [\[Herviou, 2005\]](#) was started. And as it was stated in [\[Grindon et., 2004\]](#) at that time BBN approach was novel and not yet tested on a wide scale. The results achieved during the FP5 programme were used to start the development of the Swedish tool RASTEP [\[Knochenhauer et. al., 2012\]](#) in 2008-2009. A similar German tool is called FaSTPro; description and application example can be found in [\[Hage et. al., 2018\]](#). According to the available literature, the tools based on the BBN are the most widely used for the fast source term prediction in case of the accident at the NPP, therefore in this section the focus is only on this approach. Worth to mention, that in the tools using the BBN no modelling leading to the calculation of the source term value happens, all information is pre-calculated in advance for the given type of the reactor. Therefore, the basic understanding of the Bayesian belief networks gives the idea of how all these tools work.

The Bayesian belief network [\[Pearl et. al., 2000\]](#), [\[Weber et. al., 2012\]](#) represents the probabilistic dependency model graphically with the directed acyclic graph. Any graph consists of the nodes (vertices) and edges connecting these nodes. In the direct graph the edges connecting the nodes have direction and also called arrows or arcs. The acyclic graph has no cycles. Such graphic representation of the problem is widely used in many different areas from biology and computer science to the nuclear field. The node in the BBN is the event/variable with the discrete or infinite number of possible states represented with the set of the probabilities or the probability density function. The arc going from the parent to the child one represent the casual relationship between these two nodes. That causal relationship can be represented in the form of conditional probability table showing the probability of the given state of the child node, if the state of the parent node is known and equals the given value. When state of one node is changed, it affects immediately all other nodes directly or indirectly linked to that one.

BBN applied to the nuclear safety field helps to define the type of the accident and give the prediction about the source term. BBN nodes in that case can be:

- Status of a safety system (failed or working correctly).
- Event (happened or nor).
- Threshold for a given measured parameter (temperature is above the given value or not).

Example of the BBN from FaSTPro tool [\[Hage et. al., 2016\]](#) is presented at **Figure 2-5**. In the three left nodes one can see the following variables describing the status of the plant – pressurizer level, pressure in the containment and the temperature of the core. On all these questions user gives an answer choosing from the available options. If as it is shown in the figure the user does not know anything about these parameters and set option ‘unknown’, the system based on that cannot give the answer, whether the loss of coolant accident (LOCA) is happening, and the status of the ‘LOCA_Exist’ node is also unknown. The node ‘Initiating_Event_PSA’ is related to the probabilistic safety analysis (PSA), which itself relies on the Boolean algebra to

describe the probability of failure (fault tree) and of occurrence of events (event tree) of a complex system. The node related to the actual observation and the one related to the PSA also performed in advance both influence on the node ‘Initiating_Event_Final’, which is giving in the case the 20% chances that LOCA happens and 80%, that it is a transient. The ‘Initiating_Event_Final’ influences on the two other nodes - ‘CD_IE_PSA’ and ‘Source_Terms’. The ‘CD_IE_PSA’ and the ‘CD_Final’ nodes are related to the core damage status. The ‘CD_Final’ gives the user probabilities of whether the core damage is taking place based on the observations and the PSA results. As presented in the figure there is 26% chances of the core damage in that case. The ‘Source_Terms’ node is showing the possibility of different source term, and in presented case the probability of the loss of coolant accident with the core damage and the corresponding source term value is only 2%. As one can see, the presented Bayesian belief network is accumulating the information from different sources (the observations made by the user and the results of the PSA) and going through various nodes to the final answer about the source term. Of course, the source term value is not provided just as a single value of the probability, it is presented to the user of the tool as an evolution in time of the release rate in Bq/h or the integral release in Bq for different elements and their isotopes.

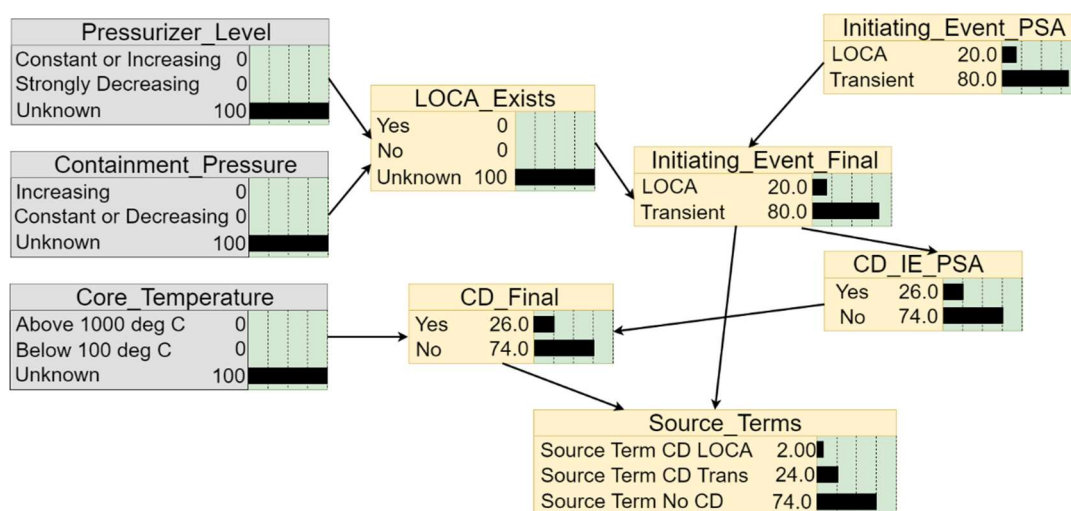


Figure 2-5 – Example from the FaSTPro tool of a Bayesian belief network providing the status of the core damage and the given source term probability based on the user answers about the plant status and the PSA results. Based on [Hage et. al., 2016].

Creating a BBN requires a broad knowledge of the possible accident scenarios and a given plant design. This process is tightly connected to the probabilistic safety analysis [Wall et. al., 2001] and fault and event trees used for it [Choi et. al., 2003]. To construct a BBN and work with it a special software can be used, for example Netica [Norsys Software Corp., 2022]. Netica BBN engine is a part of the RASTEP tool. User interacts with the software through graphical user interface (GUI), answering the questions, and therefore changing the status of some of the BBN nodes, BBN engine update status of the whole system and giving the probability of a given ST and its value.

Adding functionality, which allows to modify ST value in real-time, was investigated in [\[Alfheim, 2012\]](#), [\[Dedda, 2013\]](#) for RASTEP tool. But, according to our knowledge up to now [\[Rocchi et. al., 2020\]](#) this option has not been introduced in RASTEP or any other tool based on BBN. Therefore, up to now using BBN with the database of pre-calculated ST values is the most widely used fast approach to obtain to ST value in case of the accident. The idea of using ANN to predict the ST [\[Santhosh et. al., 2020\]](#) or status of the plant [\[Kim et. al., 2021\]](#) floats around, while ANN are actively used in other fields (in medicine, for example). Significant amount of papers could be found already about that topic, but up to now it didn't substitute the BBN approach.

3 Mathematical description of the Monte Carlo based Bayesian approach (MOCABA) for the fast source term calculation

The MOCABA algorithm was originally developed in 2015 [\[Hoefler et. al., 2015\]](#) and can be attributed to the class of data assimilation (DA) algorithms. Initially, DA methods are developed and applied to improve the quality of weather forecasting [\[Bouttier et. at., 2001\]](#). It is a step-by-step process, which is using observations and results of previous forecasts to construct a new one. DA methods are not tied to the field of the earth sciences, of course, and are also used in other fields – as in nuclear simulations to reduce the uncertainty of some nuclear reactor core parameters like reactivity [\[Abdel-Khalik et. al., 2008\]](#). The MOCABA algorithm was developed as a DA method improved compared to another one – Generalized Linear Least Squares (GLLS) [\[Hoefler et. al., 2011\]](#) – and was initially used to predict the values of the integral functions of the reactor core, like total power or k_{eff} , and to reduce the uncertainty of such prediction.

In this work, MOCABA algorithm is applied to a results of a severe accident simulations, and the main goal is to predict the source term value as a function of time. The mathematical formulation of the algorithm divided into two parts called ‘*prior*’ and ‘*posterior*’ is described hereafter.

3.1 Mathematical formulation of the ‘*prior*’ part of the prediction algorithm

Let us describe the problem in very general terms. There is some physical process, which we can simulate, observe in reality or even set up an experiment for. In this process, we are particularly interested in some parameters, and we want to know, how they evolve in time; let us call this group ‘*predictions*’. Other parameters are measured during the process, and we call these parameters ‘*observables*’. For example, there are N_{pred} and N_{obs} parameters in these two groups, respectively, so finally, we focus on $N_{total} = N_{pred} + N_{obs}$ parameters. Assume, that we are modelling/observing this process for the time period t_{total} , which is divided into n_t time steps. When this process is simulated, some other parameters could be picked up as uncertain input parameters and varied inside given uncertainty range, which gives us a collection of process realizations. Set the number of these realizations to n_s . Taking these all into account, for each parameter Y from the ‘*predictions*’ or ‘*observables*’ group, the following matrix is filled with results of the process simulations, containing values for all samples at each time step:

$$\begin{bmatrix} Y_{1,1} & \cdots & Y_{n_s,1} \\ \vdots & \ddots & \vdots \\ Y_{1,n_t} & \cdots & Y_{n_s,n_t} \end{bmatrix}. \quad (3.1)$$

At each time step for each parameter Y its mean value $\bar{Y}_{i,j}$ is calculated as:

$$\bar{Y}_{i,j} = \frac{1}{n_S} \cdot \sum_{k=1}^{n_S} Y_{i,j}^k, \quad (3.2)$$

where $i = 1 \dots N_{total}$ (parameter index), $j = 1 \dots n_t$ (time step index), and $k = 1 \dots n_S$ (realizations/sample index). The result of applying Eq. (3.2) to data from Eq. (3.1) is the matrix \bar{Y} of parameters mean values with size (N_{total}, n_t) .

At each time step from $j = 1 \dots n_t$ the Pearson correlation coefficient between parameter Y_i and Y_m , where $i, m = 1 \dots N_{total}$, and $k = 1 \dots n_S$ can be calculated by:

$$Corr_{i,m} = \frac{\sum_{k=1}^{n_S} (Y_i^k - \bar{Y}_i) \cdot (Y_m^k - \bar{Y}_m)}{\sqrt{\sum_{k=1}^{n_S} (Y_i^k - \bar{Y}_i)^2} \cdot \sqrt{\sum_{k=1}^{n_S} (Y_m^k - \bar{Y}_m)^2}}. \quad (3.3)$$

Results of applying Eq. (3.3) is a tensor size $(N_{total}, N_{total}, n_t)$. The correlation matrix at each time step can be divided into three parts – correlations between parameters only from the ‘predictions’ group, only from the ‘observables’ group, and between parameters from different groups: $\begin{pmatrix} Corr_{pred,pred} & Corr_{pred,obs} \\ Corr_{pred,obs} & Corr_{obs,obs} \end{pmatrix}$. We use this representation of the correlation matrix later in the ‘posterior’ part of the algorithm.

The next step is to calculate correlations between time steps. For each parameter Y , correlation between two different time steps from $j = 1 \dots n_t$ can be calculated using the same Eq. (3.3), but in the first case Y_i and Y_m are the values of different parameters Y at the same time step, and now, Y_i and Y_m are the values of the same parameter Y at the different time steps. Result of calculating correlations between time steps is a tensor with shape (n_t, n_t, N_{total}) .

For each parameter Y at each time step, the standard deviation is evaluated by:

$$\sigma_{i,j} = \sqrt{\frac{1}{n_S} \cdot \sum_{k=1}^{n_S} (Y_{i,j}^k - \bar{Y}_{i,j})^2}, \quad (3.4)$$

where $i = 1 \dots N_{total}$ (parameter index) and $j = 1 \dots n_t$ (time step index). The resulting matrix of the standard deviation values has the shape (N_{total}, n_t) .

All these results are used as the input data for the next ‘posterior’ part.

3.2 Mathematical formulation of the ‘posterior’ part of the prediction algorithm

For the ‘*posterior*’ part all correlations calculated in the ‘*prior*’ part need to be converted into covariance, so each correlation value should be multiplied by the corresponding standard deviation value:

$$Cov_{i,j} = Corr_{i,j} \cdot \sigma_{i,j}^2, \quad (3.5)$$

where $i = 1 \dots N_{total}$ (parameter index) and $j = 1 \dots n_t$ (time step index).

Each parameter from the ‘*observables*’ group has corresponding measurement values with their own measurement errors. Measured data ($Meas$) and measurements errors (σ_{meas}) are matrices of the size (N_{obs}, n_t) . Assuming independence of measurements, their covariance matrix at each time step looks like:

$$Cov_{meas} = \begin{pmatrix} \sigma_{1,1}^2 & \cdots & 0 \\ \vdots & \ddots & \vdots \\ 0 & \cdots & \sigma_{N_{obs},N_{obs}}^2 \end{pmatrix}, \quad (3.6)$$

and all measurement covariances at all time-steps form a tensor size (N_{obs}, N_{obs}, n_t) .

Now let us assume that from all time steps in $1 \dots n_t$ we have measurements only for the first t_{obs} time steps. For each time step with measured data updated values for all parameters (both from ‘*predictions*’ and ‘*observables*’ groups) can be calculated according following formulas:

$$Y_{pred}^* = \overline{Y_{pred}} + Cov_{pred,obs} \cdot (Cov_{obs,obs} + Cov_{meas})^{-1} \cdot (Meas - \overline{Y_{obs}}), \quad (3.7)$$

$$Y_{obs}^* = \overline{Y_{obs}} + Cov_{obs,obs} \cdot (Cov_{obs,obs} + Cov_{meas})^{-1} \cdot (Meas - \overline{Y_{obs}}), \quad (3.8)$$

and formulas for updating values of covariance matrices:

$$Cov_{pred,pred}^* = Cov_{pred,pred} - Cov_{pred,obs} \cdot (Cov_{obs,obs} + Cov_{meas})^{-1} \cdot Cov_{pred,obs}^T, \quad (3.9)$$

$$Cov_{obs,obs}^* = Cov_{obs,obs} - Cov_{obs,obs} \cdot (Cov_{obs,obs} + Cov_{meas})^{-1} \cdot Cov_{obs,obs}^T, \quad (3.10)$$

$$Cov_{pred,obs}^* = Cov_{pred,obs} - Cov_{pred,obs} \cdot (Cov_{obs,obs} + Cov_{meas})^{-1} \cdot Cov_{obs,obs}^T. \quad (3.11)$$

After calculating updated parameters and covariance values for all time steps where measurements are available, the next step is to calculate predictions for the time steps, where no measured data exist. First, assume that only t_{past} time steps are considered to predict values for t_{future} time steps in the future at each step of prediction algorithm (note that $t_{future} \leq t_{past}$). The prediction process starting at the time point t_{obs} . After a prediction is made for the t_{future}

time steps after t_{obs} , new current point in time for the algorithm will be $t = t_{obs} + t_{future}$ and so on. Schematically this process is shown on **Figure 3-1**. To calculate the ‘predictions’ parameters values covariance between time steps (defined by Eq. (4.3) – Eq. (4.5)) are required, and from that matrix only the values for future and past time steps are to be used. Schematically this is shown on **Figure 3-2**.

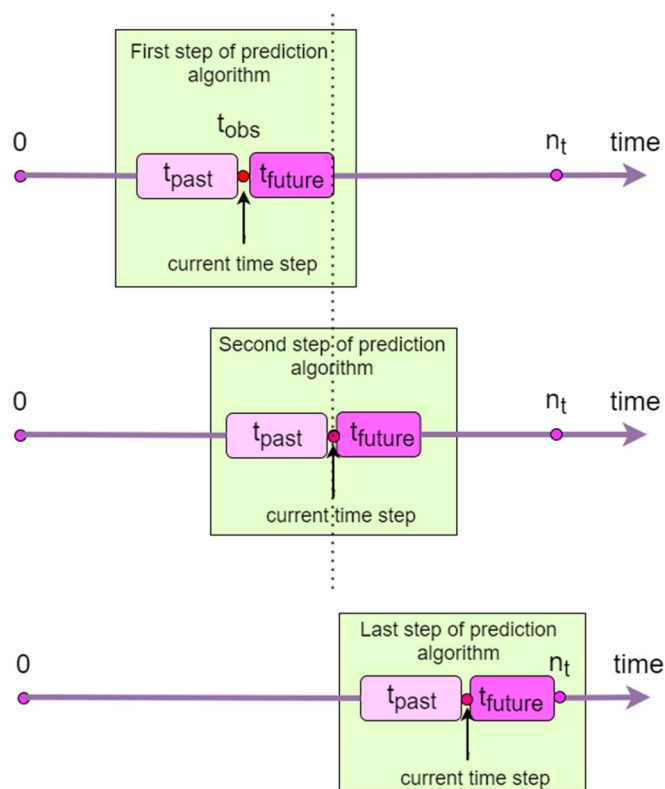


Figure 3-1 – Prediction algorithm steps in the ‘posterior’ part. At each step of its work algorithm takes t_{past} time steps to construct prediction for t_{future} time steps. Process goes till the last point of the time scale marked at n_t .

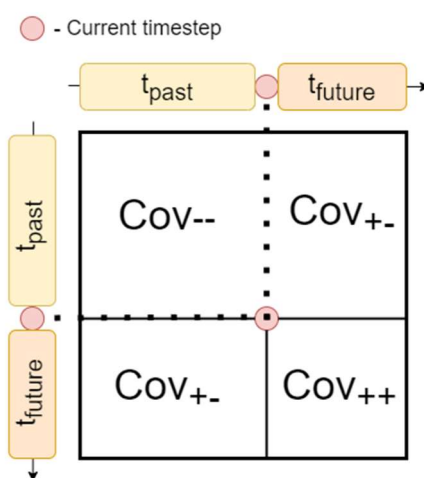


Figure 3-2 – Part of the full covariance matrix used at each step of constructing the prediction. This part has size $(t_{past} + t_{future}, t_{past} + t_{future})$. Cov_{--} - covariance between ‘past’ time steps. Cov_{++} - covariance between ‘future’ time steps. Cov_{+-} - covariance between ‘past’ and ‘future’ time steps.

Taking these all into account, predictions for future and past time steps are calculated according to following formulas:

$$Y_+^* = \bar{Y}_+ + Cov_{+-} \cdot (Cov_{--} + \sigma_{-}^{meas})^{-1} (Meas_- - \bar{Y}_-), \quad (3.12)$$

$$Y_-^* = \bar{Y}_- + Cov_{--} \cdot (Cov_{--} + \sigma_{-}^{meas})^{-1} (Meas_- - \bar{Y}_-), \quad (3.13)$$

where \bar{Y}_+ and \bar{Y}_- are the mean values (from Eq. (3.2)) of given parameter at the past time steps.

The variables $Meas_-$ and σ_{-}^{meas} at the time steps covering the time period until t_{obs} are the real measurement values and their errors. After that no measurement values exist anymore, therefore $Meas_-$ and σ_{-}^{meas} have to be evaluated using prediction results from the previous steps. **Figure 3-3** shows that predicted values of ‘observables’ parameters from the previous t_{past} time steps are the new virtual measurements.

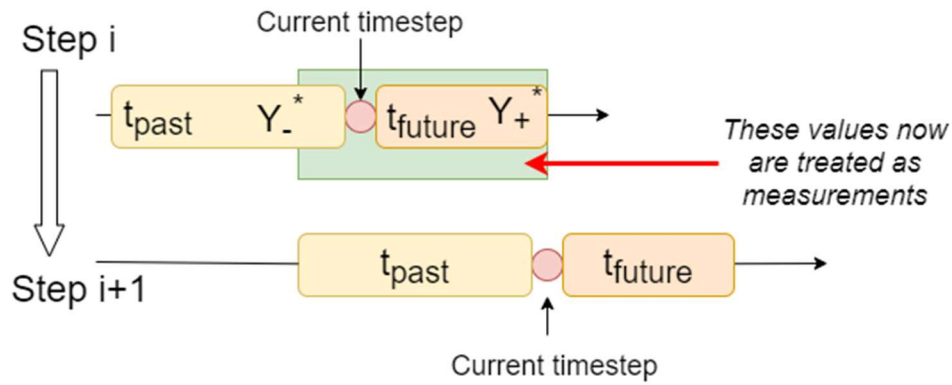


Figure 3-3 – Creating new virtual measurements values for the part of the time scale where no real measurements are available anymore. Predicted values of the ‘observables’ parameters from the last t_{past} time steps are becoming the ‘measurements’.

The same idea is applied to assigning new measurement errors values. To do so the updated values of covariances between time steps should be calculated according to the following formulas:

$$Cov_{++}^* = Cov_{++} - Cov_{+-} \cdot (Cov_{--} + \sigma_{-}^{meas})^{-1} \cdot Cov_{+-}^T, \quad (3.14)$$

$$Cov_{--}^* = Cov_{--} - Cov_{--} \cdot (Cov_{--} + \sigma_{-}^{meas})^{-1} \cdot Cov_{--}^T, \quad (3.15)$$

$$Cov_{+-}^* = Cov_{+-} - Cov_{+-} \cdot (Cov_{--} + \sigma_{-}^{meas})^{-1} \cdot Cov_{--}^T. \quad (3.16)$$

Using Eq. (3.12) – Eq. (3.16) for t_{future} time steps at each step of the algorithm creates the full prediction up to the last time step n_t . The final result of the algorithm execution is a Y_+^* values for ‘predictions’ and ‘observables’ parameters and the prediction errors defined as $\sqrt{Cov_{++}^*}$.

4 Tool for the fast source term calculation (FSTC)

The FSTC tool consists of two parts focus on their own task and can be run separately. These parts are devoted to:

- Uncertainty and sensitivity modules to generate a comprehensive database on radiological source terms;
- Predictive Bayesian inference module for the fast prediction of radiological source terms considering the database generated by previous module and measured data.

Here, after, the structure of these modules will be presented in more details. Note that words “*module*” and “*package*” are interchangeable in context of FSTC tool description.

For the generation of the database, the FSTC tool has been initially coupled with the integral severe accident ASTEC code and focused on its output file format. During the preparation of this thesis, the U&S part of the code has been improved to be easily coupled with other codes.

The generation of a representative database is itself a large and complicated task, which needs to be automated. It includes:

- The choice of uncertain input parameters.
- Sampling these parameters.
- Preparing input files for the SA code.
- Dealing with SA code execution for all considered variants of the input data.
- Collecting results of simulations.
- Performing uncertainty and sensitivity analysis.
- Finally, preparing the database for the prediction algorithm.

The existing U&S tools have been found not appropriate for the specific purpose of this dissertation, due to the overall solution approach depicted in **Figure 1-1** is bigger, that just performing U&S analysis.

Hence, the FSTC tool is developed from scratch using Python programming language so that it can be extended and improved on-demand depending of the specific tasks to be solved.

The U&S part of the FSTC tool consists of six modules (see in **Figure 4-1**) covering the tasks from sampling to U&S analysis itself. Implementation of the MOCABA prediction algorithm consists of two modules for ‘prior’ and ‘posterior’ parts. Additional module for more convenient automatic run of MOCABA algorithm on the bigger sets of data is not presented on the Figure 5-1, but will be described shortly in this chapter.

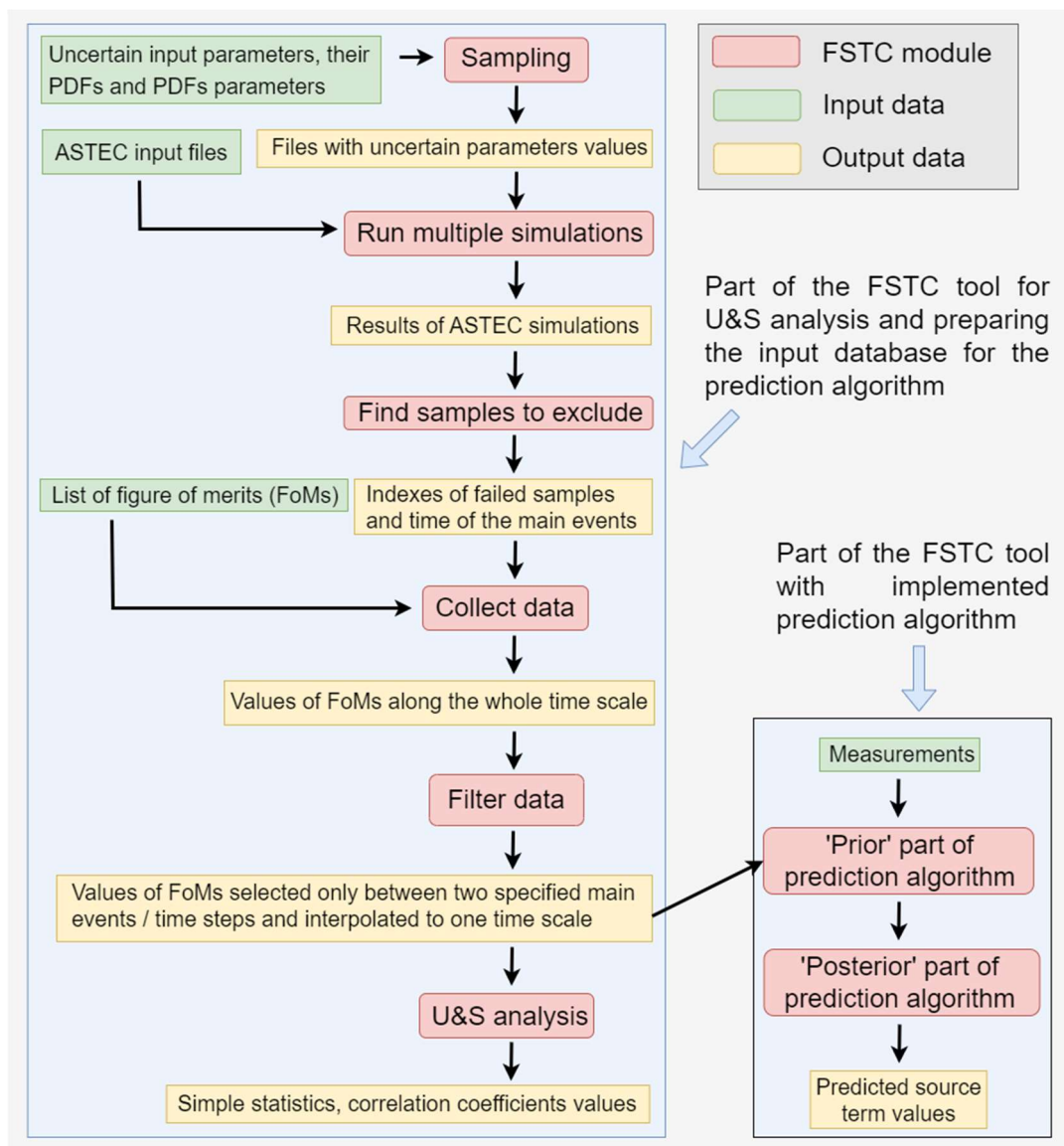


Figure 4-1 – FSTC tool scheme. Two main parts – for U&S analysis and for prediction algorithm are shown on the blue background. Separate modules are marked with red rectangles; input data – green; output results – yellow. Dataflow is shown by black arrows connecting modules with input and output data.

In [Appendix B](#) additional information related to the FSTC tool is provided, like:

- Testing of the tool.
- Creating documentation.
- Tool verification.

4.1 Database generation for the source term prediction task using the FSTC tool

4.1.1 Sampling

First step to U&S analysis is defining the list of uncertain input parameters, which potentially have a high impact on the variation of simulation results. These input parameters with their PDFs and PDFs parameters (like minimum, maximum, mode, etc.) are the input for the sampling module. Five probability density functions are currently available in the FSTC tool – uniform, normal, truncated normal, triangular and beta. Other types of PDFs could be easily added, for example, from the SciPy Python library [[SciPy, 2022](#)], which has a broad collection of such functions. The current limited collection of PDFs is based on choice of uncertain input parameters.

Sampling package performs sampling of given parameters inside a defined uncertainty range according to a given probability density function. Currently, two sampling methods are implemented – LHS [[McKay et. al., 1979](#)] and Monte-Carlo (also known as SRS).

The user prepares the input file with the following information:

- Name of sampling method.
- Number of samples.
- Description of all uncertain input parameters and correlations between them if needed.

For each uncertain parameter, the user specifies in the input file the following:

- Parameter name.
- Best estimated value.
- PDF type.
- PDF parameters.

As result of this package execution, the user can find in the output folder the following:

- Scatter plots showing how samples are distributed between minimum and maximum values.
- Plots with correlations between sampled input parameters (e.g. Pearson or Mann-Kendall [[SampleVis, 2022](#)]).
- Sampling results written in a database and in text files,
- A text file with sampling measures like L2-discrepancy [[Sheikholeslami et. al., 2017](#)].

4.1.2 Run multiple simulations

The second step is to run multiple simulations. In this work simulations with ASTEC code are time consuming and should be run in parallel. This option is available in the FSTC tool, and

user can specify number of cores, which will be used. For each individual run, the separate folder containing the individual set of input files is prepared automatically by the FSTC tool. In case of using the ASTEC code, input files describing the nodalization and activated ASTEC modules are the same for each individual simulation, and only the file with the values of uncertain input parameters is unique. In the input file for this module user specifies:

- The path to the ASTEC code executable.
- Name of the main file in the input deck. This name is used as an argument to run the ASTEC code.
- Name of the database, where the values of the sampled uncertain input parameters are stored.
- Name of the file, where the values of uncertain input parameters for each individual run are stored. This file will be called from the main file of the ASTEC input deck.

The output of this FSTC module are the results of ASTEC simulations stored in the multiple folders and ready to be used in the other FSTC modules.

4.1.3 Find samples to exclude

After all simulations are finished, their correctness are checked, and the indices of all failed simulation are provided. These failed simulations will be automatically excluded on the next step of U&S analysis.

In case of using the ASTEC code user provides in the input file for this module:

- The names the main events happening during the accident – for example, “*start of FPs release*”, “*lower head vessel failure*”, etc.
- The name of the specific ASTEC output file, where the time points of main events occurring are stored.

Due to varying values of uncertain input parameters, the SA progression also varies. The FSTC tool checks when the given main events happen in each individual simulation. This allows the user to look at how accident progression varies and focus only on the part of the process, which is further to be considered in the U&S analysis. For some correctly finished samples the accident progression can be too different from the rest of the simulations set – e.g. the lower head vessel failure could occur for some samples significantly earlier. In the U&S analysis itself the data only for particular part of the transient are analyzed – for example, the part between start of the FPs release and the lower head vessel failure. In that case, the data from the simulations output files will be extracted only up to the earliest lower head vessel failure. Therefore to broaden the time window for the U&S analysis, the samples with the earliest lower head vessel failure can be excluded. This is the optional part, and user always can perform U&S analysis using the whole

set of simulations. This option must be used very carefully, and effect from excluding samples must be investigated. That part of the analysis is very specific to the ASTEC code, which generates a specific output file, where the times of the main events are stored.

4.1.4 Collect data

Next step is to extract data from results of the multiple simulation to use it further in U&S analysis. In the input for this module user provides the following:

- Names of the parameters of interest exactly as they are named in the output files of the ASTEC code.
- Full names or extension of the ASTEC output files, where the values of the output parameters can be found.
- Indexes of the samples, which are to be excluded in addition to the failed ones. Failed samples excluded automatically and their indexes don't need to be specified.

The FSTC tool goes through all simulation results sample by sample and gets the data for the whole timescale. The output of this module is the collection of the databases, where the values of the specified in the input file parameters are stored. One database corresponds to the one parameter of the interest.

4.1.5 Filter data

Due to different values of input parameters, each single ASTEC simulation of a SA scenario has its own unique progression and main events may occur at different times. But for further U&S analysis, it is reasonable to consider only the same parts of the SA progression. For that, the '*filter data*' module takes only the data between two specified events. It guarantees that in the U&S analysis part of the FSTC tool only the same stages of the process from each individual simulation are analyzed.

To prepare the data collected at the previous step to the U&S analysis, the user specifies in the input file the following:

- Names of the two main events or two time points.
- Names of the parameters of the interest. In case if all data from the previous step is require, this field can be left blank.

Between these specified events or time points the U&S analysis will be performed in the next module. The current module:

- Reads the data from the databases created at the previous step.
- Extract the data lying between specified main events/time points.

- Interpolate all extracted data to the one time scale.

As a results, all interpolated data are stored again in the databases, like it has been done at the previous step.

4.1.6 Uncertainty and sensitivity analysis

Finally, the U&S analysis itself can be performed – calculating the simple statistics for selected parameters of interest and different correlation coefficients values between these parameters and uncertain input parameters. User provides in the input:

- Names of the parameters of interest. In case if all data from the previous step is require, this field can be left blank.
- Whether the simple statistic are to be calculated.
- Names of the correlation coefficients are to be calculated.

This module uses as the input data the output of the ‘filter data’ and ‘sampling’. Module does the following:

- Extracts the values of sampled uncertain input parameters stored in the output database of the ‘sampling’ module.
- Extracts the values of the parameters of interest stored in the output databases of the ‘filter data’ module.
- Computes simple statistics (minimum, mean and maximum values, as well as 5th, 50th and 95th percentile values) if required.
- Computes correlation coefficients for all pairs of the output-input parameters for every time steps.

Currently available correlations coefficients are – Pearson, Spearman, distance [\[Martinez-Gomez et. al., 2014\]](#) and MIC [\[Kinney et. al., 2014\]](#). The flexibility of the FSTC tool allows adding or removing functionality from the code, therefore, in case some of these coefficients are no longer required for analysis or some additional coefficient are to be computed, it can be easily done. The current choice of the correlation coefficients is driven by the fact that SA physics is very complex and non-linear relationship between input and output parameters are highly expected. Nevertheless, only Pearson and Spearman correlations values are presented in current work.

The module for U&S analysis is providing information which allows the user to make conclusions about:

- How output results can vary due to input parameter variation.
- Which input parameters could be considered as important.

-
- How correlation between given output and uncertain input parameters change over time – namely, at what stages of the process which parameter has the most impact in output results variation.

Based on this information, the user can decide whether the list of chosen input parameters should be extended or shortened, whether it looks necessary to change the PDFs on input parameters and so on.

4.2 Fast Source Term Calculation Module for the Bayesian prediction algorithm

4.2.1 Prior part

The module corresponding to the ‘prior’ part of the prediction algorithm takes the databases generated by the ‘filter data’ package. User specifies in the input file the following:

- Total number of the ‘predictions’ and ‘observables’ parameters.
- Names of the databases, where values of the ‘predictions’ and ‘observables’ parameters are stored.
- Number of the time steps are to be skipped in the time scale extracted from the original data.

‘Prior’ module does the following:

- Extracts the data from the specified databases.
- Calculates the mean values for each parameter from ‘predictions’ and ‘observables’ groups at the every time step.
- Calculates Pearson correlation coefficient between every possible pair of parameters from ‘predictions’ and ‘observables’ groups at the every time step.
- Calculates Pearson correlation coefficient between values of the given parameter at the different time steps.

All calculated results are stored in the output files. In addition, plots with the Pearson correlation coefficient values for different pairs of parameters are created. As is was mentioned before, the high Pearson correlation values between given ‘prediction’ and ‘observable’ parameters are associated with better prediction results. Therefore, before running the ‘posterior’ part of the algorithm, user can check, whether the chosen combination of ‘predictions’ and ‘observables’ was appropriate.

4.2.2 Posterior part

The module with implemented ‘posterior’ part of the prediction algorithm takes as input the output of the ‘prior’ part. In addition to it, the files with ‘measurements’ for ‘observables’ parameters are provided. These ‘measurements’ can be a real experimental data or the simulation results. In the input file for the module user provides the following information:

- Separately the number of the parameters from ‘predictions’ and ‘observables’ groups.
- Names of ‘prior’ module output files containing the mean and Pearson correlation values for chosen ‘predictions’ and ‘observables’ parameters.
- Names of the files with the ‘measurements’.
- Number of future and past time steps, which will be taken into account at the each step of constructing the prediction.

The module extract all the input data from the provided files and construct prediction taking the measurements one by one. For example, it takes measurements only for the first time step and creates a prediction based only on it for the whole process. Then takes measurements only for the first two time steps and creates a prediction, and so on. The idea is that in a real application new measured data from detectors are constantly appearing, and the algorithm should re-calculate the prediction based on fresh data. Results of these step-by-step predictions are stored in the output files and also presented in the plots.

4.2.3 Automated prediction algorithm run on the sets of data

For most of the MOCABA tests in this work, no real measured data is available (except for one case, where MOCABA was tested on real data from the QUENCH-08 experiment), so instead, additional simulations are generated which will be treated as ‘experimental’ data. Of course, it is possible to make one simulation of the process, store it as an experimental data and run the ‘posterior’ module with it. But, usually we have sets of simulation performed with different values of uncertain input parameters. To deal with data organized in that way, a special module for automatic MOCABA run has been developed.

This module uses the input data for the ‘prior’ module and a pre-calculated so-called validation data set. The validation set usually has a smaller size than the ‘prior’ set and has been made with smaller uncertainty ranges of input parameters, so the ‘prior’ set guaranteed covers the validation one. The module runs the ‘prior’ part of the algorithm, and after that takes one by one the samples from validation set, treats it as results of an experiment and runs the ‘*posterior*’ module with that data.

The problem, which one can see in the results of the ‘posterior’ module output is how to measure the prediction quality – only two curves are presented on the output plots: the ‘prior’ data and the prediction result itself, but there is no curve representing the reality. Unfortunately, in a real application it will not be possible, because the whole point of the algorithm is to predict the values of the parameters which are not measured using the actual measurements for other parameters. But in the case of using results prepared in advance, the prediction quality could be quantified by comparing the output of the ‘posterior’ part with the simulation results stored in the validation set. To do so, the AREA metric [\[Jekel et. al., 2019\]](#) from the “*similaritymeasures*” Python package [\[Similaritymeasures, 2022\]](#) has been chosen. Basically, this metric is calculating the area between the curves – the closer the curves are, the smaller the AREA is, which is indicating a good prediction.

After execution of the module, the following output results are available for each sample from the validation set:

- All output files of the prior module.
- Plots showing how the ‘experimental’ data (values of the ‘predictions’ and ‘observables’ parameters) is lying inside the uncertainty range of the ‘prior’ data.
- For each step of the prediction algorithm, prior, experimental and prediction curves are presented in the one plot. In real cases, we do not know the values of the parameters of interest, but here ‘experimental’ results are simulated in advance.
- Plots with the values of the AREA metric.

Running this module allows to investigate the prediction algorithm deeply on the different sets of data and give some insights about its limitations and expected prediction quality.

5 Integral validation of the FSTC-MOCABA approach by the QUENCH-08 experiment

5.1 QUENCH-08 experiment and its ASTEC model

A series of QUENCH experiments were performed at KIT to investigate the hydrogen source term and the bundle degradation during water reflooding of an overheated dried out reactor core. The possible drawback of the reflooding measure is that it can cause further degradation with generation of a significant amount of hydrogen, which in turn can threaten the containment integrity. To be able to apply this SAM measure safely, a detailed understanding of the physical processes is needed and the influence of different parameters (for example, time of reflooding, materials in the core, water injection rate, temperature of the coolant) is investigated. A summary description of the influence of particular parameters has been analyzed in different QUENCH tests can be found, for example, in [\[Steinbrück et. al., 2010\]](#).

Here, the QUENCH-08 experiment performed in 2003 is analyzed, its detailed description can be found in [\[Stuckert et. al., 2005\]](#). Scheme of the test facility is shown in **Figure 5-1**. Test bundle is cooled by superheated steam and argon from the bottom end. The mixture of steam, argon and produced hydrogen leaves the bundle at the top of the test section. The superheated steam is changed to the saturated steam during the cooldown phase of the experiment. The test bundle itself consists of 21 fuel rod simulators approximately 2.5m long, in which one central rod is unheated and the other 20 are heated electrically by tungsten heating elements inserted in the center of each rod simulator. These heaters are surrounded by ZrO₂ pellets, which are in turn surrounded by Zry cladding. In addition, 4 corner rods are installed in the test bundle, one of them is removable and is used for evaluation of the oxide layer thickness before the cool-down phase. Fuel rod simulators and corner rods together are surrounded by Zry shroud, then by a layer of ZrO₂ fiber insulation and after that by a stainless-steel cooling jacket. A cross section of the test bundle is shown at **Figure 5-2**. All QUENCH tests undergo similar phases: heat-up, pre-oxidation, transient and cool-down. The QUENCH-08 experiment starts with heating up from room temperature up to ~873 K. Then, a second phase of heating up continues up to ~1700 K. In the pre-oxidation phase, electrical power is regulated to balance input from electrical heat-up and oxidation and keep temperature constant around ~1700-1740 K. During the last heat-up phase – transient – the temperature is rising from ~1700K up to ~2200K, and after that reflooding phase is initiated. Up to the cooldown phase, the test bundle coolant is argon and superheated steam (both with flow rate 3 g/s), and in the cool-down phase, saturated steam is injected with a flow rate of 15 g/s. These phases and total electrical power during the experiment are shown in **Figure 5-3**.

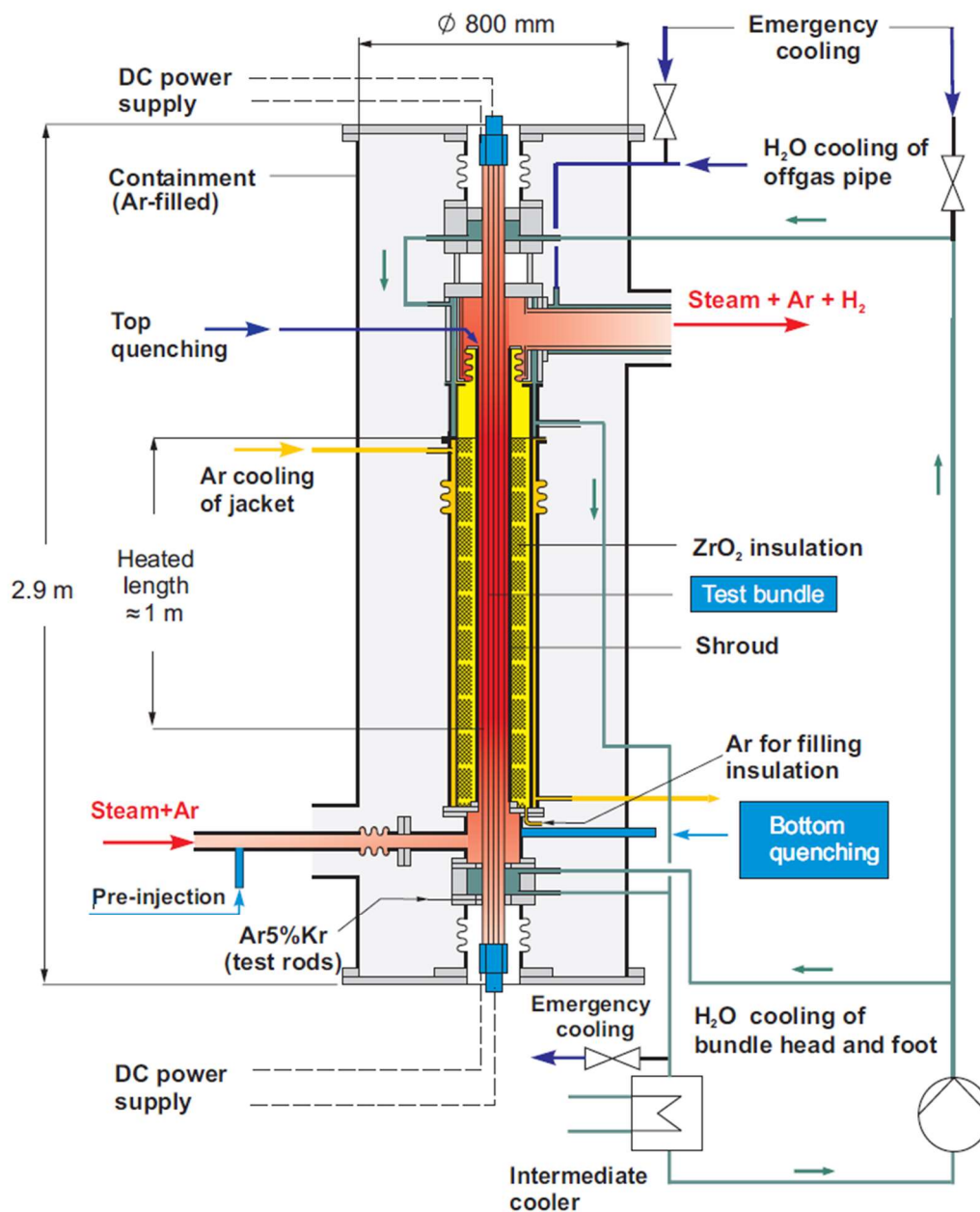


Figure 5-1 – Schematic set-up of the QUENCH test facility (from [Stuckert et. al., 2005]).

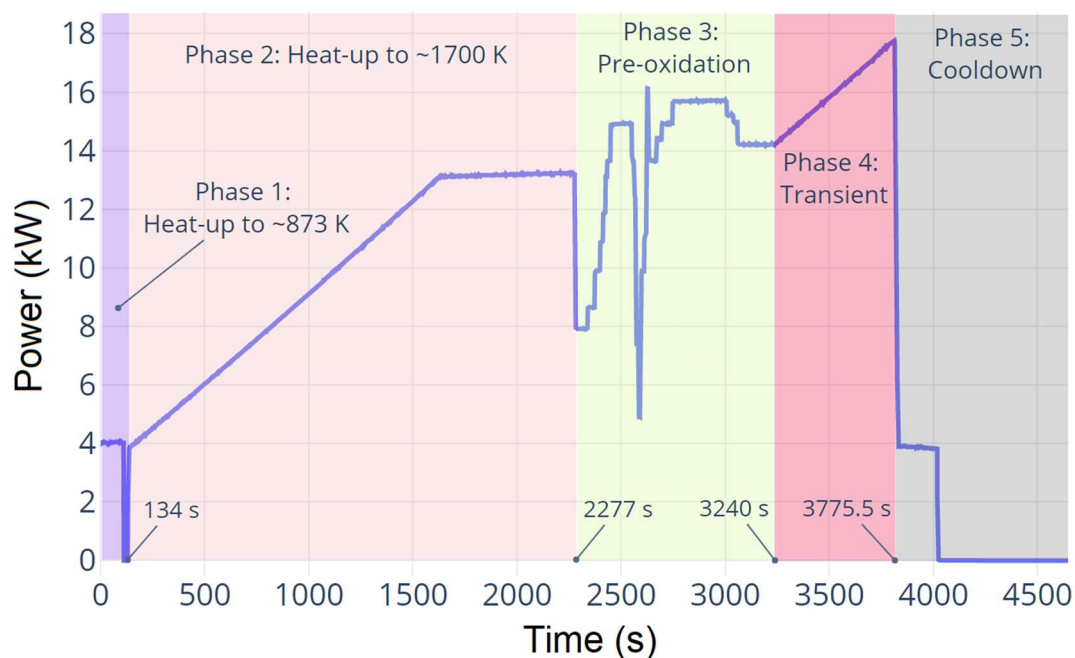


Figure 5-3 – Temporal evolution of the electric power provision to the fuel pin simulators in the QUENCH-08 experiment and assignment of the corresponding experimental phases.

Temperatures have been measured with thermocouples mounted at different axial elevations and angular orientations of the test bundle, where temperatures of the fuel rod simulators, shroud and cooling jacket are recorded. Axial locations for the temperature measurements are shown in **Figure 5-4**. In the ASTEC model it is also possible to extract temperature values of different structures at various elevations, but not at different orientations. The amount of hydrogen produced during the experiment has been measured by a mass spectrometer and a special hydrogen detection system. In the ASTEC simulations, the mass of the hydrogen is computed as output from model assumptions. All detailed descriptions about the measurements during the experiment can be found in the report [\[Stuckert et. al., 2005\]](#).

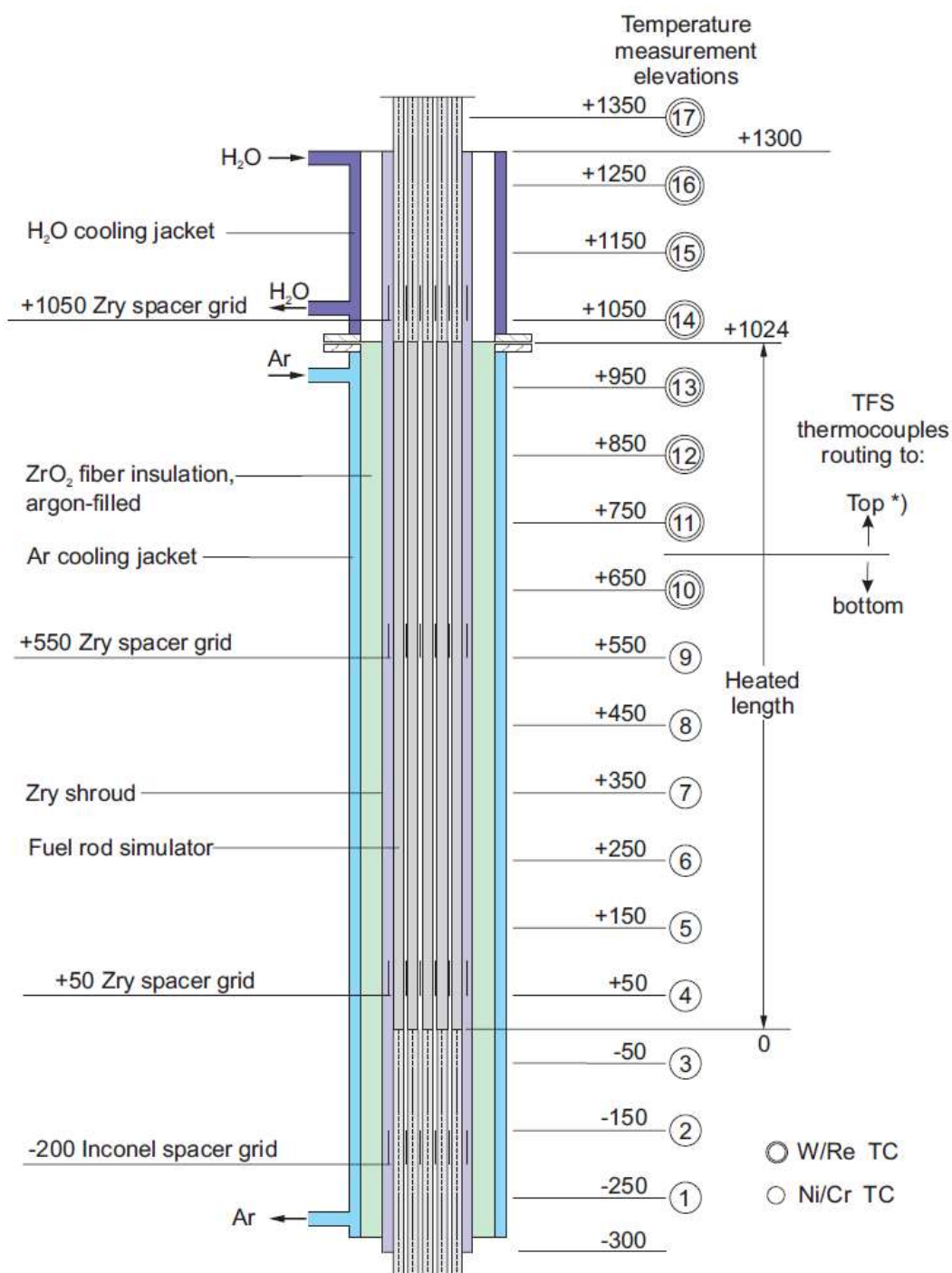


Figure 5-4 – Axial location of the thermocouples in the QUENCH-08 test section (from [Stuckert et. al., 2005]).

The QUENCH-08 simulations have been made with ASTEC code [Chailan et. al., 2019] (version 2.2_b). The ASTEC input used here is based on previous work – see [Gabielli et. al., 2018] and [Gómez-García-Toraño, 2017].

Radial and axial nodalization of the ASTEC model are shown at the **Figure 5-5** on the left and right parts respectively. In the ASTEC code, the QUENCH-08 test bundle described above is represented as a group of concentric structures. To do so the central unheated rod and nearest 8 heated rod simulators are combined to one channel 'Channel_1'. The other 12 heated rods and 4

corner rods in another channel 'Channel_2'. The shroud, following insulation layer and cooling jacket are already cylindrical and simulated without any changes. In the results of simulations only the temperature of the whole ASTEC model structure at the given elevation is available, while in the real experiment the temperature can be measured at the each individual rod simulator. Nevertheless, the ASTEC simulation reproduces the experimental results quite well, which has been shown in [\[Gómez-García-Toraño et. al., 2017\]](#).

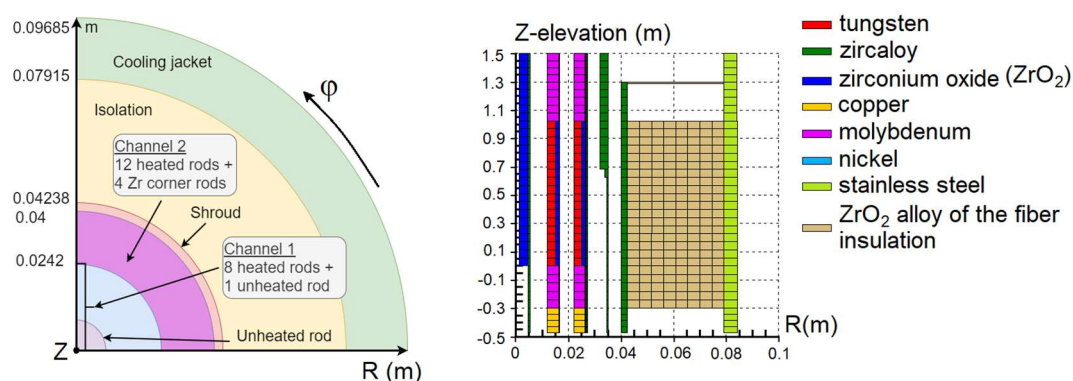


Figure 5-5 – Schematic cross-sectional (left) and axial (right) representation of the QUENCH-08 experiment in the ASTEC code. Colors denote materials. Based on [\[Stakhanova, 2022a\]](#).

Two ASTEC modules have been used to model the QUENCH-08 experiment – ICARE and CESAR – to simulate in-vessel core degradation and thermal-hydraulics, respectively. The following physical processes of QUENCH experiment were simulated: convective, conductive and radial radiative heat transfer; oxidation of different materials and structures; structures integrity; transport of the melted materials. The parameters of some of used ASTEC models as well as the boundary conditions (like steam and argon flow rates) are considered as uncertain input parameters and used in U&S analysis.

5.2 Uncertain input parameters for QUENCH-08 simulations

The main figure-of-merit of the QUENCH-08 simulations is the hydrogen mass released considered as source term. To investigate its possible variation, 24 parameters have been chosen for uncertainty propagation. These parameters cover geometry, initial and boundary conditions and the following ASTEC models: melted corium relocation (MOVEMAG), melt oxidation by steam (UZOXMAG), radiation heat exchange (RADB), convective heat transfer (CONV) and integrity criteria (INTE). Names of the models are provided here for the reader to find their description easily in the ASTEC code documentation. The model choice is based on the more relevant to current experiment physical processes. The choice of the PDFs and PDF parameters has been based on available information from the literature, such results of U&S analysis for the CORA-W2 experiment [\[Kozbar et. al., 1997\]](#), ASTEC documentation [\[Belon et. al., 2017a\]](#) and

[\[Coindreau, O., 2017\]](#) and engineering judgement. Five of the selected parameters have normal distribution. This distribution is used usually for the parameters measured in the experiment, for example, steam mass flow rate, which error is associated with the error of the measurement device. The other nineteen parameters have uniform distribution, which is usually used in case of the lack of information (lack of experimental data, for example).

The full list of uncertain input parameters with all relevant information is presented in **Table 5-1**. Please note, that some of the uncertain input parameters (like, steam and argon mass flow rates) are the coefficients varying around 1.0 value and then in ASTEC input are multiplied by the actual best estimated value of the model parameter. That has been done for the purposes of debugging.

| Parameter | PDF | PDF parameters | Description | Source |
|---|---------|--------------------------------|--|--------|
| <i>Parameters of the melted corium relocation model</i> | | | | |
| CRES | Uniform | [0.8 – 1.20] | Coefficient to modify the residual saturation | 1. |
| KEXP | Uniform | [2. – 4.] | Exponent for the saturation in the relative permeability | |
| KSMX | Uniform | [0.9 – 1.10] | Maximum value of the ratio permeability/viscosity (sampled value is multiplied by 0.1 in the ASTEC input file) | |
| <i>Parameters of the model of melt oxidation by steam</i> | | | | |
| GRDR | Uniform | [0.9 – 1.10] | Corrective factor for the gradient in the crust interfacing with the liquid (sampled value is multiplied by 6.0 in ASTEC input file) | 1. |
| GREX | Uniform | [0.9 – 1.10] | Corrective factor for the gradient in the crust interfacing with the steam | |
| HSLX | Uniform | [0.9 – 1.10] | Maximum value for the mass transfer coefficient between solid and liquid (sampled value is multiplied by 0.1 in ASTEC input file) | |
| MULT | Uniform | [0.9 – 1.10] | Multiplying factor applied on the exchange area | |
| OXLQ | Uniform | [0.9 – 1.10] | Factor for increasing/decreasing the external oxygen flux to the pure liquid when all the crust has disappeared | |
| RDZR | Uniform | [0.9 – 1.10] | Relative diffusivity of Zr in the melt. (sampled value is multiplied by 0.01 in ASTEC input file) | |
| <i>Parameters of integrity criteria</i> | | | | |
| ZrO2T | Uniform | [2248. – 2500.] K | Failure temperature of ZrO ₂ layer [K] | 2. |
| ZrO2Thi | Uniform | [200 - 400] 10 ⁻⁶ m | Thickness of ZrO ₂ layer [m] | |
| <i>Geometry parameters</i> | | | | |
| d_int | Uniform | [0.99 – 1.01] | Parameter used to calculate internal diameters in the ASTEC nodalization of the QUENCH-08 experiment test bundle | 2. |
| s_thic | Uniform | [0.99 – 1.30] | Parameter related to the shroud thickness used to calculate geometric parameters in the ASTEC nodalization of the QUENCH-08 experiment test bundle | |
| j_thic | Uniform | [0.99 – 1.01] | Parameter related to the cooling jacket thickness used to calculate geometrical parameters in the ASTEC nodalization of the QUENCH-08 experiment test bundle | |
| <i>Initial and boundary condition parameters</i> | | | | |
| stFlow | Normal | $\mu = 1., \sigma = 0.05$ | Coefficient used to calculate the steam flow value at different time points | 2. |
| arFlow | Normal | $\mu = 1., \sigma = 0.05$ | Coefficient used to calculate the argon flow value at different time points | |
| cTime | Uniform | [0. – 10.] s | Possible delay of steam injection [s] | |
| fpres | Normal | $\mu = 1., \sigma = 0.02$ | Output pressure of the test bundle [Pa] (sampled value is multiplied by 2.0·10 ⁵ in input ASTEC file) | |
| fpp | Uniform | [0.99 – 1.01] | Argon pressure in the gap | |
| <i>Radiation heat exchange parameters</i> | | | | |
| frani | Uniform | [0. – 1.] | Rod reflection anisotropic factor | 3. |
| fsani | Uniform | [0. – 1.] | Shroud reflection anisotropic factor | |
| <i>Convective heat transfer model parameters</i> | | | | |
| fhd | Normal | $\mu = 100., \sigma = 0.05$ | Average additional heat transfer coefficient due to droplet projection | 3. |
| fzd | Normal | $\mu = 0.8, \sigma = 0.05$ | Height above the quench front concerned by droplet projection | |
| falpha | Uniform | [0.99 – 0.999] | Threshold void fraction to allow exchange with liquid droplets | |

1. [Kozbar et al., 1997], [Gabrielli et al., 2018], [Belon et al., 2017], [Coindreau, 2017]; 2. [Stuckert et al., 2005], [Gabrielli et al., 2018]; 3. [Gabrielli et al., 2018], [Belon et al., 2017], [Coindreau, 2017]

Table 5-1 – Uncertain input parameters of QUENCH-08 ASTEC model

5.3 Results of U&S analysis

An extensive U&S analysis of the QUENCH-08 ASTEC results has been performed [[Stakhanova et. al., 2022a](#)], investigating:

- Which uncertain input parameters most strongly influence the hydrogen source term values.
- How changing the number of samples can affect the source term, correlation coefficients values and the consistency of the simulation results.
- Whether any effect could be observed due to randomness effect from the sampling.

After the uncertain input parameters have been selected, the next step in U&S analysis is to choose the number of samples. According to the literature, the required number of samples is usually calculated by the Wilks [[Wilks, 1941](#)] formula using the desired level of confidence and percentile value. Despite that Wilks formula is practically a standard for U&S analysis in the nuclear safety field, a discussion about the limits of that approach and possible improvements exist, see for example the following publications [[Frepoli et. al., 2011](#)], [[Honga et. al., 2011](#)], [[Lee et. al., 2014](#)], [[Zhang et. al., 2016](#)]. One of the questions is how well the high-dimensional input space is covered using a particular number of samples and the given sampling algorithm. This issue, according to the literature, is usually addressed in different fields outside of nuclear safety – for example, in machine learning or environmental studies, because problems in these fields are typically very high-dimensional. Some examples are given in [[Pedergnana et. al., 2016](#)], [[Sheikholeslami et. al., 2017](#)]. A deeper investigation of that topic and its application to our high-dimensional problems seems quite interesting, but due to the time limits and that the main goal of the thesis is different, only very preliminary investigation has been made using a brute-force approach. For the time-consuming calculations like nuclear accident simulations with severe accident codes the number of samples is always a balance between desired level of the confidence and available time and computer resources. Taking all these into account for the QUENCH-08 simulations the preliminary investigation has been made to check, whether number of samples influence on the U&S analysis results. The single ASTEC simulation of the QUENCH-08 experiment takes ~1 hour, and it is acceptable using available computer resources (32 core machine) to run up to 800 simulations.

In the following U&S analysis two widely used correlation coefficients – Pearson and Spearman – are calculated. The Pearson correlation is widely used in the nuclear safety, but it reflects only the strength of linear relationship between the variables. The Spearman correlation coefficient shows whether the relationship between the two variables exists and can be described with a monotonic function not necessarily linear. This correlation is more appropriate to use in U&S analysis of the severe accident, which is shown later in the chapter, due to the complex non-

linear physical processes involved. First of all, the Pearson and Spearman correlation coefficient values for all considered uncertain input parameters at the end of the transient are shown in the **Figure 5-6**. Here the results for the maximum considered number of samples, which is 800, are presented. Note that the short names of the uncertain input parameters are used on the figures in this chapter. The full description of the parameters is provided above. The ranking of a relationship strength between two variables can vary from one field or one work to another. In this thesis we consider the correlation values in range:

- [0.0; 0.2) / (-0.2; 0.0] – very weak positive/negative;
- [0.2; 0.4) / (-0.4; -0.2] – weak positive/negative;
- [0.4; 0.6) / (-0.6; -0.4] – moderate positive/negative;
- [0.6; 0.8) / (-0.8; -0.6] – strong positive/negative;
- [0.8; 1.0] / [-1.0; -0.8] – very strong positive/negative.

From that ranking, at the last time step of the process only the steam mass flow rate is affecting the hydrogen release.

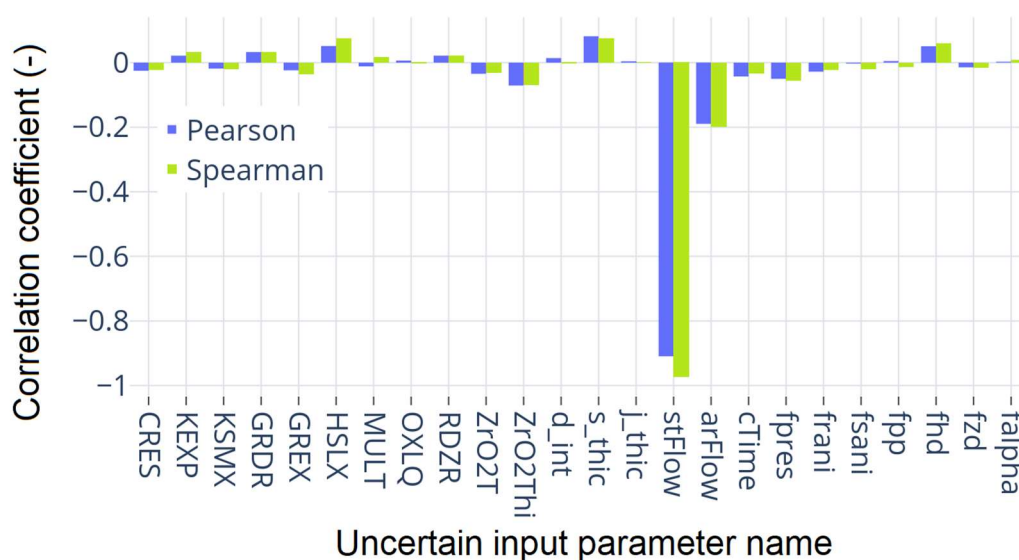


Figure 5-6 – Pearson and Spearman correlation coefficients value between hydrogen mass and uncertain input parameters at the last time step of the simulations. Results of 800 simulations are used.

The influence on the figure-of-merit from different uncertain input parameters can change during the transient, therefore it is important to look how correlation coefficient values evolve in time. For the most uncertain input parameters the correlation values lie in the range [-0.2; 0.2], which is very weak correlation according to our ranking, and not considered in the analysis. On the **Figure 5-7** is shown how the Pearson and Spearman correlation values evolve in time for the rest four uncertain input parameters governing: steam (*stFlow*) and argon (*arFlow*) mass flow rates; diameter of the ASTEC model structures (*d_int*); radiative heat exchange (*frani*). The difference in the correlation coefficients (both Pearson and Spearman) between *arFlow* and

stFlow parameters can be explained by the difference in the specific heat capacity – for steam it is around 4 times higher, than for argon. Therefore, uncertainty of steam flow rate mainly affects the variation in hydrogen production.

The presented evolution in time of the Spearman and Pearson correlation coefficient are quite different for the steam and argon mass flow rate parameters. The Pearson correlation coefficients are starting to decrease (in absolute value) at the beginning of the pre-oxidation phase, reach their minimum at the end of this phase and after that increase again during the transient. To investigate that behavior, let us look closer at the curves with hydrogen production for all 800 samples shown in **Figure 5-8**. One can see that at the beginning of the pre-oxidation phase, a group of samples with very fast increasing amount of hydrogen is diverging from the rest of the samples. The most important uncertain parameter according to the results presented in **Figure 5-7** is the steam mass flow rate. Therefore, let us look closer at the amount of hydrogen as a function of the steam mass flow rate parameter at four different time points: 1500s (heat-up phase), 2400s (close to the beginning of the pre-oxidation phase), 3000s (close to the end of pre-oxidation phase), 3600s (in the middle of the transient phase). One can see from **Figure 5-7 (B)** and **Figure 5-8** that at time 1500 s the Pearson and Spearman correlation values are nearly identical and all 800 hydrogen curves also lie together. At the 3000 s the difference between Pearson and Spearman correlation values reaches its maximum, and difference between minimum and maximum values of the mass of hydrogen reaches ~200 g. The scatter plots for four selected time points presented in **Figure 5-9** show the relationship between mass of produced hydrogen and steam mass flow rate parameter. One can see, that at time 1500s the relationship between hydrogen mass and *stFlow* parameter values is linear and that explains the high (in absolute value) values of the Pearson correlation coefficient and the fact that Pearson and Spearman correlation values are identical. At the beginning of the pre-oxidation phase some samples have much higher values of produced hydrogen mass, therefore relationship between hydrogen mass and *stFlow* parameter is not linear anymore and cannot be explained using Pearson correlation coefficient. Taking this into account further only the Spearman correlation values are presented.

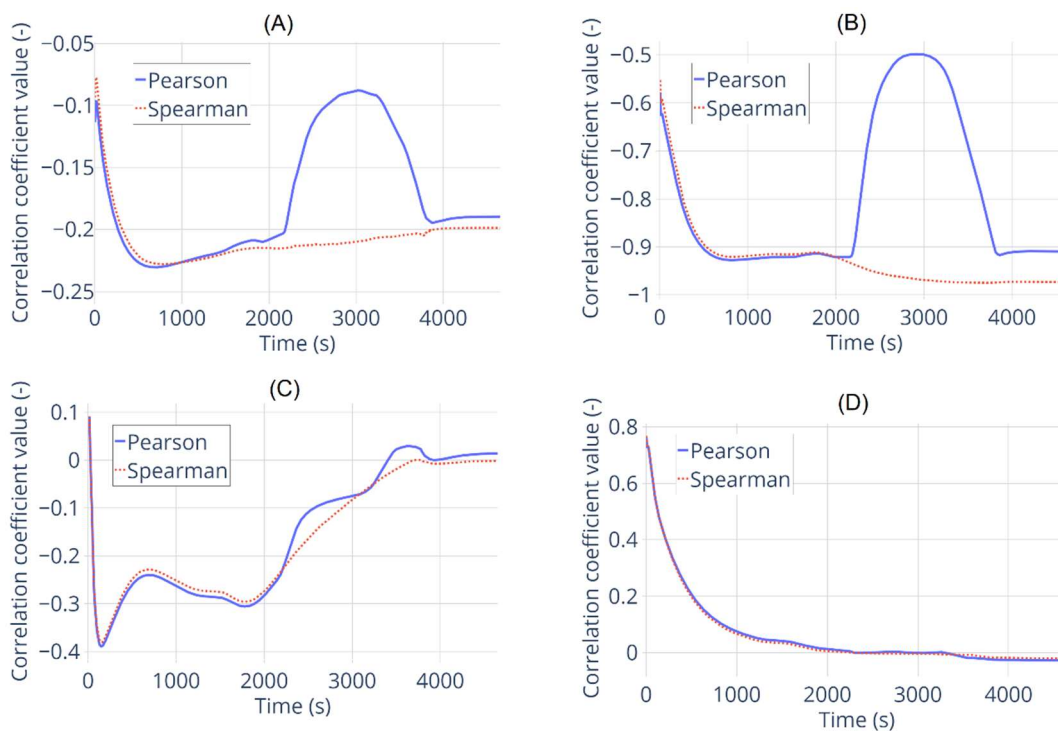


Figure 5-7 – Pearson and Spearman correlation coefficients evolution in time between the produced hydrogen mass and uncertain input parameters governing the (A): argon mass flow rate; (B): steam mass flow rate; (C): internal diameter of the test bundle ASTEC model structures; (D): radiative heat exchange. Results of 800 QUENCH-08 simulations.

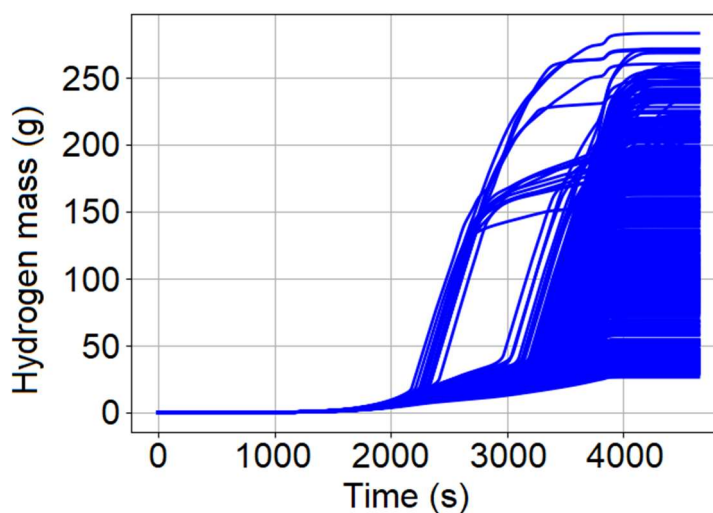


Figure 5-8 – Simulated hydrogen mass evolution in time. 800 ASTEC simulations of the QUENCH-08 experiment.

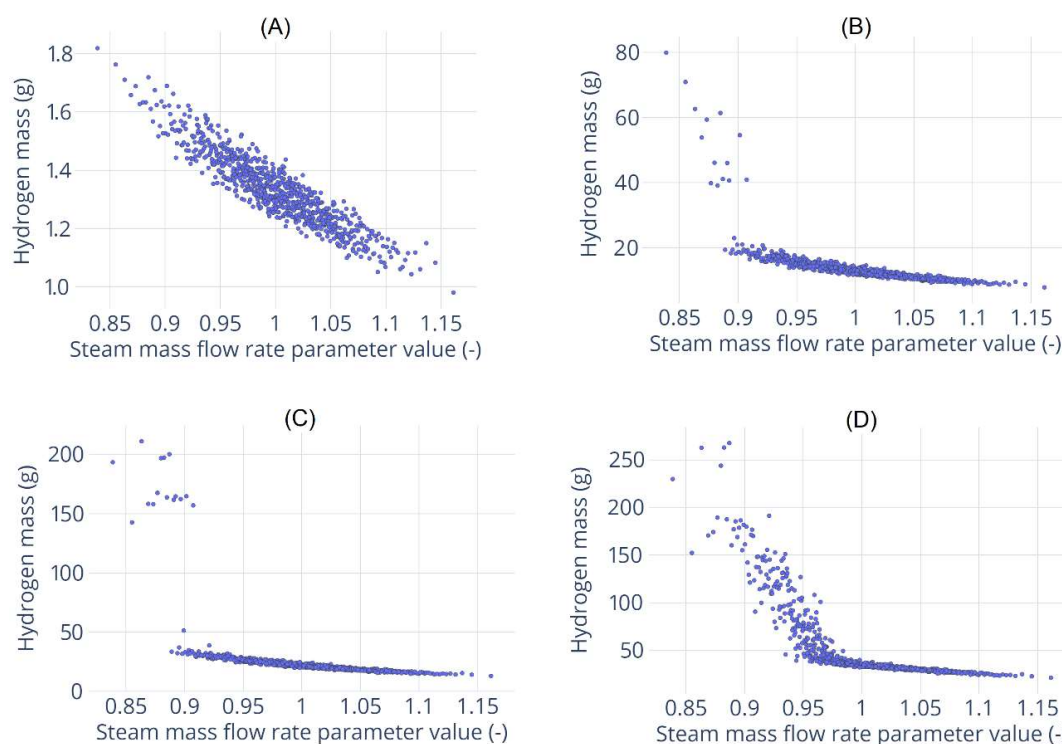


Figure 5-9 – Relationship between the hydrogen mass and uncertain parameter governing steam mass flow rate for four different time points. (A): 1500s (second half of the heat-up phase); (B): 2400s (close to the beginning of the pre-oxidation phase); (C): 3000s (close to the end of pre-oxidation phase); (D) 3600s (middle of the transient phase). Results of 800 simulation.

Results presented above were calculated using the 800 simulations of the QUENCH-08 experiment – the maximum number considered in this work. Below presented how the number of samples influence on the U&S analysis results. The goal is to make preliminary analysis to answer the question, what number of samples is sufficient for this U&S analysis, whether number of samples influence on the results and on conclusions made based on these simulations. In this analysis the number of samples is varied from 50 up to 800. On **Figure 5-10** is shown how changing the number of samples influence on the 95th percentile values of the temporal evolution of the hydrogen production. The maximum difference between the curves is observed during the transient phase in the time frame ~3200 – 3500 s, where the hydrogen production is going with different speed, the difference here can reach up to ~30%. In other phases of the process, the difference in values is much smaller, for example, in time frame ~4000 – 4500 s it is ~3-7%, on other parts of the experiment simulations this difference is even less. The same results are observed for 5th and 50th percentile values. Therefore, changing number of samples practically not influence on the hydrogen simple statistics and there is no reason to perform too many simulations, in case the goal is only to look at the hydrogen production values. The different effect can be observed, if one looks at the Spearman correlation value evolution in time calculated for sets of simulations with different number of samples. These results for four uncertain input parameters are presented in **Figure 5-11**. The most important uncertain input parameter governing

the steam mass flow rate is independent from the number of samples as shown in **Figure 5-11 (B)**. The parameter governing the argon mass flow rate (**Figure 5-11 (A)**) according to our classification of the Spearman correlation values can be considered as negligible. The values of Spearman correlation for this parameter calculated for 100 samples and 200 samples anyhow differs along the whole time scale ~ 2 times – see for example the values ~ -0.15 and ~ -0.3 at time equals 1000 s, which can potentially affect the conclusion about the degree of correlation between the selected variables. For the parameter governing the internal diameter of the ASTEC model structures representing the test bundle (**Figure 5-11 (C)**) the difference in Spearman correlation values observed in time window ~ 500 s – 2000 s can change the status of the correlation from negligible to moderate according to our classification. The level of Spearman correlation value for the parameter governing the radiative heat exchange changes from high to moderate at the very beginning of the transient during the first ~ 500 s of the heat-up phase. The correlation value decreases with different speed depending on the number of samples used to perform simulations.

To investigate it a bit deeper, an additional consistency test was made for the following number of samples – 50, 200, 400 and 600 has been executed. The results here are shown only for 50 samples and 600 samples tests. The idea is to run the whole U&S analysis multiple times keeping the list of uncertain input parameters and their PDFs the same. It can give some preliminary idea of how the sampling algorithm is covering the high-dimensional input space for a given number of samples, how it impacts on the output results in order to draw conclusions on the effect of uncertain input parameters. Even though the QUENCH-08 simulation takes only one hour, performing hundreds of simulations, especially multiple times, is time consuming. Therefore, for each fixed number of samples, the simulations are executed only 5 times. It can be not enough to make final conclusions, also this analysis is very straightforward; therefore, more advanced techniques have to be applied for that task. 95th percentile values for produced hydrogen mass evolution in time are presented in **Figure 5-12**. The difference between the five results of simulations each performed with 50 samples (see in **Figure 5-12 (A)**) is practically the same as shown in **Figure 5-10**. It can reach $\sim 30\%$ during the transient phase in time frame $\sim 3200 - 3500$ s, and at the end of the process is $\sim 5\%$. For five simulations sets with the 600 samples each the maximum difference is around $\sim 20\%$ at the same time frame $\sim 3200 - 3500$ s as shown in **Figure 5-12 (B)**. From all presented results at least for simple statistics values like 95th percentile the increasing number of samples does not leads to any significant improvements. The effect from re-sampling and running simulations again is the same as from increasing the number of samples. Therefore, using the Wilks formula can be perfectly enough for the hydrogen mass temporal evolution simulations with the giving level of confidence.

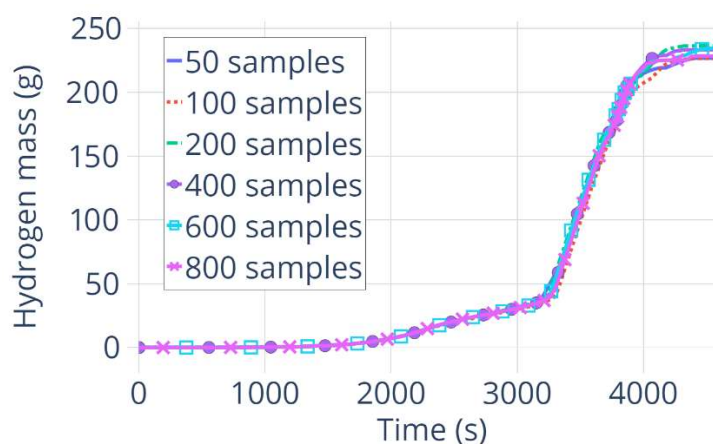


Figure 5-10 – Simulated impact of samples number of 95th percentile of the temporal evolution of the hydrogen mass in the QUENCH-08 experiment.

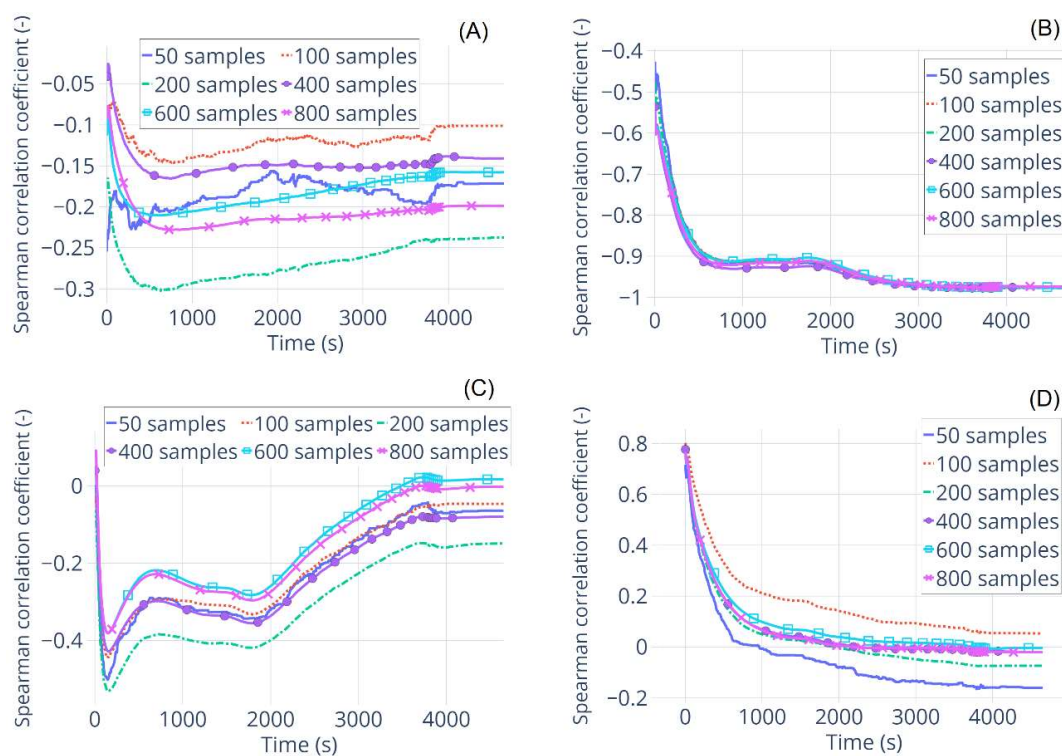


Figure 5-11 – Evolution of the Spearman correlation coefficient value in time calculated for four uncertain input parameters for sets of simulations with different number of samples. (A): argon mass flow rate; (B): steam mass flow rate; (C): internal diameter of the test bundle ASTEC model structures; (D): radiative heat exchange.

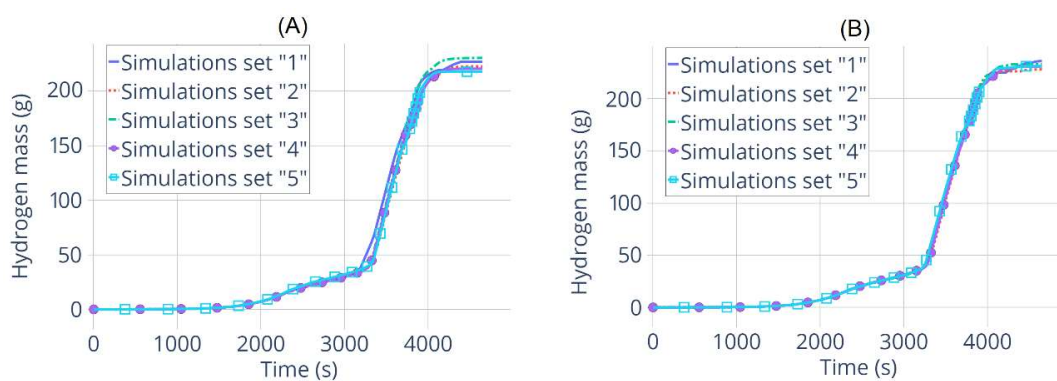


Figure 5-12 – Consistency investigation. 95th percentile values for the simulated hydrogen mass evolution in time in the QUENCH-08 experiment. Results of the five sets of simulations performed with (A). 50 samples for each set; (B): 600 samples for each set.

How re-sampling and re-running the simulations affects the Spearman correlation values for three selected uncertain input parameters is shown in **Figure 5-13**. For the most influential uncertain input parameter governing the steam mass flow rate results look quite consistent for 50 and 600 samples simulation sets as shown in **Figure 5-13 (A) and (B)** respectively. It means that the same conclusions are made about the impact of the given parameter at the given stage of the transient regardless the number of samples of re-running the simulations. Only at the very beginning of the time scale for 50 samples simulations the values of Spearman correlation for steam mass flow rate parameter differs significantly from ~ -0.7 up to ~ -0.45 , but after that results from different simulation sets converge very fast. The different picture is observed for the uncertain parameter related to inner diameter of the ASTEC QUENCH-08 model structures (see correlation values in **Figure 5-13 (C) and (D)**) and for the parameter governing the radiative heat exchange (**Figure 5-13 (E) and (F)**). Spread of the Spearman correlation values for the 600 samples simulations set is lower, than for 50 samples set. For example, for radiative heat exchange parameter in case of the 50 samples simulations set the wrong conclusion about this parameter influence during the whole transient can be made – see the red curve for “Simulation set 2” in **Figure 5-13 (E)**. For the parameter related to ASTEC model geometry the conclusion about the negligible correlation can be made from the results of “Simulation set 4” in **Figure 5-13 (C)**, while for “Simulations set 1” the correlation value is moderate from ~ 100 s up to ~ 2000 s. Therefore, the bigger amount of samples (at least 600) can be recommended for the QUENCH-08 experiment U&S analysis, as well as, deeper investigation of the discussed issues.

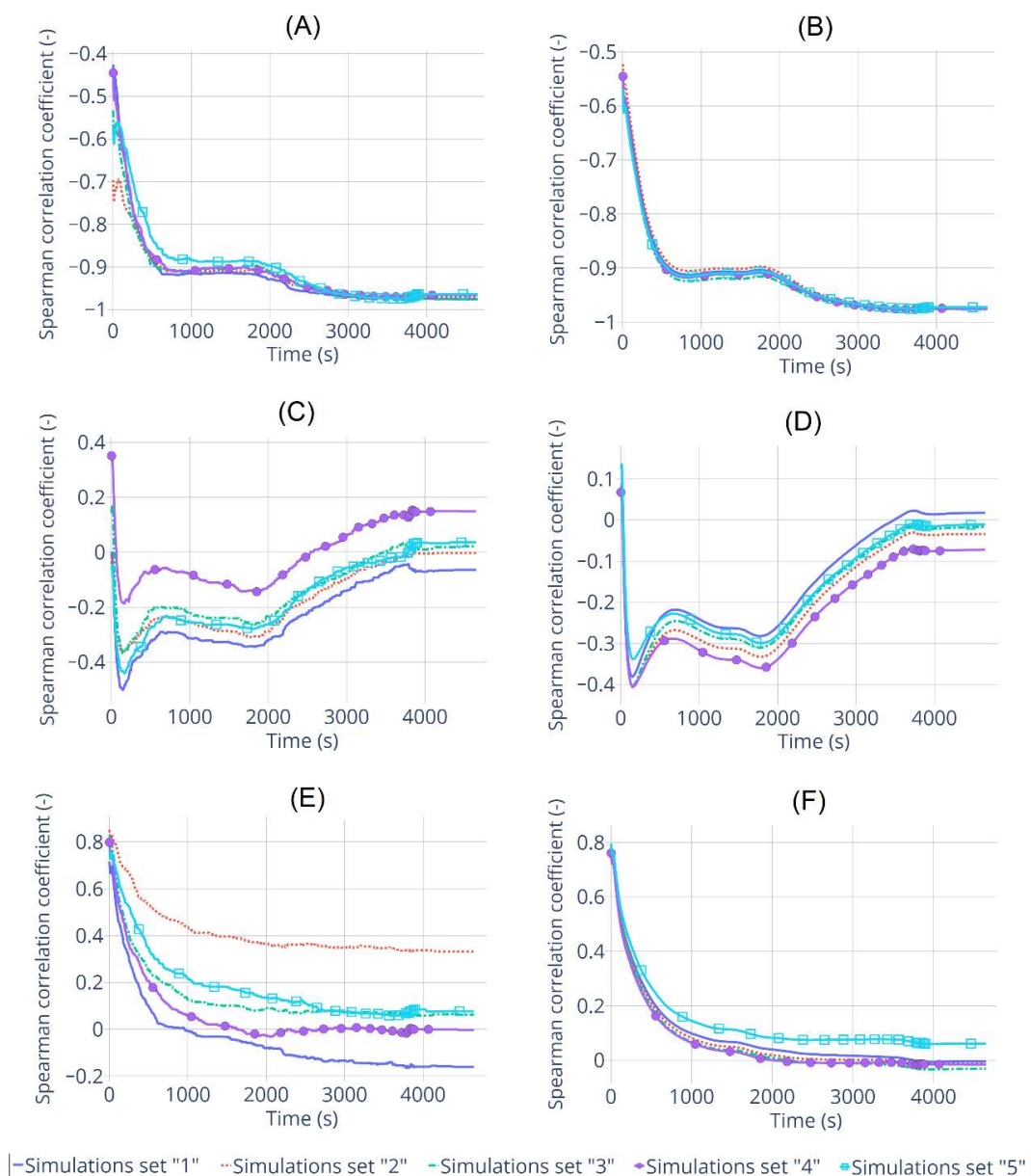


Figure 5-13 – Spearman correlation value evolution in time for three uncertain input parameters calculated for five sets of simulations 50 or 600 samples each. (A): steam mass flow rate, 50 samples; (B): steam mass flow rate, 600 samples; (C): internal diameter of the test bundle ASTEC model structures, 50 samples; (D): internal diameter of the test bundle ASTEC model structures, 600 samples; (E): radiative heat exchange, 50 samples; (F): radiative heat exchange, 600 samples.

5.4 Results of applying MOCABA algorithm for hydrogen source term prediction

In this section, results of applying the MOCABA algorithm implemented in the FSTC tool to QUENCH-08 simulations will be presented. The goal is to predict the released amount of hydrogen using temperature values of different ASTEC model structures at the different

elevations. First, results of such an application performed only with simulated data are presented. After that an attempt to apply MOCABA algorithm using real experimental data is shown.

5.4.1 Predictions using simulation data as measurements

In this example of the prediction algorithm application, the goal is to predict the amount of hydrogen produced during the experiment ($H2mass$ parameter) using three temperatures (see the elevation, where thermocouples are located in the experiment in **Figure 5-4**): of the inner circle of fuel rods imitators (see ‘Channel_1’ structure of the ASTEC model in **Figure 5-5**) at the 950 mm elevation – $T2_950$ parameter; of the outer circle of fuel rods imitators (see ‘Channel_2’ structure at **Figure 5-5**) at the 850 mm elevation – $T3_850$ parameter; shroud temperature at the 950 mm elevation – $Tshroud_950$ parameter. Therefore, the hydrogen mass produced during the experiment is the ‘prediction’ parameter, and the three temperatures act as ‘observables’ parameters. To apply the MOCABA algorithm on results of the QUENCH-08 experiment simulations, two sets are prepared:

- The so-called “prior set”: the results of 400 samples simulations used as an input data for the ‘prior’ part of the MOCABA algorithm.
- The so-called “validation set”: the results of 50 samples simulations. From this set each sample is treated as individual ‘experiment’ realization. It allows to obtain more results of MOCABA prediction to investigate better its limitations and constraints.

For both sets, the list of uncertain input parameters as well as their PDFs and PDF parameters stay the same corresponding to those in **Table 5-1**.

When the ‘predictions’ and ‘observables’ parameters are selected, the ‘prior’ part of the prediction algorithm runs using the ‘prior’ set as input data. After that, each sample from the validation set is treated as an individual ‘experiment’ realization, and the ‘posterior’ part of the algorithm runs with this data. The following factors can influence on the prediction results as it has been discussed before in investigation of prediction algorithm constraints and limitations:

- The Pearson correlation values between the ‘predictions’ and ‘observables’ parameters. Higher correlation values leads to a better prediction results.
- Similarity between the ‘experimental’ and ‘prior’ curves shapes. More similarity between the ‘experimental’ and ‘prior’ curves leads to a better prediction.
- ‘Experimental’ data must lie inside the range of the ‘prior’ data.

Unfortunately, for these factors there is no clear quantification currently exist, to transform these statements to a quantified metrics additional investigations and calculations can be performed. One attempt of such investigation on a simple ‘toy’ model is presented in [Appendix D](#). The quality of prediction can be evaluated using the AREA metric, which practically counts

the space between two given curves – the less this space, the closer and more similar these curves are. AREA metric was taken from the “*similaritymeasures*” Python package [[Similaritymeasures, 2021](#)].

The Pearson correlation coefficients values for three pairs of selected ‘predictions’ and ‘observables’ parameters are shown in **Figure 5-14**. The correlations are close to 1 for most of the process length from ~ 500 s up to ~ 4000 s.

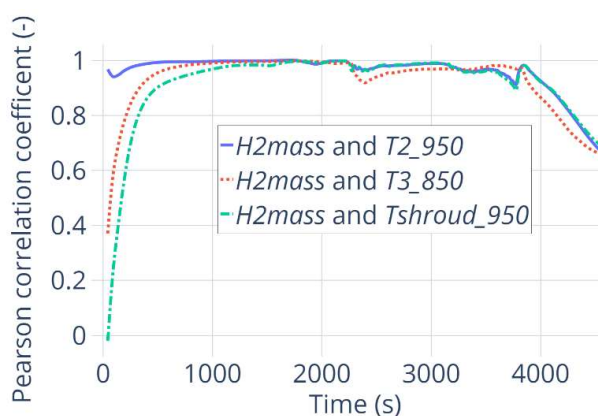


Figure 5-14 – Pearson correlation coefficients time evolution between selected ‘predictions’ and ‘observables’ parameters from the QUENCH-08 experiment simulations results. Calculated for the 400 samples ‘prior’ set of data. Selected parameters are: hydrogen mass – ‘H2mass’; temperature of the ‘Channel_1’ structure at 950 mm elevation – ‘T2_950’; temperature of the ‘Channel_2’ structure at 850 mm elevation – ‘T3_850’; temperature of the ‘shroud’ structure at 950 mm elevation – ‘Tshroud_950’.

For the demonstration purposes, results for 2 out of 50 samples are shown. On the **Figure 5-15** is presented, how the hydrogen mass values for these selected samples presents, how hydrogen mass values for chosen samples (№1 and 3) lie inside the range of the ‘prior’ data. On **Figure 5-16** the same is shown for the one parameter from the ‘observables’ group – ‘T2_950’. For other two ‘observables’ parameters the picture is very similar to the one presented in **Figure 5-16** and not shown here. ‘Predictions’ and ‘observables’ parameters values for samples №1 and 3 lie inside the range of the ‘prior’ data – between the minimum and maximum values. The shapes of the hydrogen curves are different from the ‘prior’ one for the both selected samples. The hydrogen production for sample №1 goes faster, than in average represented by the ‘prior curve’ during the time period ~ 3500 s – 4000 s, and the final hydrogen mass value for this sample is higher, than average. Sample №3 lie close to the minimum hydrogen mass values and these curves are very similar along the whole time scale. The shapes of the temperature curves for samples №1 and 3 are also different from the shape of the ‘prior’ curve. Temperature for sample №1 first increases faster, than average during the time period ~ 3500 s – 3800 s, and after that decreases faster than average from the time point ~ 3800 s till the end of the transient. The temperature values for sample №3 are lying very close to the minimum curve during the whole transient. Note that, the range of the ‘prior’ data is very narrow – before time ~ 2200 s for the hydrogen mass parameter, and before time ~ 1500 – 1600 s for the temperature parameters.

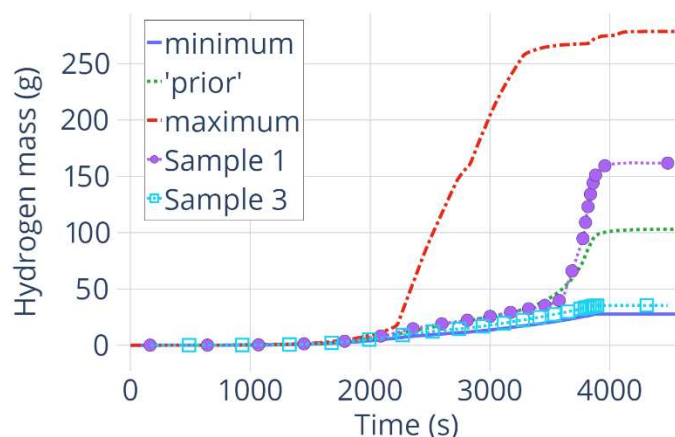


Figure 5-15 – Simulated hydrogen mass evolution in time. Minimum, ‘prior’ and maximum values are from the ‘prior’ set of data. Two samples 1 and 3 are from the ‘validation’ set of data.

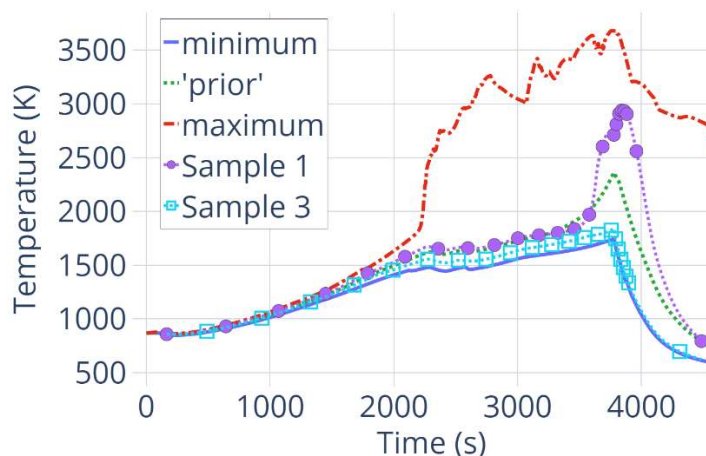


Figure 5-16 – Simulated temperature evolution in time of the ‘Channel_1’ structure. Minimum, ‘prior’ and maximum values are from the ‘prior’ set of data. Two samples 1 and 3 are from the ‘validation’ set of data.

Values of the AREA metric for samples №1 and 3 are shown at the **Figure 5-17**. All AREA values are normalized to the AREA value between the ‘prior’ and given ‘experimental’ curve. The minimum of the AREA curve means that at that time point the best prediction is achieved – namely, the prediction curve is closer to the experimental one, than in all other cases. In case presented here, after the global minimum the AREA metric value is growing again, which means that adding more measurements makes the prediction worse – the reason of such behavior is not yet clear, one of the hypothesis is the difference between the ‘experimental’ and ‘prior’ curves shapes at that time region. The almost constant value of the AREA metric up to the ~3000 s can be because ‘experimental’ and ‘prior’ curves in that region are very close to each other (see the **Figure 5-15** and **Figure 5-16**) and adding measurements here, probably, makes no real difference.

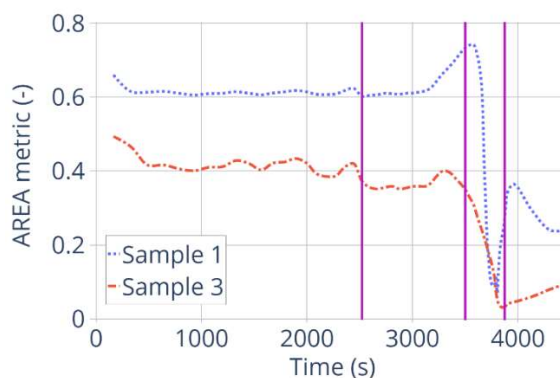


Figure 5-17 – AREA metric values for samples №1 and 3 from the 50 samples validation set. Time points up to which the ‘measured’ data are used to construct prediction for the illustration are marked by the vertical lines at 2521 s, 3500 s and 3875 s respectively.

On the **Figure 5-18** and **Figure 5-19** prediction results and prediction error are shown for the samples №1 and 3. It is shown how the prediction and prediction error change with adding more and more ‘measurements’. For the sample №1 the predictions using the ‘measurements’ up to 3500 s significantly underestimate the ‘experimental’ values. The better predictions can be constructed using the ‘measurements’ up to ~ 3800 s. The prediction constructed with the ‘measured’ data up to 3875 s predicts quite well the hydrogen generation at the time region ~ 3500 s – 3900 s, where the hydrogen mass increases sharply. But the final value of the hydrogen mass is overestimated. For the sample №3 first two prediction results overestimate the hydrogen mass value, but the prediction constructed with the ‘measurements’ up to the 3875 s lie very close to the ‘experimental’ curve – the difference is $\sim 5\%$. The computed prediction error can, unfortunately reach up to 30% in the time frame around ~ 3700 – 3800 s, when the algorithm is using ‘measurements’ up to ~ 2521 s or up to ~ 3500 s. This can happen when ‘measurements’ very close to the ‘prior’ curves are used and when one tries to predict values in a region which is already far from ‘prior’ values. One can see, that when ‘measurements’ are used up to ~ 3875 s, the prediction error is significantly smaller. Additional investigations can be done to provide a clear answer, why the prediction errors have particular values.

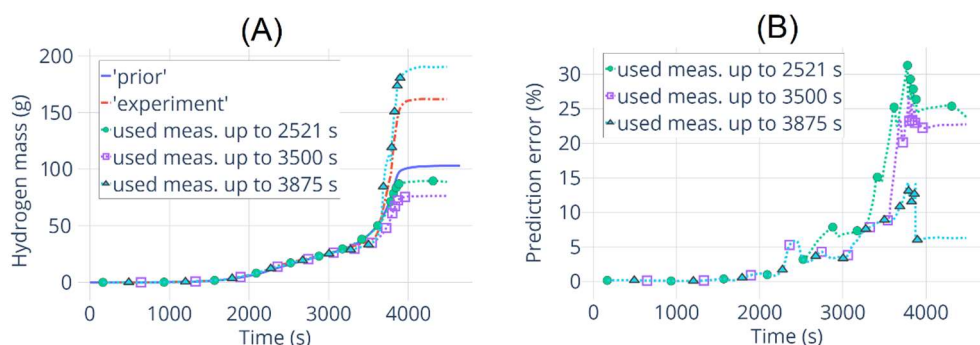


Figure 5-18 – Prediction results (A) and errors (B) for the sample №1 from the validation set. Results are presented for the different amount of measured data used for calculating the prediction.

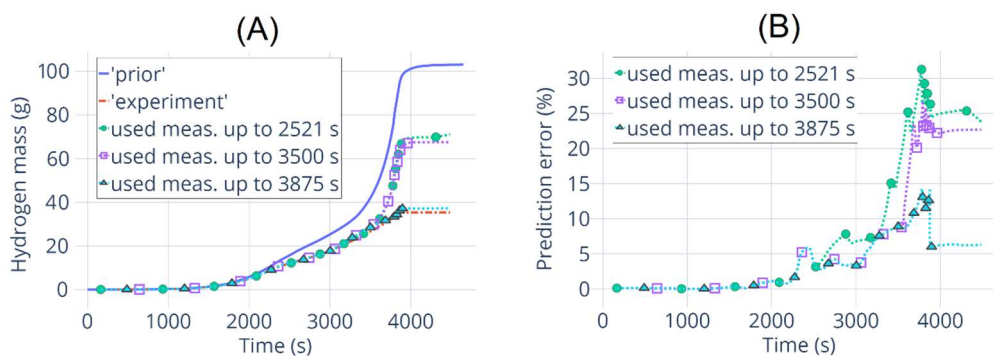


Figure 5-19 – Prediction results (A) and errors (B) for the sample №3 from the validation set. Results are presented for the different amount of measured data used for calculating the prediction.

5.4.2 Predictions using real experimental data as measurements

The MOCABA prediction algorithm is also applied to the real data from the QUENCH-08 experiment. Initially, the ‘prior’ set of data is the same, as has been used in the previous MOCABA application. Firstly, from all thermocouples only the non-failed ones are chosen. After that it is checked whether the data from non-failed thermocouples are lying inside the uncertainty range of the prepared ‘prior’ data. Unfortunately, the measured in the experiment temperature values lie usually too close to the minimum curve from the prepared ‘prior’ data set or even slightly lower it. To overcome that issue, another ‘prior’ set with increased up to 20% uncertainty for the two most important input parameters governing the steam and argon mass flow rate has been prepared, and after that data from all thermocouples has been checked again. From all experimental data, only two thermocouples left:

- 1) The thermocouple named “TFS 2/5”, which is located at the fuel rod simulator next to the central one from on the left side at the 150 mm elevation. From the ‘prior’ data the temperature of the ASTEC model structure ‘Channel_1’ at the elevation 150 mm corresponds to this thermocouple and named ‘T1_150’.
- 2) The thermocouple named “TSH 12/180 P”, which is located at the shroud outer surface at the 850 mm elevation. From the ‘prior’ data the temperature of the ASTEC model ‘shroud’ structure at the elevation 850 mm corresponds to this thermocouple and named ‘Tshroud_850’.

The **Figure 5-2** and **Figure 5-4** as well as the **Table 3** and **Figure 8** in experimental report [\[Stuckert et. al., 2005\]](#) can help to understand better the thermocouples location. The ASTEC model radial and axial representations are show in **Figure 5-5**.

Next step is to check the Pearson correlation values between the ‘prediction’ parameter (hydrogen mass) and the suggested ‘observable’ parameters. As shown in **Figure 5-20**, the Pearson correlation coefficient for suggested observable ‘T1_150’ changes significantly during

the transient and reaches values lower than 0.3 at the time ~ 2500 s and between $\sim 3600 - 3800$ s. Therefore, this ‘observable’ parameter has been excluded.

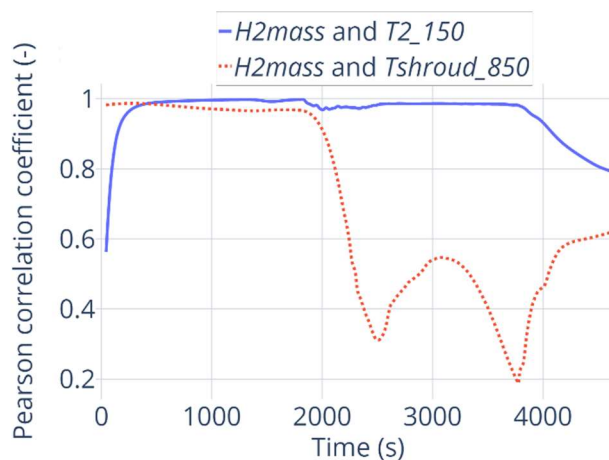


Figure 5-20 – Pearson correlation coefficients time evolution between selected ‘predictions’ and ‘observables’ parameters from the QUENCH-08 experiment simulations results. Calculated for the 400 samples ‘prior’ set of data. Selected parameters are: hydrogen mass – ‘H2mass’; temperature of the ‘Channel_1’ structure at 150 mm elevation – ‘T2_150’; temperature of the ‘shroud’ structure at 850 mm elevation – ‘Tshroud_850’.

At **Figure 5-21 (A)** is shown, how the data from the selected thermocouple “TSH 12/180 I” lie inside the uncertainty range of the ‘prior’ data. One can see, that the measured temperature values lie inside the simulated range, and up to ~ 2000 s the measured temperature curve is going along the ‘prior’ one, after that up ~ 3800 s the temperature rises slower, than in was simulated and presented by the ‘prior’ curve, from ~ 3800 s till the end of the transient the temperature decreases with the same speed as in average, but the curve itself lie under the ‘prior’ one. For the hydrogen mass evolution in time presented in **Figure 5-21 (B)** from the time point ~ 2200 s the experimental values differs significantly from ‘prior’ ones – the hydrogen mass values during the time window $\sim 2200 - 3700$ s increases much slower in the experiment, than it has been simulated here, and the final value is lower, than the ‘prior’ one.

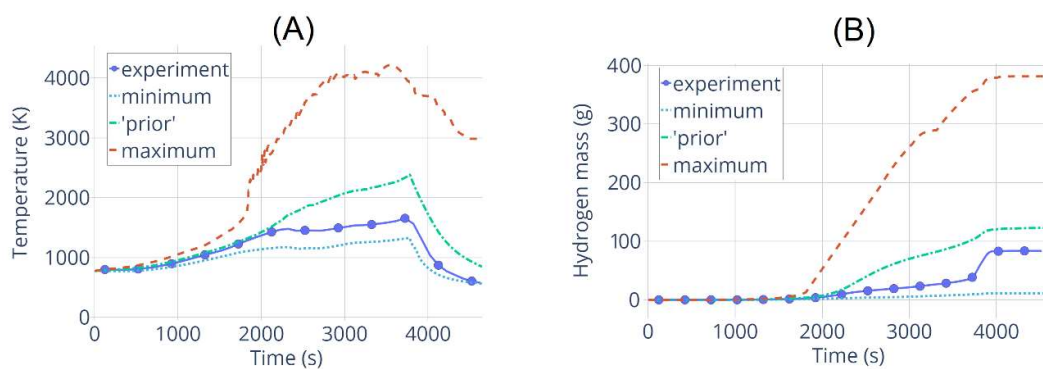


Figure 5-21 – ‘Prior’, minimum and maximum simulated values and experimental data. (A): Simulated temperature evolution in time of the ‘shroud’ structure at the elevation 850 mm and data from the thermocouple “TSH 12/180 I”. (B): Simulated hydrogen mass evolution in time and the experimental data.

On **Figure 5-22** the prediction results calculated with different amount of measured data are presented. The prediction constructed with minimal amount of measured data (**Figure 5-22 (A)**) repeats well the very beginning of the process up to ~ 2200 s and also predicts well the final values of produced hydrogen mass, but does not repeat the experimental curve during the pre-oxidation and transient phases $\sim 2200 - 3800$ s. In addition to it, the prediction error is very high and can reach up to $\sim 50\%$. The prediction constructed with the measured data up to 2423 s (**Figure 5-22 (B)**) repeats the experimental curve quite well up to ~ 3500 s, after that the prediction starts to deviate and underestimates the final hydrogen mass by $\sim 25\%$. The prediction errors are still high, especially from ~ 3800 s till the end of the transient and can be $\sim 35 - 50\%$. The prediction calculated with the measured data up to the end of the transient phase (**Figure 5-22 (C)**) is even worse, that the previous one, it underestimates the final hydrogen mass by $\sim 50\%$ from the real experimental value, but prediction errors are lower and have value $\sim 20\%$ during the cooldown phase. The last prediction calculated with using all available measured data (**Figure 5-22 (D)**) does not differ much from the previous one, but has much worse prediction error at the end of the time scale reaches up to $\sim 70\%$.

Results presented here are not satisfactory, probably due to the differences in the experimental and 'prior' curves shapes. Overcoming that issue can be a topic of a future investigation.

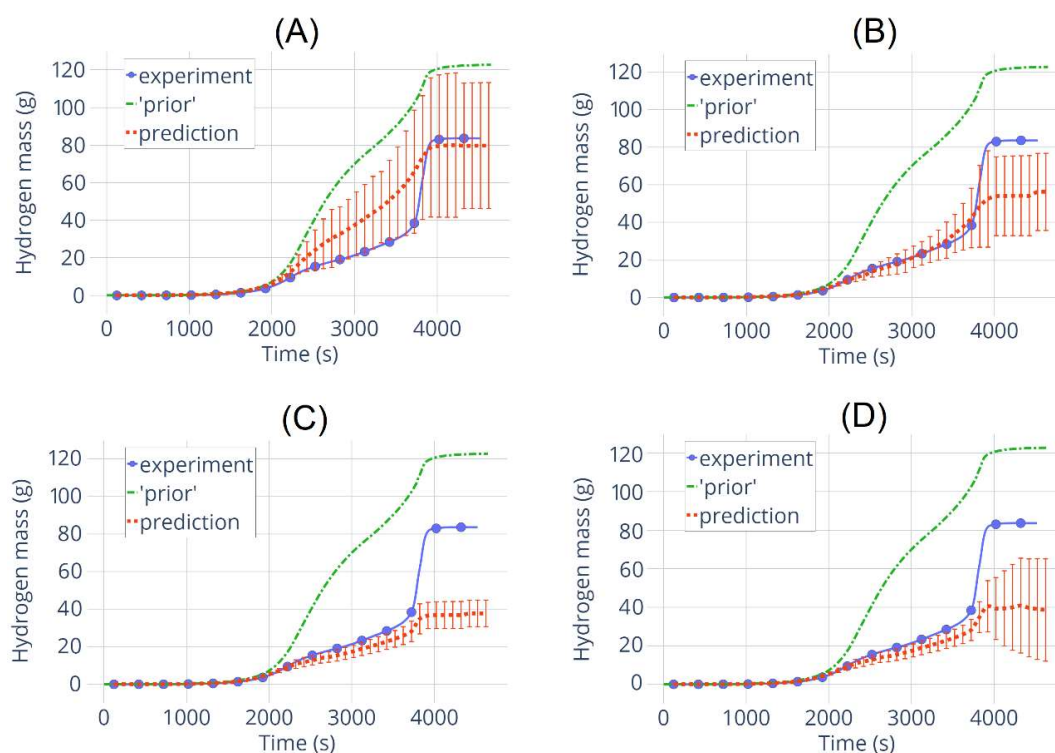


Figure 5-22 – Prediction results and errors for the hydrogen mass. Results are presented for the different amount of measured data used for calculating the prediction – (A): up to 223 s; (B): up to 2423 s; (C): up to 3823 s; (D): up to 4623 s.

6 Integral validation of the FSTC-MOCABA approach by the KONVOI-1300 pressurized water reactor

6.1 KONVOI NPP and its ASTEC model

KONVOI is a type of German PWR made by Kraftwerk Union company (KWU).

Three reactors of this type currently operate in Germany:

- Isar-2 located in lower Bavaria; in operation since 1988;
- Emsland located in lower Saxony; in operation since 1988;
- Neckarwestheim-2 located in Baden-Württemberg; in operation since 1989.

All three are considered to shut down by the end of 2022 due to the decision of the German government. Due to the changes in the Atomic Energy Act (Atomegesetz) from 9th December 2022 the lifespan of these NPPs have been extended until 15th April 2023.

A KONVOI plant has 4 coolant loops, a pressurizer, 4 steam generators and 4 reactor coolant pumps. More details about the plant design may be taken from [\[Kuschel et. al., 1991\]](#), [\[Czech et. al., 1996\]](#).

The ASTEC input used for simulations in this work is based on previous work made for the CESAM project [\[Nowack et. al., 2018\]](#), [\[Gómez-García-Toraño, 2017\]](#). The current project executed in cooperation with Framatome GmbH, uses a ‘generic’ input as described in [\[Gabrielli et. al., 2021\]](#), [\[Stakhanova et. al., 2022b\]](#). Comparing to the original ‘generic’ input deck, all ASTEC modules are activated, the model for the containment leakage is revised, no filtering is assumed, and realistic fuel inventories are computed by Framatome using the ORIGEN-ARP tool.

Scheme of the primary and secondary circuits is shown at the **Figure 6-1**. Four loops of KONVOI NPP is represented in that model in two loops – A and B. Loop B is connected to the pressurizer, and three loops of the real NPP are combined here in loop A. The coolant path in the loops is marked by arrows – coolant leaves the core through the upper plenum; goes through the hot legs and upper head; from hot legs enters the SGs and goes through their U-tubes, then enters the cold legs; enters the MCPs; goes to the downcomer through the cold legs collectors. Feedwater of the secondary circuits marked with white arrows – it enters the SGs downcomers from the top, goes down along the downcomers, enters the riser region (divided into eight cells) and leaves this region as a humid steam (marked with red arrows). Humid steam goes to the main steam line (MSL) leading to the steam collector.

On **Figure 6-2** the core and containment nodalizations are shown. The active zone is divided into equidistant slices (300 mm thick), and axially – in 8 rings (6 represented the core, and the other 2 – bypass and downcomer). Lower head is modelled as one cell. The containment is divided

into the compartments connected by junctions. On the **Figure 6-2**, the annulus is divided into three zones, the containment and the annulus, as well as the annulus and the environment are connected with fan.

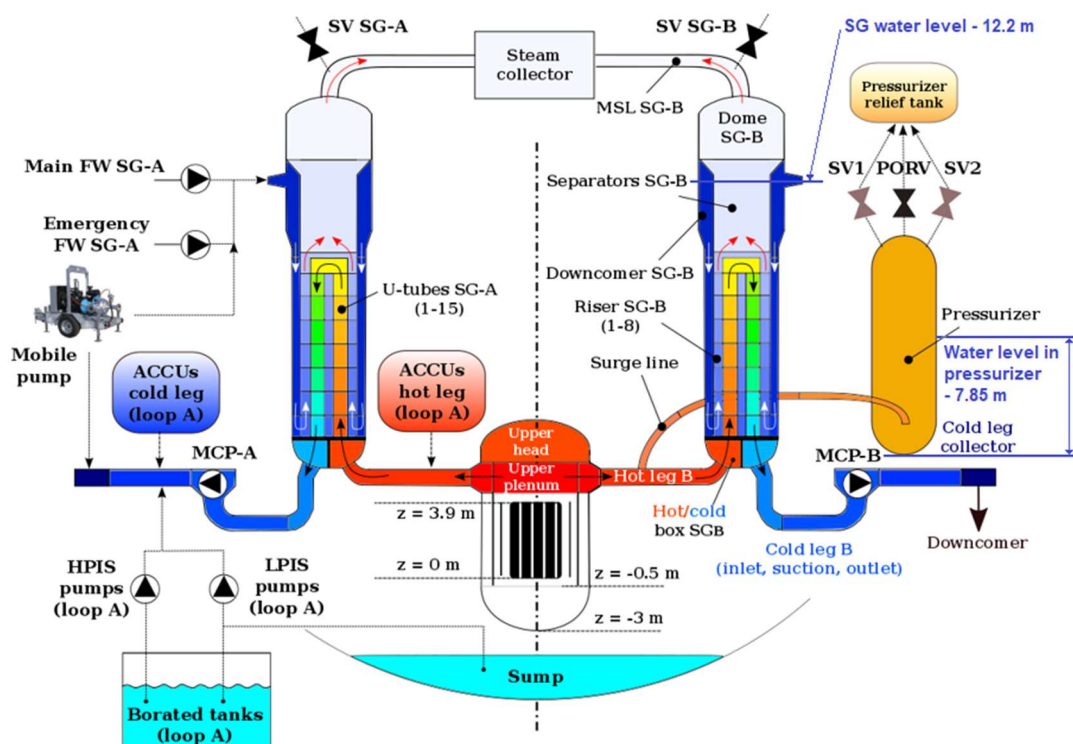


Figure 6-1 – Primary and secondary circuit modelling of a generic KONVOI NPP by the ASTEC code. Based on [\[Gómez-García-Toraño 2017\]](#).

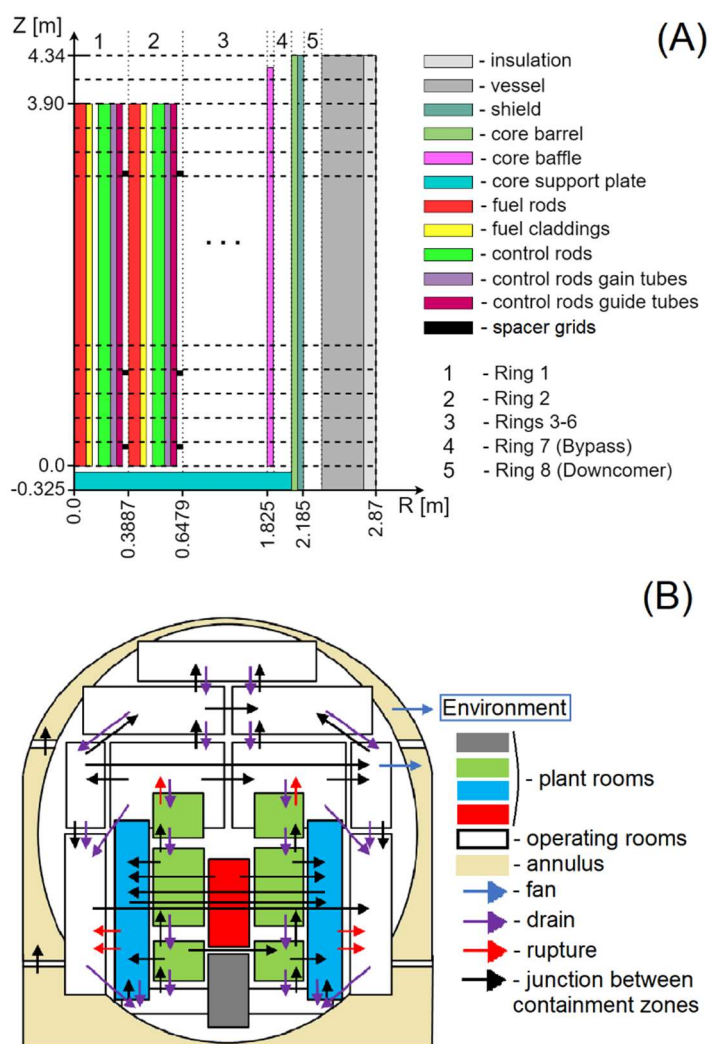


Figure 6-2 – Core (A) and containment (B) nodalization in the ASTEC model of a generic KONVOI NPP. Based on [\[Gabrielli et. al., 2022\]](#).

6.2 Uncertain input parameters for considered scenarios

To choose the uncertain input parameters, first, the phenomena affecting the selected FoMs must be identified. In our case, the main FoM is the source term, and it is affected by: FPs released from the fuel (ELSA module of the ASTEC code), the conditions at the start of core degradation (integrity criteria) and FPs transport to the containments and their behavior (SOPHAEROS module of the ASTEC code). After identifying the main phenomena, parameters from corresponding ASTEC models are selected. Information related to these parameters, like PDFs and PDF parameters, are taken from literature (code documentations, experimental results, code models verification, etc.) or by engineering judgement.

The list of uncertain input parameters chosen for ASTEC simulations of a KONVOI NPP is given in the **Table 6-1** and consists of 16 variables. Four parameters (*par1*, *par2*, *par5*, *par5a*) are from the ELSA module, which simulates FP and structural material release in the core

degradation phase. The parameters in this context are related to surface/volume ratio of fuel pellets and governing geometrical parameters of the grains. Three parameters (*par14* – *par16*) are from the INTE structure managing the integrity of macro-components (according to the ASTEC code terminology, it is physical object corresponding to any solid structure in the reactor core, e.g. fuel rods) – two for the threshold temperatures (for cladding and oxide layer) and one for the threshold thickness of oxide layer. Seven parameters (*par31* – *par37*) are chosen from AEROSOLS ASTEC structure of the SOPHAEROS module. These parameters describe particle geometry and physical properties of aerosols. The last two parameters in the list are not related to ASTEC models and represent coefficients governing the leakage rate from containment to the annulus (*par41*) and the number of effective full power days of the current fuel cycle (*parBU*). PDFs for these parameters have been chosen according to the available information from the literature, and all links are provided in the **Table 6-1**. For example, default values for parameters *par1* and *par2* are the results of the ELSA model validation described in [\[Brillant et. al., 2013a\]](#), [\[Brillant et. al., 2013b\]](#).

Correlations between uncertain input parameters have been introduced for correctness of the modeling, while propagating the uncertainties. In **Figure 6-3** the correlation matrix of input parameters is shown. For example, *par1* and *par2* are directly pre-correlated, because an increase of the roughness of the fuel pellet surfaces will most likely limit the oxygen access to the fuel. In order to take into account the effect of non-symmetrical shapes, *par1* is anti-correlated with the *par5a*. An increase of the temperature threshold for the dislocation of the cladding (*par14*) should be consistent with the increase of the temperature threshold of the dislocation of the oxide layer (*par15*) and with the minimum limit for the thickness of the oxide layer (*par16*). Therefore, these three parameters are positively correlated with each other. The *par31* is directly pre-correlated with the *par32*, since the thermal conductivity (*par31*) and the specific heat (*par32*) are both increasing with the temperature.

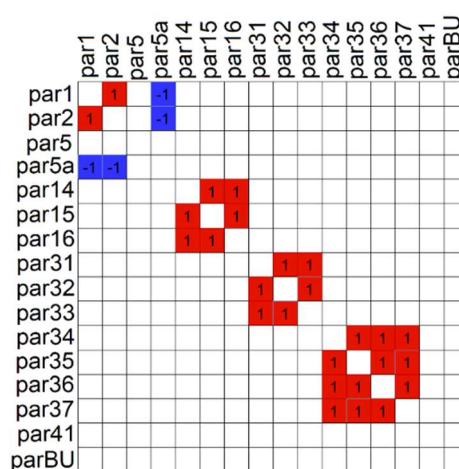


Figure 6-3 – Correlation matrix of uncertain input parameters (left). Correlation matrix after applying Iman-Conover method (right)

| Parameter name | Probability density function (PDF) | PDF parameters | Parameter meaning and corresponding ASTEC model/structure | Source |
|----------------|------------------------------------|--|--|---|
| par1 | Normal | $\mu = 5.0$; $\sigma = 30\%$ (truncated at $\pm 3\sigma$) | STRU ELSA: Correction factor for the surface/volume ratio of the fuel pellets due to roughness | [Ikeda et. al., 2003] , [Brillant et. al., 2013a] , [Brillant et. al., 2013b] |
| par2 | Normal | $\mu = 0.03$; $\sigma = 30\%$ (truncated at $\pm 3\sigma$) | STRU ELSA: Correction factor for the surface/volume ratio of the fuel pellets for the limited steam access | |
| par5 | Normal | $\mu = 1.2E-5$; $\sigma = 30\%$ (truncated at $\pm 3\sigma$) | STRU ELSA: Geometrical diameter of the grain | [Pastore et. al., 2015] , [Song et. al., 2000] |
| par5a | Triangular | mode = 2.0E-6; min = 1.6E-6; max = 3.4E-6 | STRU ELSA: Standard deviation of geometrical diameter of the grain | |
| par14 | Normal | $\mu = 2500.0$; $\sigma = 10\%$ (truncated at $\pm 3\sigma$) | VESSEL:INTE: Threshold Temperature of the cladding Dislocation [K] | [NRC, 2018] , [Pontillon et. al., 2005] |
| par15 | Normal | $\mu = 2300.0$; $\sigma = 10\%$ (truncated at $\pm 3\sigma$) | VESSEL:INTE: Threshold Temperature of the oxide layer Dislocation [K] | [Hofmann et. al., 1999] |
| par16 | Normal | $\mu = 250.0E-4$; $\sigma = 20\%$ (truncated at $\pm 3\sigma$) | VESSEL:INTE: Threshold thickness of the oxide layer [mm] | |
| par31 | Uniform | min = 2.975; max = 4.025 | SOPHAEROS:AEROSOLS: Particle mean thermal conductivity (J/m/K) | Engineering judgement |
| par32 | Uniform | min = 714.0; max = 966.0 | SOPHAEROS:AEROSOLS: Average specific heat (J/kg K) of the aerosol | |
| par33 | Triangular | mode = 3000.0; min = 2610.0; max = 10000.0 | SOPHAEROS:AEROSOLS: Particle mean density (kg/m ³) | [NRC, 2012] |
| par34 | Triangular | mode = 1.1E-8; min = 1.0E-8; max = 2.0E-07 | SOPHAEROS:AEROSOLS: SIZE particle minimum geometrical radius (m) | [Helton et. al., 1986] |
| par35 | Triangular | mode = 1.99E-5; min = 5.0E-6; max = 2.0E-5 | SOPHAEROS:AEROSOLS: SIZE particle maximum geometrical radius (m) | |
| par36 | Triangular | mode = 1.0; min = 0.9, max = 1.0 | SOPHAEROS:AEROSOLS:SHAPE Shape factor relative to particle coagulation | [NRC, 2012] |
| par37 | Beta | $\alpha = 1.0$; $\beta = 5.0$, min = 1.0; max = 3.0 | SOPHAEROS:AEROSOLS:SHAPE Shape factor relative to Stokes velocity | [NRC 2018] |
| par41 | Uniform | min = 1.0; max = 30.0 | Coefficient for the leakage rate | Engineering judgement |
| parBU | Uniform | min = 10.0; max = 328.0 | Effective full power days | |

Table 6-1 – Uncertain input parameters of KONVOI ASTEC model

6.3 Description of the MBLOCA SA Scenario

The MBLOCA scenario starts at time $t=0$ s assuming a break of 440 cm² cross-section in the cold leg. When the pressure in the Reactor Coolant System (RCS) is lower than 132 bar or containment overpressure is higher than 30 mbar, a SCRAM is initiated by the Reactor Protection System (RPS). After that Feed Water Pumps (FWPs) trip no feed water (FW) is injected to the Steam Generators (SGs) anymore. The steam flow into the turbine is blocked, because the turbine valves are closed after SCRAM. If two of three conditions are met, which means an overpressure in the containment greater than 30 mbar, a RCS pressure lower than 110 bar or a level of the liquid in the pressurizer lower than 2.30 m – the Emergency Core Cooling System (ECCS) is activated. The Extra Borating System (EBS) is also activated when the pressurizer water level is lower than 2.30 m. The ECCS consists of passive accumulators (ACCUs) and the active High and Low Pressure Injections Systems (HPIS and LPIS). The ACCUs discharge at an initial pressure of 25 bar into the hot and cold legs of the RCS. Each train of the HPIS injects up to 75 kg/s below 110 bar; each train of the LPIS – up to 150 kg/s below 12 bar. Each train of the HPIS and the LPIS has water supply from a different borated water tank (with a capacity of 480 m³ each) and injects it into the cold leg collector. Following the ECCS criterion, the Main Coolant Pumps (MCPs) are coasted down and the pressure regulation in the pressurizer is switched off. The Emergency Feed Water System (EFWS) is activated when the level of the liquid in one of the SGs falls below 4.50 m.

In the MBLOCA scenario, the availability of 3 out of 4 trains of the HPIS and the LPIS (the fourth is assumed to be under maintenance) and the failure of the sump recirculation mode are assumed. As a result, the HPIS and the LPIS remain active up to the tanks are empty. After such instant, no more cooling is available in the core leading to severe accident.

The computed time for the occurrence of the main events important for the simulated SA progression with best estimated values of chosen uncertain input parameters are presented in **Table 6-2**. Note that all ASTEC simulations have been stopped 6000s after lower head vessel failure. That has been done to save computational time, because the simulation of the ‘full’ MBLOCA scenario up to a basemat rupture is much longer.

| Event | Time |
|---|---------|
| Break opening | 0 s |
| SCRAM | 1 s |
| Turbine valves closed. FWPs shut down | 1.5 s |
| ECCS signal. Activation EBS | 6 s |
| MCPs coast down. EFWS activation | 7 s |
| Start of FPs release | 564 s |
| First material slump into the LP | 794 s |
| 20 tons of corium relocated into the LP | 5734 s |
| 50 tons of corium relocated into the LP | 11724 s |

| | |
|---|---------|
| 70 tons of corium relocated into the LP | 11744 s |
| Lower head vessel failure | 12054 s |
| End of the corium slump from lower head to the cavity | 12071 s |
| End of simulations | 18054 s |

Table 6-2 – Sequence of the events occurring during the MBLOCA scenario. Results for the reference case.

6.4 Results of U&S analysis

Results of the U&S analysis of the MBLOCA scenario are described here in the following manner. At first, the time of the occurrence of the main events during the transient is analyzed to illustrate how the varying uncertain input parameters causes a different temporal accident progression. For the four fission products (xenon, iodine, cesium and molybdenum) a simple statistics of their release into the containment and the environment and Spearman correlation coefficient values for the most important uncertain input parameters are provided. The release values are presented hereafter as a fraction of initial inventory.

Because the uncertain input parameters have different values for each individual simulation, progression of the accident can go quite differently, and it can be illustrated with the time values when the main events are occurring during the accident. At the **Figure 6-4** time for the start of FPs release and the lower head vessel failure are shown for all non-failed ASTEC simulations. In addition to that, time of the main events for simulation with best estimated (BE) values of uncertain input parameters is also given. One can see that time of the start of FPs release is not varying much across the simulations, but after that the time of lower head vessel failure from 2240 s (minimum value for that set of simulations) up to 33200 s (maximum value for that set of simulations). This significant difference in the speed of SA progression makes the U&S analysis quite challenging in terms of interpreting the results. In this work only the data between two selected events are extracted in following manner: the left bound of time scale is the maximum time when the first event occurred; the right bound of the time scale denotes the minimum time when second event occurred. For example, data between start of FPs release and the time of the lower head vessel failure are extracted. Practically that means that data are extracted for time period from the latest release of FP across all samples until the earliest lower head vessel failure across all samples. If all non-failed simulations are kept, the U&S analysis can be performed only up to the minimal time of the lower head vessel failure, which is 2240 s. To extend the time window for the analysis, the samples with early lower head vessel failure can be excluded from the statistics. In that case, the separate U&S analysis can be done with and without some selected samples, to see how it affects the results.

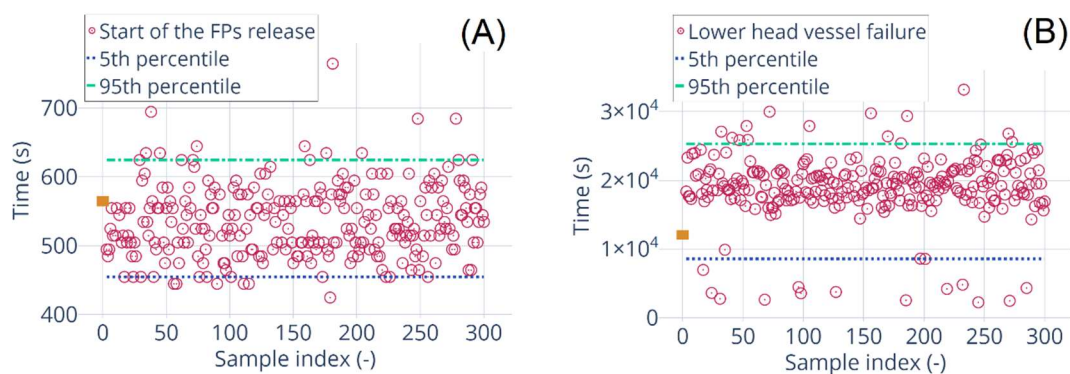


Figure 6-4 – Time of the main events for the all non-failed MBLOCA simulations from the 300 simulations set. (A): time of the start of the FPs release; (B): time of the lower head vessel failure. With orange rectangle the results of the simulation with the best estimated values of the uncertain input parameters are marked.

Simple statistics for the selected elements released in the environment is presented in **Figure 6-5**. The same for the containment – in **Figure 6-6**. Data is presented as fraction of initial inventory varying from 0 to 1. Most of the xenon (Xe) released during the course of the accident is located in the containment and only a small fraction is released to the environment due to the small leakage from the containment. The amount of Xe in the containment reaches a plateau very fast at the beginning of the transient and a second release is happening around the time of the first slump of the corium. Before the time of the vessel failure all Xe is already released into the containment. The amount of iodine released into the environment at least one magnitude smaller than for Xe. At the end of the transient, in the containment amount of iodine can reach ~ 0.35 of the initial inventory, however, the median value is ~ 0.02 , due to significant amounts of iodine remain in the primary system. The median amount of cesium released into the environment is higher than for iodine, but still lower than for xenon. Median amount cesium released into the containment is ~ 10 time higher than for iodine (~ 0.2 and ~ 0.02 of the initial inventory, respectively), and 95th percentile values can reach ~ 0.4 of the initial inventory. And as well as for I, most of the Cs will stay in the primary system. Most of molybdenum will stay in the vessel, and only ~ 0.02 (95th percentile value at the end of the transient) reaches the containment and $\sim 10^{-6}$ (95th percentile value at the end of the transient) reaches the environment.

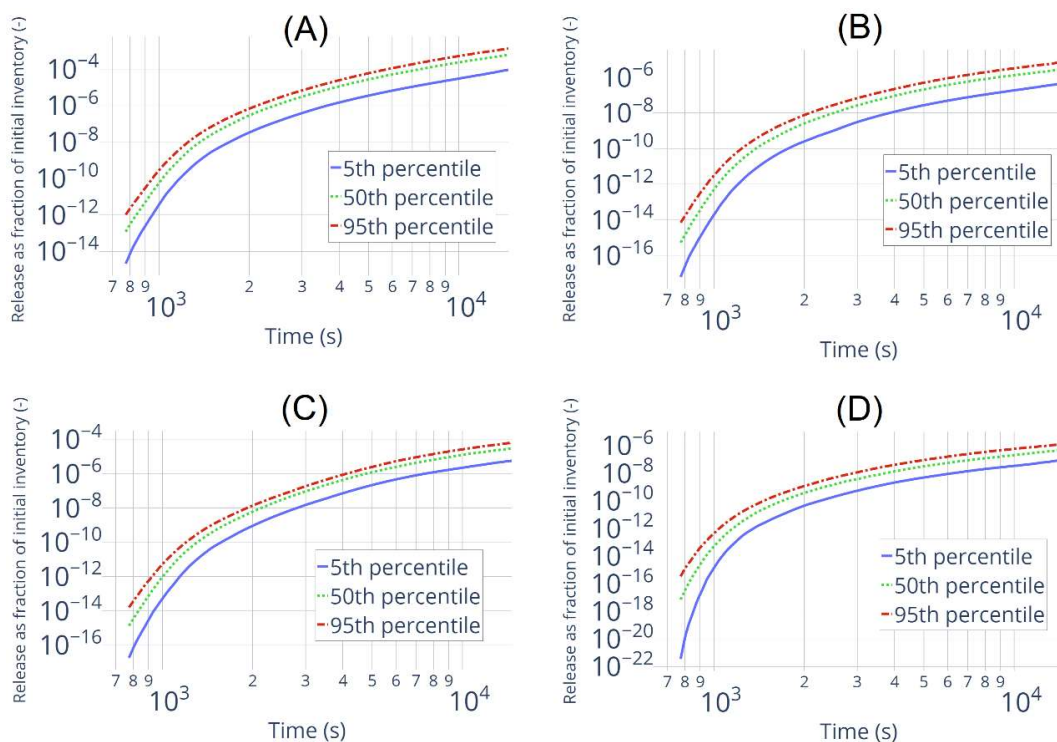


Figure 6-5 – Simple statistics for the release into the environment as fraction of initial inventory. (A) – Xenon (Xe); (B) – Iodine (I); (C) – Cesium (Cs); (D) – Molybdenum (Mo).

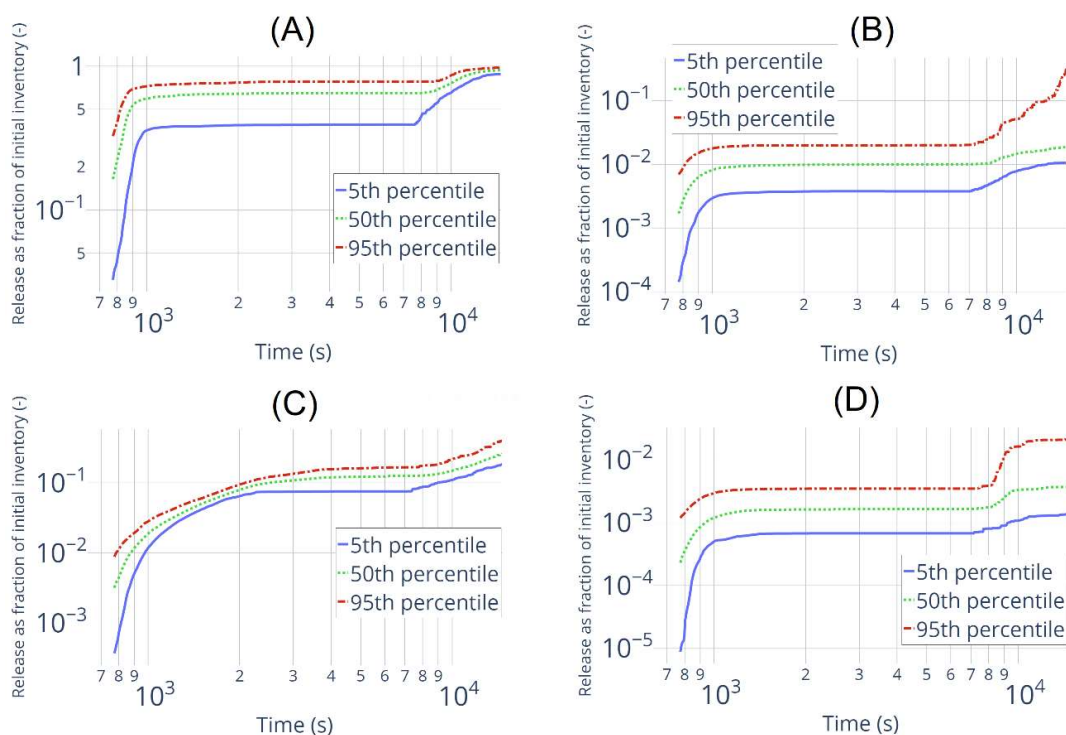


Figure 6-6 – Simple statistics for the release into the containment as fraction of initial inventory. (A) – Xenon (Xe); (B) – Iodine (I); (C) – Cesium (Cs); (D) – Molybdenum (Mo).

Calculating the correlations between figures of merit (FoMs) and uncertain input parameters allows to investigate which parameters have the biggest influence on the release at the different stages of the process. On **Figure 6-7** is shown the Spearman correlation values for the most important uncertain input parameters affecting the release into the environment. For all four selected fission products the parameter governing the leakage rate is the most important – the Spearman correlation value reaches the level $\sim 0.8 - 1.0$ and stays on that level for the rest of the transient. This results is quite obvious, the bigger the leakage between containment and environment the bigger amount of fission products reaches the environment. Another important parameter influencing release into the environment is the one governing the burnup rate (from beginning to the end of the fuel cycle). The Spearman correlation values for this parameter are high at the very beginning of the transient, when the fission products release start, and after that decrease very fast. The most important parameter affecting the release into the containment is the one governing the burnup rate, as presented in **Figure 6-8**. It is important at the beginning of the transient, when the fission product release starts, after that Spearman correlation values remains constant (at least for the xenon, iodine and molybdenum), while the release into the containment is also constant, and after that the correlation value decreases. In addition to it for the release into the containment of the low-volatile fission product like molybdenum the parameters from the ELSA ASTEC model simulating the fission products release from the fuel pellets play a role. On the **Figure 6-8** the Spearman correlation coefficient for the parameter representing the correction factor for the surface/volume ratio of the fuel pellets due to roughness is shown. The Spearman correlation values for another two uncertain input parameters from the same ASTEC model (correction factor for the surface/volume ratio of the fuel pellets for the limited steam access and diameter of the grain) are not shown, due to their correlation with already presented parameter. The correlation value is moderate during the most part of the transient. For other selected uncertain input parameters the correlation values are negligible and not presented here.

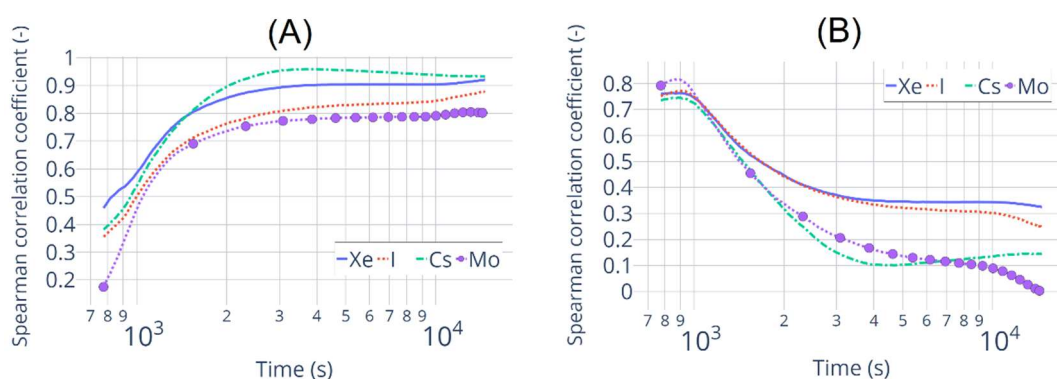


Figure 6-7 – Spearman correlation coefficient evolution in time for the amount selected fission product (xenon, iodine, cesium and molybdenum) released into the environment and uncertain input parameter governing (A): the leakage between containment and environment; (B): the burnup.

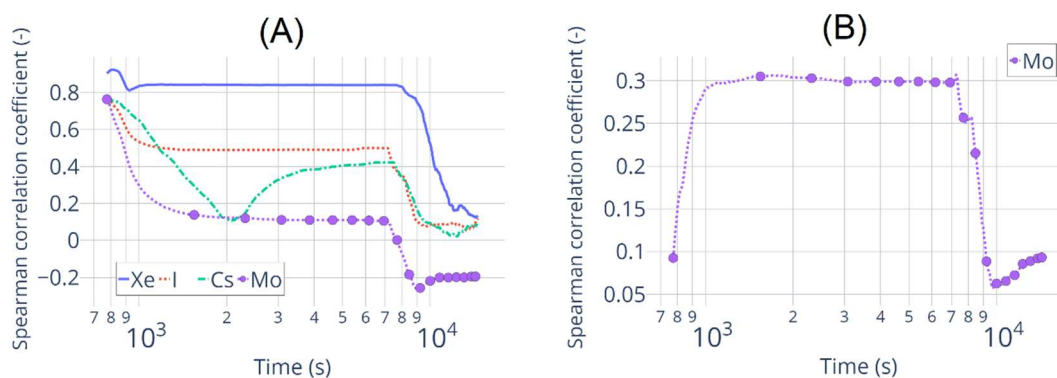


Figure 6-8 – Spearman correlation coefficient evolution in time for the amount selected fission product (xenon, iodine, cesium and molybdenum) released into the containment and uncertain input parameter governing (A): the burnup; (B): the correction factor for the surface/volume ratio of the fuel pellets due to roughness.

In order to increase the confidence about the results of U&S analysis, additional investigation is probably worth to be done. A consistency test, which is executed for the QUENCH-08 simulations, is not as easy to perform for KONVOI simulations not only due to time consuming, but also because of the difficulties with U&S analysis mentioned above, like differences in the progression of the SA from one sample to another.

6.5 Results of applying the MOCABA algorithm for the source term prediction in MBLOCA SA scenario

To test the MOCABA algorithm on the results of MBLOCA scenario simulations, two sets of data have been prepared as it has been done for the QUENCH-08 simulations. One set of data consists of 300 simulations and has been used as the input data for the ‘prior’ part of the MOCABA algorithm. Another one consists of 100 samples and is used as a so-called ‘validation’ set, where each sample is considered as an individual experiment realization. For these two sets of data, the same list of input parameters (see the **Table 6-1**) with the same uncertainty ranges has been used.

The goal of this example is to predict the amount of xenon (as fraction of initial inventory) released into the environment. At first, two parameters have been checked as potential ‘observables’ – the total dose rate in the annulus and the total dose rate in containment. Total dose rate in annulus consists of dose rates from isotopes of noble gases Xenon and Krypton (Kr-85, Kr-87, Kr-88, Xe-133, Xe-135, Xe-138). Total dose rate in containment consists of dose rate from isotopes of Barium, Cesium, Iodine, Krypton, Lanthanum, Molybdenum and Xenon (Ba-140, Cs-134, Cs-137, Cs-138, I-131, I-132, I-133, I-134, I-135, Kr-85, Kr-87, Kr-88, La-140, Mo-99, Xe-133, Xe-135, Xe-138). From results of the ‘prior’ part of the prediction algorithm it has been observed, that Pearson correlation coefficient values between ‘prediction’ parameter and the total

dose rate in containment are low (see in **Figure 6-9**), therefore only total dose rate in the annulus has been left as an ‘observable’ parameter.

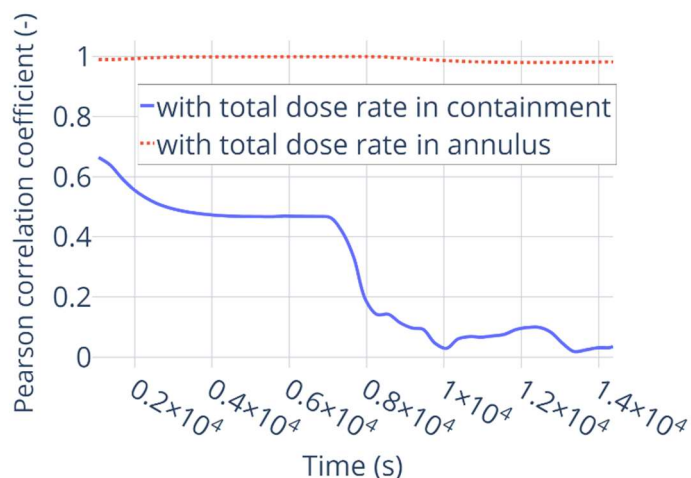


Figure 6-9 – Pearson correlation coefficients between ‘prediction’ parameter (amount of Xenon released into the environment) and two initially suggested ‘observable’ parameters (total dose rate in the annulus and total dose rate in containment)

To present the results of prediction two samples from the ‘validation’ set has been chosen. On **Figure 6-10** is shown how total dose rate in annulus and Xenon release values for these two samples lie inside of the uncertainty range of the ‘prior’ data. It has been discussed already, that ‘prior’ data have to cover possible ‘measurements’ values and also the similarity in the curves shapes between ‘measurements’ and ‘prior’ values can affect the prediction results. For sample №3 both Xenon release and the total dose rate in the annulus are increasing faster, than in average, while for the sample №26 – slower.

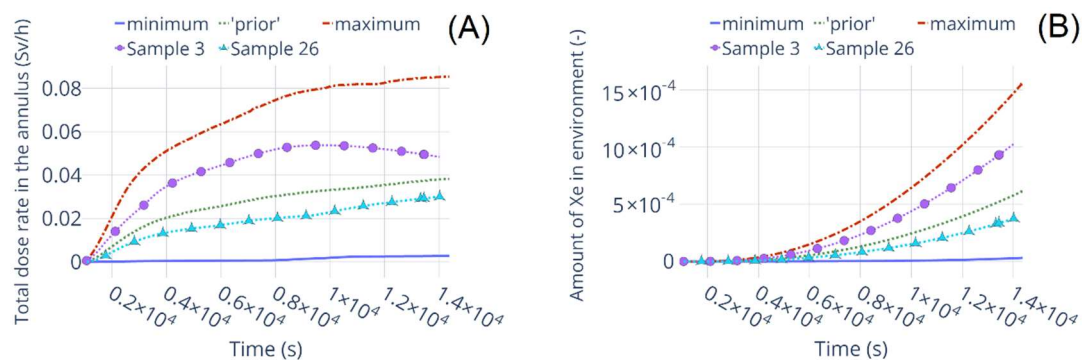


Figure 6-10 – Simulated total dose rate in the annulus (A) and amount of Xenon released into the environment (B) evolution in time. Minimum, ‘prior’ and maximum values are from the ‘prior’ set of data. Two samples 3 and 26 are from the ‘validation’ set of data.

Values of the AREA metric indicating the prediction quality for these two samples are presented at **Figure 6-11**. For samples №3 and №26 the best prediction (global minimum of the AREA metric curve) is achieved around the time ~ 8700 s and ~ 9800 s respectively. The quality

of prediction for the sample №3 along the whole transient is better, than for the sample №26. The reason of such results is not yet clear.

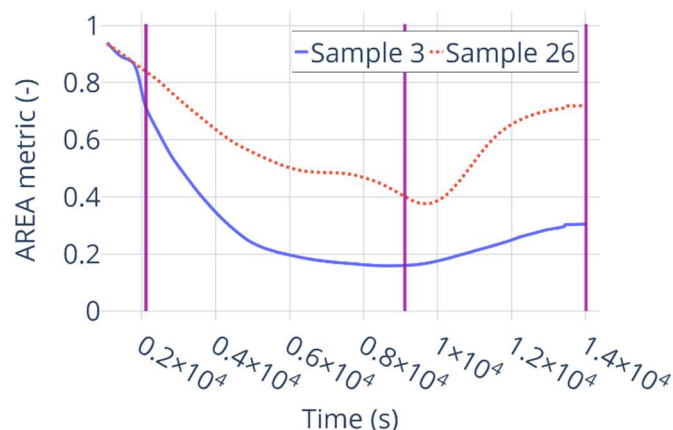


Figure 6-11 – AREA metric values for samples №3 and 26 from the 100 samples validation set. Time points up to which the ‘measured’ data are used to construct prediction for the illustration are marked by the vertical lines at 2114 s, 9114 s and 14014 s respectively.

Prediction results and prediction error are presented for the samples №3 and №26 in **Figure 6-12** and **Figure 6-13** respectively. In both cases the prediction goes closer to the ‘experimental’ data with adding more measurements, but the last prediction performed with all measurements is not the best one (as also shown in **Figure 6-11** with AREA metric values). The reason of that behavior is not yet clear. The prediction errors can be really high at the beginning of the process, but decreasing really fast and reach some kind of plateau $\sim 20 - 40\%$. Currently it is difficult to say, why the prediction errors have exactly these values.

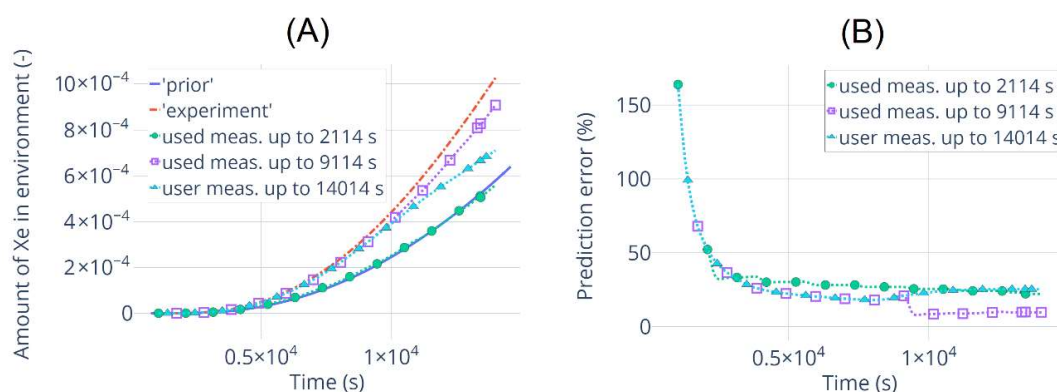


Figure 6-12 – Prediction results and errors for the sample №3 from the validation set. Results are presented for the different amount of measured data used for calculating the prediction.

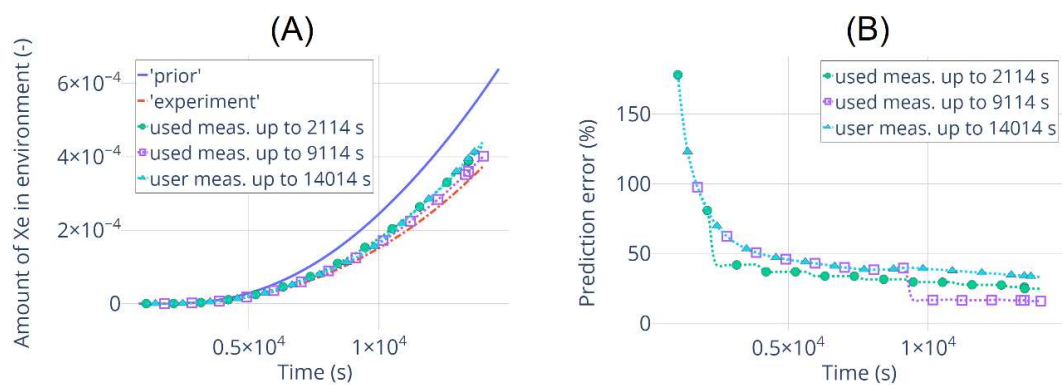


Figure 6-13 – Prediction results and errors for the sample №26 from the validation set. Results are presented for the different amount of measured data used for calculating the prediction.

7 Conclusions and future work

The main objective of this thesis is the developing, implementing and testing the methodology for fast source-term calculations in case of severe accidents to support the emergency team and providing data about potential release of radiological substances to the authorities. SA codes can make very detailed simulations of the accident progression, but they are time-consuming and cannot be used in cases when results should be provided in minutes or even seconds. In this work, the MOCABA algorithm is suggested to apply it to the source term prediction. In contrast to the widely-used approach based on the BBN, MOCABA is not only using pre-calculated results, but calculates prediction values by using measured data, which allows it to correct the prediction according to the real situation during accident progression.

The main results to present in this thesis is the ST prediction made with MOCABA using simulation results of accident scenarios (so-called '*prior*' data) at a KONVOI-type NPP. To prepare this database so that it will represent the simulated process correctly, U&S analysis is needed, which allows investigating the possible variations in accident progression and uncertain input parameters influence on the Figures-of-Merit. Therefore, a big part of the thesis is devoted to the generation of a lot of SA simulations and performing U&S analysis of the chosen accident scenarios.

To perform the U&S analysis and to implement the MOCABA algorithm, the FSTC tool has been developed. The verification of the U&S analysis part of the tool against URANIE platform has been conducted. The verification of the MOCABA algorithm implementation against proprietary tool developed in Framatome has also been done.

At first the whole methodology has been analyzed for the QUENCH-08 experiment. Since the simulations of this experiments using the ASTEC SA code are faster than for KONVOI NPP, but the QUENCH phenomena are complex enough to be a suitable task for U&S analysis. These steps demonstrated the potential of MOCABA algorithm and paved the way for application of the methodology to a KONVOI NPP. The MOCABA algorithm itself is not constrained to any particular physical process and can be arbitrarily applied to different tasks.

Even though it was already more or less obvious which uncertain input parameters from the suggested list for QUENCH-08 experiment simulations were the most important, another test provided some interesting information. The number of samples in the U&S analysis in the nuclear safety field is usually chosen based on Wilks formula [[Wilks, S.S., 1941](#)]. In this work, using the results of QUENCH-08 simulations with different numbers of samples and results of the 'consistency' test, one could show that this choice is not so easy to make and results of the simulations (Pearson and Spearman correlation coefficients, for example) could be quite

inconsistent, especially for a small number of samples, and that inevitably affects the conclusions made from these results.

The MOCABA algorithm is firstly applied to results of QUENCH-08 simulations to predict the amount of released hydrogen using temperature values from different elevations. Predictions of very different quality have been obtained during this test, but in general results of the MOCABA test of QUENCH-08 simulations showed that this approach is working.

Simulations of KONVOI NPP have been performed for the MBLOCA SA transient. As a result a list of uncertain input parameters has been identified consisting of 16 parameters in total. 14 are related to different ASTEC code models, one parameter governing the leakage rate from containment to annulus (*par41*) and another one governing the burnup (*parBU*). The U&S analysis of the KONVOI simulations shows that regarding the FPs release in the environment the most important input parameters are *par41* and *parBU*. For FPs release into the containment *parBU* is even more important for all elements. Also parameters related to the ELSA model are playing a role for less volatile fission products. But, all these conclusions should be made with enough caution due to the mentioned requirement of additional ‘consistency’ tests. The results of the MBLOCA+SBO scenario simulations are presented in [Appendix C](#).

The MOCABA algorithm has been applied to simulation results of the MBLOCA scenario. From all available FPs only the amount of Xe in the environment has been chosen as a ‘*predictions*’ parameter, and its values are to be predicted using dose rate in the annulus (individual dose rates from different isotopes calculated by ASTEC were summed up). The total dose rate in containment was not considered as ‘*observable*’ parameter due to a sharp decrease in Pearson correlation value between it and the amount of Xe released into environment. The quality of prediction results is different for different samples, and it is still quite difficult to understand the reasons behind the given AREA metric values and their evolution depending on the amount of used measurements.

Additional tests have been made with a simple ‘toy’ example to investigate the limitations of the MOCABA algorithm. Results are presented in [Appendix D](#). It is definitely quite sensitive to correlations between the ‘*predictions*’ and ‘*observables*’ parameters as was expected. The measurements lying outside of the ‘prior’ data range do not always drastically affect the prediction quality, which is probably due to the simplicity of the model. But this investigation is very preliminary and need to be extended.

To conclude, the new first-of-its-kind approach to predict the source term values in real-time based on the MOCABA algorithm has been implemented in the FSTC tool and the training database has been assessed by employing the European reference ASTEC code for ST evaluations in SA simulations. This approach allows to predict the chosen parameter values based on available measured data. The MOCABA algorithm implemented in the FSTC tool has been successfully

applied to QUENCH-08 and KONVOI NPP simulation results and an investigation of its limitations has been initiated. Further testing is required to make clear conclusions about its limitations and potential integration into bigger systems, which are using actual data from detectors.

The U&S analysis part of the FSTC tool (from '*sampling*' to '*uncertainty and sensitivity analysis*' package) after the end of the WAME project was detached and got a new name – Karlsruhe Tool for Uncertainty and Sensitivity Analysis (KATUSA). It is planned to be used in the INR institute in the RPD group as an in-house tool for U&S analysis. A GUI should be developed, to make the tool more user-friendly. A Tkinter framework [Tkinter, 2022] was selected for that task. Preliminary requirements and draft of the GUI were collected in the documents, and implementation of some parts were started to test the collected ideas and selected framework. This work will be continued further. The KATUSA tool has been refactored to be easily couple with other codes. Those changes have been tested on the TwoPorFlow code [Chavez et. al., 2022] during the student internship in RPD group in June-August 2022.

Many sets of simulations have been already performed during work on this thesis for U&S analysis of QUENCH-08 and KONVOI, and this provides a large amount of data which could be further analyzed, for example a deeper investigation about using different correlation coefficients, not only Pearson and Spearman, can be made. Also, more simulations can be performed for KONVOI to check the consistency of results. The further investigation of possible prediction approaches could be continued by using ANNs, for example. ST prediction results could be used as input data for a JRODOS decision support system [Landman et. al., 2014] to evaluate the SA consequences.

References

- Abdel-Khalik, H., Turinsky, P., Jessee, M., Elkins, J., Stover, T., and Iqbal, M. “Uncertainty quantification, sensitivity analysis, and data assimilation for nuclear systems simulation”. *Nuclear Data Sheets*, 109, no. 12 (2008), pp.2785-2790. DOI: <https://doi.org/10.1016/j.nds.2008.11.010>
- Adamov, E.O., Cherkashov, Y.M., and Podlazov, L.N. “Chernobyl accident causes: overview of studies over the decade”. *IAEA International conference – One decade after Chernobyl: Nuclear Safety Aspects, Vienna, Austria, April 1-3, 1996*. 1996, pp. 46-83.
- Alfheim, P. “Definition and evaluation of a dynamic source term module for use within RASTEP: A feasibility study”. Dissertation. Uppsala University, Department of Physics and Astronomy, 2012. URN: <urn:nbn:se:uu:diva-177253>
- Alfonsi, A., Rabiti, C., Mandelli, D., Cogliati, J.J., Wang, C., Talbot, P.W., Maljovec, D.P., Smith, C., and Abdo, G. Mohammad. “RAVEN Theory Manual”. *Idaho National Lab, INL/EXT-16-38178, Revision 4* (2022a).
- Alfonsi, A., Rabiti, C., Mandelli, D., Cogliati, J.J., Wang, C., Talbot, P.W., Zhou, J., Burli, P., and Abdo G. Mohammad. “RAVEN User Manual”. *Idaho National Lab, INL/EXT-18-44465, Revision 1* (2022b).
- Antcheva, I., Ballintijn, M., Bellenot, B., Biskup, M., Brun, R., Buncic, N., Canal, P., Casadei, D., Couet, O., Fine, V., and Franco, L. “ROOT—A C++ framework for petabyte data storage, statistical analysis and visualization”. *Computer Physics Communications*, 180, no. 12 (2009), pp.2499-2512. DOI: <https://doi.org/10.1016/j.cpc.2009.08.005>
- Asmolov, V. and Tsurikov, D. “MASCA project: major activities and results”. *OECD/CSNI Workshop, MASCA Seminar 2004, Aix-en-Provence, France, 10-11 June 2004*. 2004.
- Atkhen, K., Dru, J., and Laroche, Y. “An Overview of Severe Accident Approach at EDF—Contribution of R&D Programs”. *In the Proceedings of the 20th Pacific Basin Nuclear Conference, Beijing, China, April 2016*, Volume 1, pp. 97-117 (2016). ISBN: 978-981-10-2311-8.
- Bandini, G., Gauntt, R.O., Okkonen T., Suh K. Y., Sheperd I., and Linnemann T. “Molten material relocation into the lower plenum: A status report”. *ENEA, NEA/CSNI/R(97)34 Technical Report* (1998).
- Barrachin, M., De Luze, O., Haste, T., and Repetto, G., 2013. “Late phase fuel degradation in the Phébus FP tests”. *Annals of Nuclear Energy*, 61, (2013), pp.36-53. DOI: <https://doi.org/10.1016/j.anucene.2013.03.041>
- Belon, S., Carenini, L., Chatelard, P., Coindreau, O., and Topin, V. “Draft Manual for ASTEC V2.1: ICARE Module. User manual”. *IRSN, PSN-RES. SAG/2016-00421 Technical report* (2017a).
- Belon, S., Bouillet, C., Topin, V., Bonneville, H., Andrews, N., and Faucett, C. “Insight of core degradation simulation in integral codes throughout ASTEC/MELCOR crosswalk comparisons and ASTEC sensitivity studies”. *In the Proceedings of the 8th European Review Meeting on Severe Accident Research – ERMSAR 2017, Warsaw, Poland, 16-18 May, 2017*. 2017b. Paper 611.
- Blanchard, J.B., Damblin, G., Martinez, J.M., Arnaud, G., and Gaudier, F. “The Uranie platform: an open-source software for optimisation, meta-modelling and uncertainty analysis”. *arXiv preprint arXiv:1803.10656* (2018). DOI: <https://doi.org/10.48550/arXiv.1803.10656>
- Bocanegra Melián, R. “Towards a BEPU methodology for containment safety analyses” Dissertation, Polytechnic University of Madrid (UPM), Department of Ingeniería Energética, 2019. DOI: <https://doi.org/10.20868/UPM.thesis.55578>
- Bonnet, J.M., Cranga, M., Vola, D., Marchetto, C., Kissane, M., Robledo, F., Farmer, M.T., Spengler, C., Basu, S., Atkhen, K., and Fargette, A. “State-of-the-Art Report on Molten Corium

- Concrete Interaction and Ex-Vessel Molten Core Coolability”. *OECD NEA, NEA/CSNI/R(2016)15, Technical Report* (2017).
- Boyack, B.E., Catton, I., Duffey, R.B., Katsma, K.R., Lellouche, G.S., Levy, S., Wilson, G.E., and Zuber, N. “Quantifying reactor safety margins part 1: an overview of the code scaling, applicability, and uncertainty evaluation methodology”. *Nuclear Engineering and Design*, 119, no. 1 (1990), pp.1-15. DOI: [https://doi.org/10.1016/0029-5493\(90\)90071-5](https://doi.org/10.1016/0029-5493(90)90071-5)
- Bouttier, F. and Courtier, P. “Data assimilation concepts and methods March 1999”. European Center for Medium-Range Weather Forecasts (ECMWF), Meteorological training course lecture series, Lecture notes (2001).
- Brillant, G., Marchetto, C., and Plumecocq, W. “Fission product release from nuclear fuel I. Physical modelling in the ASTEC code”. *Annals of Nuclear Energy*, 61, (2013a), pp.88-95. DOI: <https://doi.org/10.1016/j.anucene.2013.03.022>
- Brillant, G., Marchetto, C., and Plumecocq, W. “Fission product release from nuclear fuel II. Validation of ASTEC/ELSA on analytical and large scale experiments”. *Annals of Nuclear Energy*, 61, (2013b), pp.96-101. DOI: <https://doi.org/10.1016/j.anucene.2013.03.045>
- Buck, M., Bürger, M., Miassoedov, A., Gaus-Liu, X., Palagin, A., Godin-Jacqmin, L., Tran, C.T., Ma, W.M., and Chudanov, V. “The LIVE program—Results of test L1 and joint analyses on transient molten pool thermal hydraulics”. *Progress in Nuclear Energy*, 52, no. 1 (2010), pp.46-60. DOI: <https://doi.org/10.1016/j.pnucene.2009.09.007>
- Cantrel, L., Cousin, F., Bosland, L., Chevalier-Jabet, K., and Marchetto, C. “ASTEC V2 severe accident integral code: Fission product modelling and validation”. *Nuclear Engineering and Design*, 272 (2014), pp.195-206. DOI: <https://doi.org/10.1016/j.nucengdes.2014.01.011>
- Castro, E., Ahnert, C., Buss, O., Garcia-Herranz, N., Hofer, A., and Porsch, D. “Improving PWR core simulations by Monte Carlo uncertainty analysis and Bayesian inference”. *Annals of Nuclear Energy*, 95 (2016), pp.148-156. DOI: <https://doi.org/10.1016/j.anucene.2016.05.007>
- Chailan, L., Bosland, L., Carénini, L., Chambarel, J., Cousin, F., Chatelard, P., Draï, P., Kioseyan, G., Phoudiah, S., and Topin, V. “Overview of ASTEC integral code status and perspectives”. In *the Proceedings of the 9TH European Review Meeting on Severe Accident Research – ERMSAR-2019, Prague, Czech Republic, 18-20 March 2019*. 2019. Paper 096, pp. 18-20.
- Chatelard, P. and Laborde, L. “Synthesis of the ASTEC V2.2 code validation vs. experimental data”. In *the Proceedings of the 10th European Review Meeting on Severe Accident Research – ERMSAR-2022, Karlsruhe, Germany, 16-19 May, 2022*. 2022. Paper 302, pp. 1609-1620.
- Chauliac, C., Janot, L., Jouzier, A., and Rague, B. “Diagnosis and prognosis of the source term by the French Safety Institut during an emergency on a PWR”. *Training in management and analysis of severe accidents, Budapest, Hungary, 13-24 January, 1992*. 1992. INIS-MF-13573.
- Chavez, V.J., Imke, U., and Sanchez-Espinoza, V.H. “Implementation and validation of CHF-models in the two-phase porous-media code TWOPORFLOW”. *Nuclear Engineering and Design*, 388, 111631 (2022). DOI: <https://doi.org/10.1016/j.nucengdes.2021.111631>
- Choi, Y., Jeong, K.S., and Park, S. “Severe Accident Management using PSA Event Tree Technology”. *International Journal of Safety*, 2, no. 1 (2003), pp.50-56.
- CMake (2022). *CMake – Build with CMake. Build with Confidence*. URL: <https://cmake.org/> (Accessed: 04.04.2023).
- Coindreau, O. “ASTEC V2. 1: physical modelling of the ICARE module”. *IRSN, PSNRES/SAG/2016-00422 Technical report* (2017).
- Coryell, E.W. “Summary of important results and SCDAP/RELAP5 analysis for OECD LOFT experiment LP-FP-2”. *Nuclear Regulatory Commission, NUREG/CR-6160, Technical Report* (1994). DOI: <https://doi.org/10.2172/10147963>

- Crestaux, T., Le Maître, O., and Martinez, J.M. “Polynomial chaos expansion for sensitivity analysis”. *Reliability Engineering & System Safety*, 94, no. 7 (2009), pp.1161-1172. DOI: <https://doi.org/10.1016/j.ress.2008.10.008>
- Crichton, M.T., and Flin, R. “Identifying and training non-technical skills of nuclear emergency response teams”. *Annals of Nuclear Energy*, 31, no. 12 (2004), pp.1317-1330. DOI: <https://doi.org/10.1016/j.anucene.2004.03.011>
- Czech, J., Feigel, A., Meyer, P.J., and Kremayr, A. “Technical information on design features of Siemens Konvoi PWR”. IAEA, IAEA-TECDOC-861, Technical Report (1996).
- Dalbey, K., Eldred, M., Geraci, G., Jakeman, J., Maupin, K., Monschke, J.A., Seidl, D., Tran, A., Menhorn, F., and Zeng, X. “Dakota, A Multilevel Parallel Object-Oriented Framework for Design Optimization, Parameter Estimation, Uncertainty Quantification, and Sensitivity Analysis: Version 6.16 Theory Manual”. *Sandia National Lab, SAND2022-6172, Technical Report* (2022).
- D’auria, F., Debrecin, N., and Galassi, G.M. “Outline of the uncertainty methodology based on accuracy extrapolation”. *Nuclear technology*, 109, no. 1 (1995), pp.21-38. DOI: <https://doi.org/10.13182/NT109-21>
- D'auria, F.S., Dusic, M., Dutton LM, C., Fry, C., Glaeser, H., Kim I, G., Lee S, H., Mavko, B., Pelayo, F., Petruzzi, A., and Sandervag, O. “Deterministic Safety Analysis for Nuclear Power Plants. IAEA Specific Safety Guide”. IAEA, *IAEA Safety Standards Series* (2009). ISBN: 978-92-0-113309-0.
- D’auria, F., Camargo, C., and Mazzantini, O. “The Best Estimate Plus Uncertainty (BEPU) approach in licensing of current nuclear reactors”. *Nuclear Engineering and Design*, 248 (2012), pp.317-328. DOI: <https://doi.org/10.1016/j.nucengdes.2012.04.002>
- DataCamp (2022). *Docstrings in Python*. URL: <https://www.datacamp.com/community/tutorials/docstrings-python> (Accessed: 04.04.2023).
- Dedda, F. “Definition of a dynamic source term module within RASTEP: Linking with a fast running deterministic code”. Dissertation. Chalmers University of Technology, Department of Applied Physics, 2013. ISSN 1653-4662.
- Deutsch, J.L., and Deutsch, C.V. “Latin hypercube sampling with multidimensional uniformity”. *Journal of Statistical Planning and Inference*, 142, no. 3 (2012), pp.763-772. DOI: <https://doi.org/10.1016/j.jspi.2011.09.016>
- Dinh, T.N., Bui, V.A., Nourgaliev, R.R., Green, J.A., and Sehgal, B.R. “Experimental and analytical studies of melt jet-coolant interactions: a synthesis”. *Nuclear engineering and design*, 189, no. 1-3 (1999), pp.299-327. DOI: [https://doi.org/10.1016/S0029-5493\(98\)00275-1](https://doi.org/10.1016/S0029-5493(98)00275-1)
- Eldred, M.S., Bohnhoff, W.J., and Hart, W.E. “DAKOTA, A multilevel parallel object-oriented framework for design optimization, parameter estimation, sensitivity analysis, and uncertainty quantification”. *Sandia National Lab, SAND99-0000, Technical Report* (1999).
- Elsalamouny, N. and Kaliasatka, T. “Uncertainty Quantification of the PHEBUS FPT-1 Test Modelling Results”. *Energies*, 14, no. 21, 7320 (2021). DOI: <https://doi.org/10.3390/en14217320>
- Frepoli, C. and Iyengar, S. “A comparison of non-parametric tolerance limits with linear combinations of order statistics in safety analysis”. *In the Proceedings of the International Congress on Advances in Nuclear Power Plants – ICAPP-2011, Nice, France, 2-5 May 2011*. 2011, pp. 1392-1401.
- Frigo, M. and Johnson, S.G. “The design and implementation of FFTW3”. *Proceedings of the IEEE*, 93, no. 2 (2005), pp.216-231. DOI: <https://doi.org/10.1109/JPROC.2004.840301>
- Gabrielli, F., Sanchez-Espinoza, V. H. “Uncertainty and Sensitivity Analysis by means of ASTEC/URANIE Platform of the QUENCH-08 Experiment”. *In the Proceedings of the 24th International QUENCH Workshop, Karlsruhe, Germany, November 2018*. 2018, pp. 354-375.

Gabrielli, F., Sanchez-Espinoza V. H., Stakhanova, A., Hoefler, A., and Pauli, E. “Source term evaluation following MBLOCA and SBLOCA scenarios in a generic KONVOI-1300 NPP by means of the ASTEC code”. In *the Proceedings of the EUROSAFE-2021, Paris, France 22-23 November, 2021*.

Gabrielli, F., Sanchez Espinoza, V.-H., Stakhanova, A., Hoefler, A., Pauli, E.-M., and Feldmann, H. “Impact of Realistic Fuel Inventories on the Radiological Consequences of a Severe Accident Scenario in a Generic Konvoi Plant by Means of the ASTEC Code”. In *the Proceedings of the KERNTECHNIK 2022, Leipzig, Germany, 21-22 June, 2022*.

Gao, P., Zhang, B., Li, J., and Shan, J. “Development of mechanistic cladding rupture model for severe accident analysis and application in PHEBUS FPT3 experiment”. *Nuclear Engineering and Technology*, 54, no. 1 (2022), pp. 138-151. DOI: <https://doi.org/10.1016/j.net.2021.07.029>

Gómez-García-Toraño, I. “Further development of Severe Accident Management Strategies for a German PWR Konvoi Plant based on the European Severe Accident Code ASTEC”. Dissertation, Karlsruher Institut für Technologie, Fakultät für Maschinenbau, 2017. DOI: 10.5445/IR/100073683.

Gómez-García-Toraño, I., Sánchez-Espinoza, V.H., Stieglitz, R., Stuckert, J., Laborde, L., and Belon, S. “Validation of ASTECV2. 1 based on the QUENCH-08 experiment”. *Nuclear Engineering and Design*, 314 (2017), pp.29-43. DOI: <https://doi.org/10.1016/j.nucengdes.2016.12.039>

Gómez-García-Toraño, I., Laborde, L., Fichot, F., and Mutelle, H. “Reflooding of degraded cores in ASTEC V2. 1: Modelling and validation on PEARL experiments”. *Nuclear Engineering and Design*, 393, 111768 (2022). DOI: <https://doi.org/10.1016/j.nucengdes.2022.111768>

Girault, N., Bosland, L., Dickinson, S., Funke, F., Güntay, S., Herranz, L.E., and Powers, D. “LWR severe accident simulation: Iodine behaviour in FPT2 experiment and advances on containment iodine chemistry”. *Nuclear Engineering and Design*, 243 (2012), pp.371-392. DOI: <https://doi.org/10.1016/j.nucengdes.2011.11.011>

Glaeser, H. “Results from the application of uncertainty methods in the CSNI uncertainty methods study (UMS)”. In *the Proceedings of the Seminar on the transfer of competence, knowledge and experience gained through CSNI activities in the field of thermal-hydraulics, Pisa, Italy, 5-9 May, 2008*. 2008a, pp. 305-316.

Glaeser, H. “GRS method for uncertainty and sensitivity evaluation of code results and applications”. *Science and Technology of Nuclear Installations*, 2008, 798901 (2008b). DOI: <https://doi.org/10.1155/2008/798901>

Glaeser, H. “Summary of existing uncertainty methods”. Presented on *OECD/CSNI Workshop on Best Estimate Methods and Uncertainty Evaluations; Barcelona, Spain, 16-18 November 2011, NEA-CSNI-R-2013-8*. 2013.

Grindon, E. and Kinniburgh, C.G. “SPRINT: a tool for probabilistic source term prediction for use with decision support systems”. *Radiation protection dosimetry*, 109, no. 1-2 (2004), pp.35-39. DOI: <https://doi.org/10.1093/rpd/nch267>

Hage, M. and Löffler, H. “A probabilistic approach for source term prediction in case of severe accidents”. In *the Proceedings of the 13th International Conference on Probabilistic Safety Assessment and Management – PSAM 13, Seoul, Korea, 2-7 October, 2016*.

Hage, M., Kowalik, M., and Johst, S. “Source Term Prediction Software in Case of Severe Accidents: FaSTPro for Shutdown States”. In *the Proceedings of the 13th International Conference on Probabilistic Safety Assessment and Management – PSAM-14, Los Angeles, USA, September 2018*.

Haste, T., Payot, F., Manenc, C., Clément, B., March, P., Simondi-Teisseire, B., and Zeyen, R. “Phébus FPT3: overview of main results concerning the behaviour of fission products and structural materials in the containment”. *Nuclear Engineering and Design*, 261 (2013), pp.333-345. DOI: <https://doi.org/10.1016/j.nucengdes.2012.09.034>

Helton, J.C., Iman, R.L., Johnson, J.D., and Leigh, C.D. “Uncertainty and sensitivity analysis of a model for multicomponent aerosol dynamics”. *Nuclear technology*, 73, no. 3 (1986), pp.320-342. DOI: <https://doi.org/10.13182/NT86-A16075>

Herviou, K. and Calmtorp, C. “Methodology and tools for source term assessment in case of emergency”. *Radiation protection dosimetry*, 109, no. 1-2 (2004), pp.53-57. DOI: <https://doi.org/10.1093/rpd/nch244>

Herviou, K. “Development of a methodology and of a computer tool for source term estimation in case of nuclear emergency in a light water reactor (ASTRID)”. *IRSN, ASTRID/04.39 v1.1, Technical report*, (2005).

Hofer, A., Buss, O., and Neuber, J.C. “How confident can we be in confidence intervals for the computational bias obtained with the generalized linear least squares methodology?-a toy model analysis”. *In the Proceedings of the Ninth International Conference on Nuclear Criticality – ICNC2011. Edinburgh, Scotland, 19-22 September, 2011.*

Hofer, A., Buss, O., Hennebach, M., Schmid, M. and Porsch, D. “MOCABA: A general Monte Carlo–Bayes procedure for improved predictions of integral functions of nuclear data”. *Annals of Nuclear Energy*, 77 (2015), pp.514-521. DOI: <https://doi.org/10.1016/j.anucene.2014.11.038>

Hofmann, P., Stuckert, J., Miassoedov, A., Veshchunov, M.S., Berdyshev, A.V., and Boldyrev, A.V. “ZrO₂ dissolution by molten Zircaloy and cladding oxide shell failure. New experimental results and modelling”. *Forschungszentrum Karlsruhe, FZKA 6383, Technical report* (1999).

Honga, I.S., Oh, D.Y., and Kim, I.G. “Generic Application of Wilks’ Tolerance Limit Evaluation Approach to Nuclear Safety”. *In the Proceedings of the OECD/CSNI Workshop on Best Estimate Methods and Uncertainty Evaluations, Barcelona, Spain, 16-18 November, 2011.* 2011, pp. 16-25.

Humphries, L.L., Figueroa, V.G., Young, M.F., Louie, D., and Reynolds, J.T. “MELCOR Computer Code Manuals”. *Sandia National Lab, SAND-2015-6692R, Technical report* (2015). DOI: <https://doi.org/10.2172/1433918>

Humphries, L.L. “Quicklook overview of model changes in MELCOR 2.2: Rev 6342 to Rev 9496”. *Sandia National Lab, SAND2017-5599, Technical report* (2017). DOI: <https://doi.org/10.2172/1367442>

Ikeda, T., Terada, M., Karasawa, H., Nakahara, K., and Yamagishi, M. “Analysis of core degradation and fission products release in Phebus FPT1 test at IRSN by detailed severe accidents analysis code, IMPACT/SAMPSON”. *Journal of nuclear science and technology*, 40, no. 8 (2003), pp.591-603. DOI: [10.1080/18811248.2003.9715396](https://doi.org/10.1080/18811248.2003.9715396)

Ikonen, T. and Tulkki, V. “The importance of input interactions in the uncertainty and sensitivity analysis of nuclear fuel behavior”. *Nuclear Engineering and Design*, 275 (2014), pp.229-241. DOI: <https://doi.org/10.1016/j.nucengdes.2014.05.015>

Ikonen, T. “Comparison of global sensitivity analysis methods–application to fuel behavior modeling”. *Nuclear Engineering and Design*, 297 (2016), pp.72-80. DOI: <https://doi.org/10.1016/j.nucengdes.2015.11.025>

Iman, R.L. and Conover, W.J. “A distribution-free approach to inducing rank correlation among input variables”. *Communications in Statistics-simulation and Computation*, 11, no. 3 (1982), pp.311-334. DOI: <https://doi.org/10.1080/03610918208812265>

International Atomic Energy Agency (IAEA). “Generic assessment procedures for determining protective actions during a reactor accident”. *IAEA, IAEA-TECDOC-955, Technical report* (1997).

International Atomic Energy Agency (IAEA). “Severe accident management programmes for nuclear power plants”, *IAEA, IAEA Safety Standards Series No. NS-G-2.15, Safety guide* (2009).

International Nuclear Safety Advisory Group (INSAG). “Radionuclide Source Terms from Severe Accidents to Nuclear Power Plants with Light Water Reactors”. *IAEA, 75-INSAG-2, Technical report* (1987).

International Nuclear Safety Advisory Group (INSAG). “Basic Safety Principles for Nuclear Power Plants”. *IAEA, 75-INSAG-3, Technical report* (1988).

International Nuclear Safety Advisory Group (INSAG). “Probabilistic Safety Assessment”. *IAEA, 75-INSAG-6, Technical report* (1992).

International Nuclear Safety Advisory Group (INSAG). “Defence in Depth in Nuclear Safety”. *IAEA, INSAG-10, Technical report* (1996).

Itoh, A., Kobayashi, Y., Suzuki, A., Sato, T., Shirasu, N., Nagae, Y., and Kurata, M. “Thermodynamic approach for determination of fuel relocation condition in severe accident progression”. *Journal of Nuclear Materials*, 529, 151925 (2020). DOI: <https://doi.org/10.1016/j.jnucmat.2019.151925>

Jekel, C.F., Venter, G., Venter, M.P., Stander, N., and Haftka, R.T. “Similarity measures for identifying material parameters from hysteresis loops using inverse analysis”. *International Journal of Material Forming*, 12, no. 3 (2019), pp.355-378. DOI: <https://doi.org/10.1007/s12289-018-1421-8>

Jones, A.V., Dickinson, S., De Pascale, C., Hanniet, N., Herranz, L., De Rosa, F., Hennes, G., Langhans, J., Housiadas, C., Wichers, V., and Birchley, J. “Validation of severe accident codes against Phebus FP for plant applications: status of the PHEBEN2 project”. *Nuclear Engineering and Design*, 221, no. 1-3 (2003), pp.225-240. DOI: [https://doi.org/10.1016/S0029-5493\(02\)00340-0](https://doi.org/10.1016/S0029-5493(02)00340-0).

Kaliatka, T., Kaliatka, A., and Vileiniskis, V. “Application of best estimate approach for modelling of QUENCH-03 and QUENCH-06 experiments”. *Nuclear Engineering and Technology*, 48, no. 2 (2016), pp.419-433. DOI: <https://doi.org/10.1016/j.net.2015.12.011>

Kang, K.H., Bae, B.U., Kim, J.R., Park, Y.S., Lee, S.W., Song, C.H., and Choi, K.Y. “Development of a phenomena identification ranking table for simulating a station blackout transient of a pressurized water reactor with a thermal-hydraulic integral effect test facility”. *Annals of Nuclear Energy*, 75 (2015), pp.72-78. DOI: <https://doi.org/10.1016/j.anucene.2014.07.050>

Kim, H., Jo, S., Kim, J., Park, G., and Kim, J. “Development of Long-Term Prediction Algorithm Based on Component States Using BiLSTM and Attention Mechanism”. *In the Proceedings of the 5th International Conference on System Reliability and Safety (ICSRS), Palermo, Italy, 24-26 November 2021*. 2021, pp. 258-264. DOI: <https://doi.org/10.1109/ICSRS53853.2021.9660631>

Kinney, J.B. and Atwal, G.S. “Equitability, mutual information, and the maximal information coefficient”. *Proceedings of the National Academy of Sciences*, 111, no. 9 (2014), pp.3354-3359. DOI: <https://doi.org/10.1073/pnas.1309933111>

Kiselev, A.E. “Codes for NPP severe accident simulation: development, validation and applications”. *Journal of Nuclear Science and Technology*, 5, no. 2 (2015), pp.7-14. DOI: <https://doi.org/10.53747/jnst.v5i2.188>

Kloos, M. “Main features of the tool SUSA 4.0 for uncertainty and sensitivity analyses”. *In the Proceedings of the 1st International Conference on Uncertainty Quantification in Computational Sciences and Engineering (UNCECOMP 2015), Crete Island, Greece, 25-27 May 2015*. 2015, pp. 25-27. ISBN: 978-960-99994-9-6.

Knochenhauer, M., Swaling, V.H., and Alfheim, P. “Using Bayesian Belief Network (BBN) modelling for Rapid Source Term Prediction. RASTEP Phase 1”. *Nordic nuclear safety research (NKS), NKS-267, Technical report* (2012). ISBN: 978-87-7893-340-9.

Kozbar, V., Voltcheck, A., Tarlakovskaya, E., Yegorova, L., and Zvonarev, Y. “Uncertainty and Sensitivity Analysis of CORA-W2 test using ICARE2/SUNSET tool”. *Nuclear Safety Institute of*

Russian Research Centre “Kurchatov Institute” (NRC KI), NSI RRC KI 2127, Technical report (1997).

Kuschel, D. and Zeitner, W. “Design procedure for the primary circuit of the Konvoi plants”. *Nuclear engineering and design*, 130, no. 3 (1991), pp.451-457. DOI: [https://doi.org/10.1016/0029-5493\(91\)90235-A](https://doi.org/10.1016/0029-5493(91)90235-A)

Landman, C., Päsler-Sauer, J., and Raskob, W. “The decision support system RODOS”. In “*The Risks of Nuclear Energy Technology*”, Springer, Berlin, Heidelberg, 2014, pp. 337-348. ISBN: 978-3-642-55115-4.

Lee, J.C. and McCormick, N.J. “Risk and safety analysis of nuclear systems”. *John Wiley & Sons, Hoboken, New Jersey, Canada*, 2011 ISBN: 978-1-118-4346-2.

Lee, S.W., Chung, B.D., Bang, Y.S., and Bae, S.W. “Analysis of uncertainty quantification method by comparing Monte-Carlo method and Wilks’ formula”. *Nuclear engineering and Technology*, 46, no. 4 (2014), pp.481-488. DOI: <https://doi.org/10.5516/NET.02.2013.047>

Li, Y., Chen, R., Guo, K., Tian, W., Qiu, S., and Su, G.H. “Numerical analysis of the dissolution of uranium dioxide by molten zircaloy using MPS method”. *Progress in Nuclear Energy*, 100 (2017), pp.1-10. DOI: <https://doi.org/10.1016/j.pnucene.2017.05.022>

Liu, F., Sun, Z., Ding, M., and Bian, H. “Research progress of hydrogen behaviors in nuclear power plant containment under severe accident conditions”. *International Journal of Hydrogen Energy*, 46, no. 73 (2021), pp.36477-36502. DOI: <https://doi.org/10.1016/j.ijhydene.2021.08.151>

Luxat, D.L., Kalanich, D.A., Hanophy, J.T., Gauntt, R.O., and Wachowiak, R.M. “MAAP-MELCOR crosswalk phase 1 study”. *Nuclear Technology*, 196, no. 3 (2016), pp.684-697. DOI: <https://doi.org/10.13182/NT16-57>

Maccari, P., Mascari, F., Ederli, S., and Manservigi, S. “SBO analysis of a generic PWR-900 with ASTEC and MELCOR codes”. *Journal of Physics: Conference Series*, 1868, no. 1 (2021), 012019. DOI: <https://doi.org/10.1088/1742-6596/1868/1/012019>

Manesse, D. and Crabol, B. “Assessment of the radiological consequences in case of an emergency on a nuclear installation”. *CEA Centre d'Etudes Nucleaires de Fontenay-aux-Roses, CEA-DAS-467, Technical report* (1988).

Mao, J.F., Zhu, J.W., Bao, S.Y., Luo, L.J., and Gao, Z.L. “Creep deformation and damage behavior of reactor pressure vessel under core meltdown scenario”. *International Journal of Pressure Vessels and Piping*, 139-140 (2016), pp.107-116. DOI: <https://doi.org/10.1016/j.ijpvp.2016.03.009>

Martin, R.P. and O’Dell, L.D. “AREVA’s realistic large break LOCA analysis methodology”. *Nuclear Engineering and Design*, 235, no. 16 (2005), pp.1713-1725. DOI: <https://doi.org/10.1016/j.nucengdes.2005.02.004>

Martinez-Gomez, E., Richards, M.T., and Richards, D.S.P. “Distance correlation methods for discovering associations in large astrophysical databases”. *The Astrophysical Journal*, 781, no. 1 (2014), pp.39-49. DOI: <https://doi.org/10.1088/0004-637X/781/1/39>

McKay M. D., Beckman R. J., and Conover W. J. “A Comparison of Three Methods for Selecting Values of Input Variables in the Analysis of Output from a Computer Code”. *Technometrics*, 21, pp. 239-245 (1979). DOI: <https://doi.org/10.1080/00401706.2000.10485979>

Meignen, R., Raverdy, B., Picchi, S., and Lamome, J. “The challenge of modeling fuel-coolant interaction: Part II—Steam explosion”. *Nuclear Engineering and Design*, 280 (2014), pp.528-541. DOI: <https://doi.org/10.1016/j.nucengdes.2014.08.028>

Meyer, L., Albrecht, G., Kirstahler, M., Schwall, M., and Wachter, E. “Large scale separate effects tests on hydrogen combustion during direct containment heating events”. *Karlsruher Institut für Technologie, KIT-SR 7663, Technical report*, (2014). ISBN: 978-3-7315-0559-9.

Minato, K., Hering, W., and Hagen, S. “Zircaloy oxidation and cladding deformation in PWR-specific CORA experiments”. *Kernforschungszentrum Karlsruhe, KfK 4827, Technical report* (1991). ISSN 0303-4003.

Minepy (2022). *Minepy – Maximal Information-based Nonparametric Exploration*. URL: <https://minepy.readthedocs.io/en/latest/> (Accessed: 04.04.2023).

Norsys Software Corp. (2022). *Netica application*. URL: <https://www.norsys.com/netica.html> (Accessed: 04.04.2023).

Nowack, H., Chatelard, P., Chailan, L., Sanchez, V., and Herranz, L. “CESAM–Code for European severe accident management, EURATOM project on ASTEC improvement”. *Annals of Nuclear Energy*, 116 (2018), pp.128-136. DOI: <https://doi.org/10.1016/j.anucene.2018.02.021>

Nuclear Regulatory Commission (NRC). “State-of-the-Art Reactor Consequence Analyses Project: Uncertainty Analysis of the Unmitigated Long-Term Station Blackout of the Peach Bottom Atomic Power Station”. *Nuclear Regulatory Commission, NUREG/CR-7155, SAND2012-10702P, Technical report* (2012).

Nuclear Regulatory Commission (NRC). “*State-of-the-art reactor consequence analyses (SOARCA) project: Sequoyah integrated deterministic and uncertainty analyses*”. Nuclear Regulatory Commission, NUREG/CR-7245, Technical report (2018).

Nuclear Regulatory Commission (NRC) (2022). *Emergency classification*. URL: <https://www.nrc.gov/about-nrc/emerg-preparedness/about-emerg-preparedness/emerg-classification.html> (Accessed: 04.04.2023).

Pastore, G., Swiler, L.P., Hales, J.D., Novascone, S.R., Perez, D.M., Spencer, B.W., Luzzi, L., Van Uffelen, P., and Williamson, R.L. “Uncertainty and sensitivity analysis of fission gas behavior in engineering-scale fuel modeling”. *Journal of Nuclear Materials*, 456 (2015), pp.398-408. DOI: <https://doi.org/10.1016/j.jnucmat.2014.09.077>

Pearl, J. and Russel S. "Bayesian networks". UCLA Cognitive Systems Laboratory, R-277, Technical Report (2000).

Pederngana, M. and García, S.G. “Smart sampling and incremental function learning for very large high dimensional data”. *Neural Networks*, 78 (2016), pp.75-87. DOI: <https://doi.org/10.1016/j.neunet.2015.09.001>

Peltier, J. “Severe accidents research at IPSN”. *In the Proceedings of the workshop on severe accident research held in Japan (SARJ-98), Tokyo, Japan, 4-6 November, 1998*. 1999, pp. 15-17

Pontillon, Y., Malgouyres, P.P., Ducros, G., Nicaise, G., Dubourg, R., Kissane, M., and Baichi, M. “Lessons learnt from VERCORS tests: Study of the active role played by UO₂–ZrO₂–FP interactions on irradiated fuel collapse temperature”. *Journal of nuclear materials*, 344, no. 1-3 (2005), pp.265-273. DOI: <https://doi.org/10.1016/j.jnucmat.2005.04.053>

Povilaitis, M., Kelm, S., and Urbonavičius, E. “The Generic Containment SB-LOCA accident simulation: Comparison of the parameter uncertainties and user-effect”. *Annals of Nuclear Energy*, 106 (2017), pp.1-10. DOI: <https://doi.org/10.1016/j.anucene.2017.03.037>

ReStructuredText (2022). *reStructuredText – Markup syntax and parser component of Docutils*. URL: <https://docutils.sourceforge.io/rst.html> (Accessed: 04.04.2023).

Rocchi, F., Devol-Brown, I., and Raskob, W. “Nuclear and radiological emergency management and preparedness”. *EPJ Nuclear Sciences & Technologies*, 6, no. 37 (2020). DOI: <https://doi.org/10.1051/epjn/2019011>

Saghafi, M. and Ghofrani, M.B. “Accident management support tools in nuclear power plants: a post-Fukushima review”. *Progress in nuclear energy*, 92, pp.1-14 (2016). DOI: <https://doi.org/10.1016/j.pnucene.2016.06.006>

Salay, M. and Fichot, F. “Modelling of corium stratification in the lower plenum of a reactor vessel”. *In the Proceedings of the MASCA Seminar, Aix-en-Provence, France, 10-11 June, 2004*.

SampleVis (2022). *SampleVis – Simple tool for sample visualization for sensitivity analysis*. URL: <https://github.com/charlesrouge/SampleVis> (Accessed: 04.04.2023).

Santhosh, T.V., Mohan, A., Vinod, G., Thangamani, I., and Chattopadhyay, J. “Source-Term Prediction During Loss of Coolant Accident in NPP Using Artificial Neural Networks”. In *the Proceedings of the 4th International Conference on Reliability, Safety and Hazard, Chennai, India, 10-13 January, 2019*. 2020, pp. 81-95. ISSN: 2195-4356. DOI: <https://doi.org/10.1007/978-981-13-9008-1>

Schanz, G., Adroguer, B., and Volchek, A. “Advanced treatment of Zircaloy cladding high-temperature oxidation in severe accident code calculations: Part I. Experimental database and basic modeling”. *Nuclear Engineering and Design*, 232, no. 1 (2004), pp.75-84. DOI: <https://doi.org/10.1016/j.nucengdes.2004.02.013>

SciPy (2022). *SciPy – Fundamental algorithms for scientific computing in Python*. URL: <https://scipy.org/> (Accessed: 04.04.2023).

Sehgal, B.R., Nourgaliev, R.R., Dinh, T.N., and Karbojian, A. “Integral experiments on in-vessel coolability and vessel creep: results and analysis of the FOREVER-C1 test” In *the Proceedings of the workshop on severe accident research held in Japan (SARJ-98), Tokyo, Japan, 4-6 November, 1998*, pp. 87-93.

Sehgal, B.R. “*Nuclear safety in light water reactors: severe accident phenomenology*”. Academic Press, Cambridge, USA, 2012. ISBN: 978-0-12-388446-6.

Sheikholeslami, R. and Razavi, S. “Progressive Latin Hypercube Sampling: An efficient approach for robust sampling-based analysis of environmental models”. *Environmental Modelling & Software*, 93 (2017), pp.109-126. DOI: <https://doi.org/10.1016/j.envsoft.2017.03.010>

Similaritymeasures (2022). *Similaritymeasures 0.4.4 – Quantify the difference between two arbitrary curves in space*. URL: <https://pypi.org/project/similaritymeasures/> (Accessed: 04.04.2023).

Song, K.W., Kim, K.S., Kim, Y.M., and Jung, Y.H. “Sintering of mixed UO₂ and U₃O₈ powder compacts”. *Journal of nuclear materials*, 277, no. 2-3 (2000), pp.123-129. DOI: [https://doi.org/10.1016/S0022-3115\(99\)00212-3](https://doi.org/10.1016/S0022-3115(99)00212-3)

Sphinx (2022). *Sphinx – Python documentation generator*. URL: <https://www.sphinx-doc.org/en/master/> (Accessed: 04.04.2023).

Stakhanova, A., Gabrielli, F., Sanchez-Espinoza V. H., Hoefler, A., and Pauli, E. “Uncertainty and sensitivity analysis of the QUENCH-08 experiment using the FSTC tool”. *Annals of Nuclear Energy*, 169, 108968 (2022a). DOI: <https://doi.org/10.1016/j.anucene.2022.108968>

Stakhanova, A., Gabrielli, F., Sanchez-Espinoza V. H., Hoefler, A., and Pauli, E. “Preliminary uncertainty and sensitivity analysis of the ASTEC simulations results of a MBLOCA scenario in a generic KONVOI plant by using the FSTC tool”. In *the Proceedings of the 10th European Review Meeting on Severe Accident Research – ERMSAR-2022, Karlsruhe, Germany, 16-19 May, 2022*. 2022b. Paper 327, pp. 861-871.

Steinbrück, M., Große, M., Sepold, L., and Stuckert, J. “Synopsis and outcome of the QUENCH experimental program”. *Nuclear Engineering and Design*, 240, no. 7 (2010), pp.1714-1727. DOI: <https://doi.org/10.1016/j.nucengdes.2010.03.021>

Stuckert, J., Boldyrev, A.V., and Miassoedov, A. “Experimental and computational results of the QUENCH-08 experiment (reference to QUENCH-07)”. *Forschungszentrum Karlsruhe, FZKA-6970, Technical report* (2005). ISSN: 0947-8620.

Suehiro, S., Sugimoto, J., Hidaka, A., Okada, H., Mizokami, S., and Okamoto, K. “Development of the source term PIRT based on findings during Fukushima Daiichi NPPs accident”. *Nuclear Engineering and Design*, 286 (2015), pp.163-174. DOI: <https://doi.org/10.1016/j.nucengdes.2015.02.005>

- Tkinter (2022). *Python interface to Tcl/Tk*. URL: <https://docs.python.org/3/library/tkinter.html> (Accessed: 04.04.2023).
- Tolman, E.L., Kuan, P., and Broughton, J.M. “TMI-2 accident scenario update”. *Nuclear Engineering and Design*, 108, no. 1-2 (1988), pp.45-54.
- US Environmental Protection Agency (2022). *Protective Action Guides*. URL: <https://www.epa.gov/radiation/protective-action-guides-pags> (Accessed: 04.04.2023).
- Unittest (2022). *Unittest – Unit testing framework*. URL: <https://docs.python.org/3/library/unittest.html> (Accessed: 04.04.2023).
- Van Dorsselaere, J.P., Chatelard, P., Cranga, M., Guillard, G., Trégourès, N., Bosland, L., Brillant, G., Girault, N., Bentaib, A., Reinke, N., and Luther, W. “Validation status of the ASTEC integral code for severe accident simulation”. *Nuclear Technology*, 170, no. 3 (2010), pp.397-415. DOI: <https://doi.org/10.13182/NT10-A10326>
- Van Dorsselaere, J.P., Albiol, T. and Micaelli, J.C. “Research on severe accidents in nuclear power plants”. In Tsvetkov, P. ed. “Nuclear Power: Operation, Safety and Environment”, 2011, InTech, Croatia. ISBN: 978-953-307-507-5, pp.155-182.
- Veshchunov, M.S., Boldyrev, A.V., and Shestak, V.E. “Modelling the formation and oxidation of molten pools”. *Annals of Nuclear Energy*, 61 (2013), pp.54-62. DOI: <https://doi.org/10.1016/j.anucene.2013.03.046>
- Wall, I.B., Haugh, J.J., and Worlege, D.H. “Recent applications of PSA for managing nuclear power plant safety”. *Progress in nuclear Energy*, 39, no. 3-4 (2001), pp.367-425. DOI: [https://doi.org/10.1016/S0149-1970\(01\)00021-X](https://doi.org/10.1016/S0149-1970(01)00021-X)
- Weber, P., Medina-Oliva, G., Simon, C., and Iung, B. “Overview on Bayesian networks applications for dependability, risk analysis and maintenance areas”. *Engineering Applications of Artificial Intelligence*, 25, no. 4 (2012), pp.671-682. DOI: <https://doi.org/10.1016/j.engappai.2010.06.002>
- Wilks, S.S. “Determination of sample sizes for setting tolerance limits”. *The Annals of Mathematical Statistics*, 12, no. 1 (1941), pp.91-96.
- Wilson, G.E. “Historical insights in the development of best estimate plus uncertainty safety analysis”. *Annals of Nuclear Energy*, 52 (2013), pp.2-9. DOI: <https://doi.org/10.1016/j.anucene.2012.03.002>
- Zhang, H., Szilard, R., Zou, L., and Zhao, H. “Comparisons of Wilks’ and Monte Carlo methods in response to the 10CFR50. 46 (c) proposed rulemaking”. In *the Proceedings of the 11th International Topical Meeting on Nuclear Reactor Thermal-Hydraulics, Operations and Safety - NUTHOS-11, Gyeongju, Republic of Korea, 9-13 October 2016*. 2016, INL/CON-16-37808.
- Zhang, X., Yu, J., Huang, T., Jiang, G., Zhong, X., and Saeed, M. “An improved method for hydrogen deflagration to detonation transition prediction under severe accidents in nuclear power plants”. *International Journal of Hydrogen Energy*, 44, no. 21 (2019), pp.11233-11239. DOI: <https://doi.org/10.1016/j.ijhydene.2019.02.219>

Appendix A: U&S analysis and existing tools.

U&S analysis plays a big part of this thesis, since a SA is a complex phenomenon characterized by high uncertainties. So, when we are simulating a SA process with SA code, we want to be sure that our simulations are representative enough. The questions are:

- What parameters are important for a given SA scenario?
- In what range these parameters can vary?
- How the values of the parameters of interest change due to variation of uncertain input parameters?

To answer these questions, a U&S analysis topic and its application to SA are mandatory. In this appendix the brief introduction into the U&S analysis applied to the SA simulations is given in [Section A.1](#) and the short description of the existing tools for the U&S analysis is provided in [Section A.2](#).

A.1 Uncertainty and sensitivity analysis applied to severe accidents

Safety analysis [[Lee et. al., 2011](#)], which main goal is to evaluate potential hazards and how the strategies to prevent or minimize effect of such hazards, are divided into deterministic and probabilistic.

Deterministic safety analysis (DSA) are based on numerical simulation tools describing the physical phenomena during a postulated accidental sequence by numerically solving a system of model equations (e.g. for fluid dynamics coupled with heat transfer). To limit the computation effort models contain a large number of empirical correlations (e.g. for the mass and heat transfer at the wall and at the interface of a single or two-phase flow, as well as for oxidation). According to [[D'auria et. al., 2009](#)] DSA is used to:

- Confirm safety functions.
- Demonstrate, that uncontrolled release is prevented for all plant states.
- Determine source term for different plant states and barriers status.
- Show that source term is acceptable and large release is practically eliminated.

DSA proves the adequacy of plant design, which will work correctly and fulfill acceptance criteria in all considered transients.

PSA relies purely on mathematical approaches e.g. Boolean algebra to describe the probability of failure (fault tree) and of occurrence of events (event tree) of a complex system such as nuclear power plant. In [[INSAG Series, 1992](#)] is stated, that PSA is used to identify the combination of the events, which could lead to the severe accident and to evaluate its probability and consequences. PSA itself has three levels: PSA-1 is focused on sequences leading to the core

damage; scope of PSA-2 is the transport of FPs from damaged core to the environment and evaluating the possibility of the off-site release; and the PSA-3 is focused on the environmental and health consequences of off-site release from PSA-2 level.

It is always possible to base analysis only on conservative assumptions. A more advanced method is called – Best Estimate plus Uncertainty (BEPU) [D’auria et. al., 2012], [Wilson, 2013]. This method allows to include different sources of uncertainty and errors – for example, uncertainty of the computer code models parameters, due to the lack of experimental data used to validate the code models; uncertainty of the experimental data itself; numerical schemes errors; simplification of geometry of the modelled structures, etc. Different level of conservativeness in, for example, DSA is illustrated in **Table A-1**.

| Option | Computer code type | Assumptions about systems availability | Type of initial and boundary conditions |
|--------------------------------|--------------------|--|---|
| Conservative | Conservative | Conservative | Conservative |
| Combined | Best estimate | Conservative | Conservative |
| Best estimate plus uncertainty | Best estimate | Conservative | Best estimate; Partly most unfavorable conditions |
| Realistic | Best estimate | Best estimate | Best estimate |

Table A-1 – Different options for numerical assessment of deterministic safety analysis (DSA), type of assumptions and boundary conditions applied, from [D’Auria et. al., 2009].

Different methodologies [Bocanegra, 2019], [Glaeser, 2008a], [Glaeser, 2013] for the BEPU analysis have been suggested by different institutions: CSAU [Boyack et. al., 1990], GRS [Glaeser, 2008b], AREVA [Martin et. al., 2005], UMAE [D’auria et. al., 1995]. In many other works devoted to the U&S analysis of SA or experiment results in SA field [Elsalamouny et. al., 2021], [Kaliatka et. al., 2016], [Povilaitis et. al., 2017] the GRS approach has been used. In this work, it is also used with some modifications regarding the choice of number of code runs and sampling method. The idea is to evaluate the uncertainty of the particular simulation code output and to identify, what uncertain input parameters influence on that output parameter. Schematically the process of performing such kind of analysis is presented at **Figure A-1**.

Steps 1 and 2 don’t require much clarification, except that information about code to code comparison studies [Belon et. al., 2017b], [Maccari et. al., 2021] and knowledge about details of the code models could be helpful for understanding the final results.

Steps 3-5 on the **Figure A-1** require knowledge about the physical processes happening during the SA progression. It is important to decide in advance on what process/group of processes to focus on. In order to do so, a PIRT [Kang et. al., 2015], [Suehiro et. al., 2015] provides a significant help. After group of phenomena are identified, it is time to look closer, how those phenomena are modelled in the chosen SA code:

- Assumptions exist in the models.
- Experiments used to validate the model.

- Parameters are available for user to change.

All these information could be found in code manuals [[Humphries et. al., 2015](#)], [[Humphries, 2017](#)] and papers describing the code validation process [[Cantrel et. al., 2014](#)]. The choice of uncertain parameters can be done iteratively – the least important parameters (namely, parameters with lowest values of sensitivity coefficients) are excluded, and after that, new set of simulations is prepared and U&S analysis of new results is performed. The choice of probability density function and uncertainty range for each considered uncertain input parameter are based on information provided in code manuals, experiment results used for code model validation or expert judgment.

Choice of the samples number (see Step 6 at **Figure A-1**) in the GRS method is simple and defined by Wilks formula [[Wilks, 1941](#)]. Anyhow, despite that Wilks formula is very widely used in U&S analysis in nuclear safety field, there is a discussion, how to choose the number of samples correctly and when Wilks approach is applicable [[Honga et. al., 2011](#)], [[Zhang et. al., 2016](#)]. The choice of the sampling methods (see Step 7 at **Figure A-1**) is mainly between simple random sampling (SRS) and Latin Hypercube Sampling (LHS) [[McKay et. al., 1979](#)]. In the GRS method the SRS is used, but in our work the LHS algorithm is chosen, because it allows to avoid clustering of sampled values, which could happen due to the completely random process of drawing the samples in SRS. Different modifications of LHS algorithm exist [[Deutsch et. al., 2012](#)], [[Sheikholeslami et. al., 2017](#)] but are not used in this work.

After the preparation work, the simulation code is run (see Step 8 at **Figure A-1**) as many times as required by chosen number of samples. Each run has its own set of sampled input uncertain parameters values. Depending on the selected SA code and details of the simulated process, a single simulation can take hours, and performing hundreds of simulations can require days. It also puts some limit on the number of samples; and it's required to use computer with sufficient amount of cores or even computer cluster.

Collected results of the all performed code runs are showing how different could be values of the output parameters of interest depending on the input parameters values. To understand the degree of influence from input parameters to the output one, different correlations coefficients [[Ikonen et. al., 2014](#)], [[Ikonen, 2016](#)] are calculated (see Step 9 at **Figure A-1**). The most commonly used correlations are Pearson and Spearman coefficients, and we used them in our U&S analysis. In the software developed in the frame of the project, other additional correlation coefficients are implemented (see in [Subchapter 3.1.6](#)) – distance [[Martinez-Gomez et. al., 2014](#)] and Maximal Information Coefficient (MIC) [[Kinney et. al., 2014](#)], but, these coefficients are not actively used in the analysis during the project.

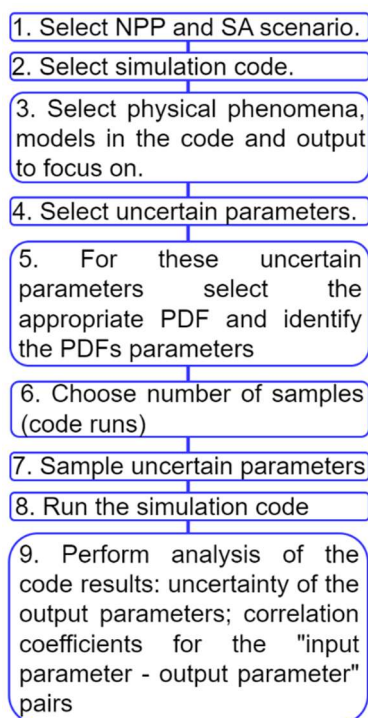


Figure A-1 – Steps of U&S analysis of SA scenario simulated with SA code.

A.2.Existing tools for U&S analysis

The tool for U&S analysis in general has the following functionality:

- Set the description of uncertain input parameters like, names, their probability density functions (PDFs) and PDFs parameters.
- Sample uncertain input parameters.
- Run the code many times with sampled values prepared at the previous step.
- Collect the output from the multiple code runs.
- Perform the U&S analysis itself – calculate simple statistics, correlation coefficients, etc.

The details of the implementation of such functionality can be different. For example, which PDFs, sampling methods, correlation coefficients, etc. are available. Also, the tool itself can be coupled with different codes and the process of coupling with a new code can be available or not. Some tools have a GUI, some are working only through the command line. Below, a brief description of some of the available tools for U&S analysis is presented.

URANIE: An open-source URANIE platform [Blanchard et. al., 2018], which has been under development for already more than 10 years in the French Alternative Energies and Atomic Energy Commission (CEA). URANIE has been used in our group, for example, for U&S analysis of the QUENCH-08 experiment [Gabrielli et. al., 2018]. For the installation and further use, URANIE requires some additional libraries – it is based on the ROOT [Antcheva et. al., 2009] framework and using some other compulsory – like CMake [CMake, 2022] and optional – like FFTW [Frigo et. al., 2005] dependencies. The platform itself is written in C++, but the user can

use C++ or Python to write the scripts for using URANIE. It can be coupled in principle with any code, which will be used as a black box, or the user can write some simple model in the script and provide it to URANIE. Users can sample variables with different PDFs (at least 16 different PDFs are available) using LHS, SRS or other sampling methods. URANIE has features for surrogate modelling, like polynomial chaos expansion [[Crestaux et. al., 2009](#)], which can help in case if running multiple simulations with original code is too time consuming. All these make URANIE a very powerful tool for U&S analysis, but it requires some time for installation, making the user familiar with the functionality, preparing all scripts for coupling URANIE with the code for simulations and for post processing. For the purposes of our project, URANIE functionality is a bit too extensive and applying it to the project requires too many additional scripts and adapting our needs to this platform.

SUSA: Another tool with a long history (from the mid-1980s) is SUSA [[Kloos M., 2015](#)], developed by the Gesellschaft für Anlagen- und Reaktorsicherheit (GRS). With the help of a GUI, SUSA guides the user through the whole process of U&S analysis – starting from choosing uncertain input parameter to calculating sensitivity coefficients. The choice of the FORTRAN programming language can be easily explained with the long history of the tool, newer tools are usually based on Python. For uncertain input parameters, around 20 PDF types are available. An option to specify correlations between input parameters is available also. Samples can be generated with SRS and LHS methods. SUSA has interfaces for some codes already and in principle can be coupled with any other code. Regarding the sensitivity analysis, SUSA provides an option to calculate Pearson, Blomquist's, Kendall's and Spearman correlation coefficients. For presenting output results in graphical form, SUSA has scatter and cobweb plots options. One of the downsides of this tool, which is crucial for us – it is available only for the Windows operating system (OS) and, therefore, cannot be used in our project, due to our multicore and high performance computers all using the Linux OS.

DAKOTA: DAKOTA from the Sandia National Labs is another open-source tool [[Eldred et. al., 1999](#)]. This tool is written in C++ and has a very extensive functionality, similar to URANIE, but in addition has a GUI, which seems to be a big advantage, and unlike SUSA, DAKOTA could be run on Windows, Linux and Mac OS. In principle that tool could be coupled with any other code. DAKOTA is regularly updated and has full set of the user guides [[Dalbey et. al., 2022](#)]. Taking these all into account, DAKOTA seems to be a good choice for the projects with U&S analysis part.

RAVEN: Another available open-source tool is RAVEN [[Alfonsi et. al., 2022a](#)], [[Alfonsi et. al., 2022b](#)] written in C, C++ and Python languages and developed at the Idaho National Laboratory since 2012. It could be run also on different OS like DAKOTA, could be coupled in principle with any code (and already coupled with MELCOR, MAAP and others), but it doesn't

have a GUI. Pearson and Spearman correlation coefficient are available for sensitivity analysis as well as the option to compute variance dependent and normalized sensitivity matrices.

All available tools, of course, cannot be described here. One can use the tool which is more suitable for the task. Supported OS, availability of GUI, possibility to easily couple the tool with other codes, available functionality for U&S analysis, PDFs, sampling methods etc. are the factors which can affect the choice of the software.

Appendix B: FSTC tool

In this Appendix the additional information about the FSTC tool is provided:

- Creating documentation is discussed in the [Section B.1](#).
- Unit testing of the source code – [Section B.2](#).
- Performance testing of the different FSTC modules on the QUENCH-08 simulation results – [Section B.3](#).
- The comparison of the U&S analysis results performed with the FSTC and the URANIE tools is shown in the [Section B.4](#).
- The comparison of the MOCABA algorithm implementation in the FSTC tool and proprietary Framatome code is presented in the [Section B.5](#).

Information provided below are supposed to be a supplementary information to the reader from software development point of view. All given examples are provided only for the illustrative purposes.

B.1. Preparing documentation for the FSTC tool

The preliminary version of the FSTC tool documentation has been prepared using the Sphinx Python documentation generator [\[Sphinx, 2022\]](#). This tool works with *reStructuredText* [\[reStructuredText, 2022\]](#) *.rst* files and extracts information from NumPy/Google style docstrings [\[Datacamp, 2022\]](#) in source code, combining all that information and produce a nice looking HTML web-page.

The main information about each FSTC module is written in its respective *.rst* file, which is named as the respective module. That information currently includes:

- The description of the module – a few sentences about main functionality.
- How to run the module.
- What to check before running the module.
- Which Python packages this module is using. It is important information for maintaining dependencies.
- How to prepare the input file.
- What output data the module produces.
- What functions the main module function calls. Basically, it is the short description of the steps during the module execution.

All links to the source code of the given module functions are provided in the other *.rst* file, named '*<module name>_functions.rst*'. It tells Sphinx where to extract docstrings from the source code.

Finally, the function details are provided in the docstrings in the source code itself. A docstring can contain the following information:

- What the function is doing.
- What input parameters it has (their names, data types, meaning).
- What the function returns.
- Additional notes. It could be any useful and important information for the user/developer.

As a result of using Sphinx to generate documentation from prepared docstrings and reStructuredText files, the main page of project documentation can look like it is shown at **Figure B-1**. Note, that the Figure is provided for the illustration purposes, and current documentation version can look differently.

FSTC

Navigation

- [Sample uncertain input parameters](#)
- [Run multiple simulations](#)
- [Find incorrect runs and additional samples to exclude](#)
- [Collect results of multiple simulations](#)
- [Extract data between two specified time points](#)
- [Perform U&S analysis](#)
- [Calculate 'priors'](#)
- [Calculate 'posteriors'](#)

Welcome to FSTC's documentation!

This site provides documentation for FSTC tool

U&S modules

Below listed packages for full uncertainty and sensitivity analysis starting from sampling uncertain parameters and ending with calculating sensitivity coefficients

- [Sample uncertain input parameters](#)
- [Run multiple simulations](#)
- [Find incorrect runs and additional samples to exclude](#)
- [Collect results of multiple simulations](#)
- [Extract data between two specified time points](#)
- [Perform U&S analysis](#)

Figure B-1 – Main page of the FSTC documentation generated by Sphinx using prepared docstrings in the source code and reStructuredText files. On the left user can click to the module name and go to the module page. The same can be done at the center of the page, where modules are also listed.

The reader can click on the package name link and gets information about its functionality, how to run it, etc – these information were specified in the module .rst file. After that, on the given module page reader can click on a given function signature link and gets more detailed information about the function, which was written in the function docstring in the source code itself.

Sphinx provides a lot of functionality and opportunities for customizing the documentation. Currently for the FSTC tool we use the very basic features.

During the preparation of the thesis the FSTC tool source code was moved to the KIT GitLab server, and documentation for the project repository has been also created here. Gitlab allows to create Wiki for each repository quite conveniently using text formatting, pictures, references, etc.

The U&S part of the FSTC tool has become a separate tool named KATUSA. The KATUSA project Wiki main page currently looks like it is shown in **Figure B-2**.

Home

Below you will find the information about KATUSA:

- [How to install and run KATUSA](#)
- [What to check before running each package](#)
- [How to prepare input files for KATUSA packages](#)
 1. [Sampling uncertain input parameters - "sampling"](#)
 2. [Run simulations - "run_multiple"](#)
 3. [Identify outliers in results - "results_preview"](#)
 4. [Collect output of interest values - "collect_results"](#)
 5. [Filter output of interest values - "filter_data"](#)
 6. [Perform uncertainty & sensitivity analysis - "unc_sens"](#)
- [Description of output files produced by KATUSA packages](#)
 1. [Sampling uncertain input parameters - "sampling"](#)
 2. [Run simulations - "run_multiple"](#)
 3. [Identify outliers in results - "results_preview"](#)
 4. [Collect output of interest values - "collect_results"](#)
 5. [Filter output of interest values - "filter_data"](#)
 6. [Perform uncertainty & sensitivity analysis - "unc_sens"](#)
- [Algorithms/Formulas/Mathematical background of the KATUSA packages](#)
 1. [Sampling](#)

Figure B-2 – Main page of the KATUSA repository Wiki on KIT GitLab account. KATUSA Wiki provides information about code installation, creating input files for different tool modules, description of the output files, etc.

B.2. Unit testing

Unit tests are used to check that each small part of a piece of software (function, for example) behaves as it was intended. The tests for the FSTC tool are written using the *'unittest'* Python framework [\[Unittest, 2022\]](#) and are currently covering only part of the code, mostly related to the function checking correctness of the modules input files.

Let us illustrate unit testing on an example with checking the correctness of the input file of the *'sampling'* module. Python file collection of the unit tests for that purpose is named *'test_check_input.py'*. Inside this file there is a one class named *'TestCheckInput'*. Each method of that class is named according to what functionality of the code it tests. For example, method named *'test_samples_num_type'* checks, whether the *'sampling'* module code reacts correctly on the incorrect value of the samples number provided by user in the input file. For example, instead of the integer value in the field *'Number of samples'* in the input file user provides some text. Of course, code must raise an error and explain to the user, where exactly the error is and the type of the error. To check that code behavior *'test_samples_num_type'* method has two pieces of data:

-
- Example of the correct module output – in that case it is the listing file, where the error message is written.
 - Example of the incorrect module input file, where instead of the integer number of samples, some text is written.

The *'test_samples_num_type'* method:

- Creates the folder.
- Puts incorrect input file in that folder.
- Runs from the folder the 'sampling' module.
- Compares the created listing file with the example.

If two listing files are identical, it means, that code behaves correctly. In other case, the unit test fails, provide some information about its failure, and it probably means, that last changes in the code has been incorrect and broken its behavior.

Other things to check in the 'sampling' module input file are, for example:

- Get sampling method and check that this method is available. Currently, only LHS and SRS methods are implemented.
- All mandatory parts of input file exist.
- Specified PDF types are available in the module.
- All required parameters of the given PDF are specified. For example, for the uniform distribution minimum and maximum values must be provided.
- All PDF parameters have correct type. All values must be type float.

For each of the mentioned above cases, a separate unit test method must be written. Tests can be combined into groups and only required groups of tests can be run allowing the flexibility in testing different parts of the source code.

Good practice is to run tests after each code change and each change of the input file structure.

For all other parts of the source code, the procedure of writing and organizing the unit tests is the same as described here.

B.3. Performance testing

The goal of the performance testing is to investigate how the system responds to a particular workload. The system, for example, can be tested on a sudden increase of users' requests. High number of users or memory consumption can also be tested. Most of these things are not applicable to the FSTC tool, because only one user is working with it simultaneously, as well as the tool does not need an internet connection, does not use any API, etc. What can be changed from one run of the FSTC tool to another is the number of samples, and as a result the amount of data produced by simulations. The tool also can be used on different machines with different

number of cores. Therefore, the execution time of different FSTC modules can be tested in these varying conditions.

Note that all following tests performed on a Linux machine with 32 cores, if other number of cores not specified. The number of uncertain input parameters was 24. Tests have been made for the QUENCH-08 experiment simulations, which are described in detail in the main body text. Information provided below can give a reader an estimation of how fast the FSTC tool is.

The ‘sampling’ module is the least time consuming from all the other FSTC tool parts, and the full executions time – reading input, sampling, creating all plots and writing results in database – varies from ~7 seconds to ~9 seconds for 100 samples and 400 samples respectively.

Because the ‘run multiple simulations’ module is the only one running the other code – in our case, ASTEC – its execution time fully depends on the time needed to perform the simulations. In case of QUENCH-08 simulations with ASTEC, one run takes ~ 1 hour at one core (ASTEC code is not parallelized), so almost 800 samples can be simulated at 32 core machine during one day.

The ‘find samples to exclude’ module has small execution time. It can vary from ~4 seconds for 100 samples till ~14 seconds for 400 samples.

The ‘collect data’ module extracts values of all parameters of interest for all time steps for all correctly finished runs, excluding samples specified by the user. Here the execution time depends on how many output parameters are considered and how many time steps are in the simulated process. For example, in case of QUENCH-08 simulations there are 2380 time steps and at most 59 output parameters (for simulations where temperatures at each elevation of the test bundle are considered as outputs). For 100 samples, the package execution takes ~ 36 seconds and for 400 samples - ~116 seconds (less than 2 minutes). Extracting the data itself from the ASTEC output files takes ~9 and ~34 seconds for 100 and 400 samples respectively. The most time consuming part of the package execution is writing extracted data into databases, it takes more than half from whole execution time - ~27 and ~78 second for 100 and 400 samples respectively, so that part of the module can potentially be parallelized.

The ‘filter data’ module is fully parallelized, and its execution time varies from ~21 seconds up to ~73 seconds for 100 and 400 samples respectively.

All these execution time values looks quite appropriate, especially taking into account how time consuming are the ASTEC simulations. Spending ~ 3.5 minutes in total for sampling, checking correctness of all runs, extracting and filtering the data for 400 QUENCH-08 simulations looks fast enough comparing to the half of the day required to perform these 400 simulations.

The ‘U&S analysis’ package consists of some intermediate steps, each of them could be parallelized. Extracting data from the databases created as with the ‘filter data’ module executed in parallel takes from 0.8 seconds for 50 samples up to ~12 seconds for 800 samples. Calculating simple statistics and percentiles is not parallelized because the execution time of that part is negligible compared to the other parts – for 800 samples it will take ~ 0.6 seconds in total. Calculation of Pearson correlation coefficients is not parallelized also, some previous tests during development phase reveal that it’s not necessary and doesn’t bring any significant speed-up. Currently calculation of Pearson correlation coefficient evolution in time (2380 time steps for QUENCH-08 test) for all possible ‘output – input’ parameters pairs (59 output and 24 input parameters for QUENCH-08 test) takes only ~1.4 seconds. The situation with calculating Spearman, distance and Maximal Information coefficients is completely different and these parts are all parallelized. Despite that, calculation of Maximal Information coefficient takes especially a long time, for example, for 800 samples the execution time of the U&S package is ~15 minutes and 90% of it is the MIC calculation. To calculate MIC, the ‘*minepy*’ Python package [\[Minepy, 2022\]](#) is used here, and the possibilities of improving the calculation time could in principle be investigated if needed by looking at the open-source code of the library. In **Figure B-3** is presented how much time ‘U&S analysis’ module needs to post-process results depending on number of samples and number of cores (using results for 200 samples simulations of the QUENCH-08 experiment).

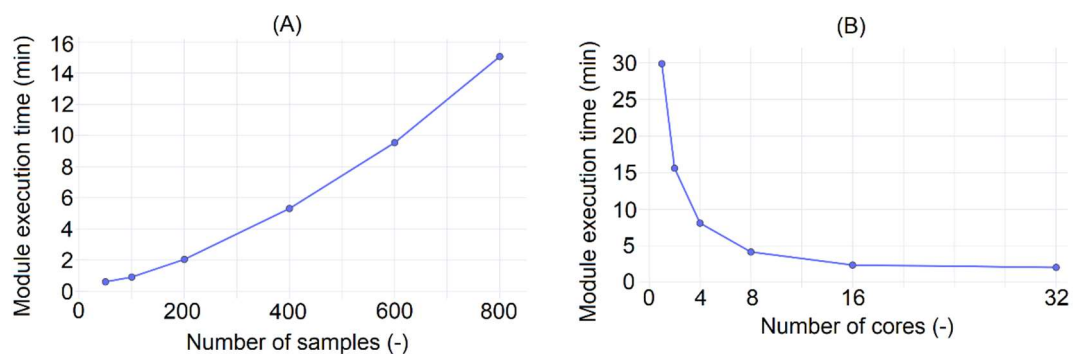


Figure B-3 –The ‘U&S analysis’ module of FSTC tool performance testing. Testing has been made on the ASTEC QUENCH-08 experiment simulations. (A): Module execution time depending on the number of samples used for the ASTEC simulations. (B): Module execution time depending on the number of the cores using the results of the 200 simulations.

The ‘prior’ part of the MOCABA algorithm implementation has the following execution times: from ~15.5 seconds up to ~53.5 seconds for 100 and 800 QUENCH-08 simulation used as an input data respectively. Both tests have been made on sparse time scale – the original time scale consisted of 2378 steps and only each 10th time step is taken to calculate priors. The most time consuming parts are extracting the input data from databases or *.dat* files and calculating Pearson correlation coefficients between the time steps. The first part depends on the number of samples and the second on how fine the time grid is.

Calculations in the ‘posterior’ part of the MOCABA algorithm are organized in a following way – first, results of the ‘prior’ calculation are extracted as well as the data from the files with ‘measurements’ values (real measurements or results of other simulations) and after that, the prediction is calculated by adding measured data one by one. In case of using this part of the FSTC tool in a real application, measured data will come up in a given interval of time (for example, every 5 minutes), therefore for the performance test it is required only to check how fast the prediction is calculated when a given amount of measured data is available. For example, in the case of QUENCH-08 simulations, a single prediction varies from ~0.007 seconds up to ~0.02 seconds, depending on how much measured data are already available and how fine the time grid is. In all MOCABA tests made up to now for the QUENCH-08 simulations the prediction always take less than a second.

As one can see from the presented results, there is some room for performance improvement, but execution time already looks good enough for potential FSTC tool usage.

B.4. Comparison of the ‘U&S analysis’ module of the FSTC tool with the URANIE platform

To check the correctness of the implemented functionality in the U&S analysis package of the FSTC tool, the U&S quantification of the ASTEC code QUENCH-08 experiment simulation results has been performed with FSTC and URANIE tools. Additional Python scripts have been written to make this process more convenient.

For this comparison, results of 200 ASTEC simulations of the QUENCH-08 experiment have been used. The details of the ASTEC model prepared for these simulations and the physical meaning of the simulation results were described in the main body of the thesis text.

Note that it is not necessary to use all output values available in the simulation results for the validation. It is enough to compare results using one output parameter – for example, mass of the hydrogen generated during the experiment.

The validation process is organized in the following way:

- The results of the ‘sampling’ and ‘filter data’ modules of the FSTC tool are used as an input data for the validation process.
- Hydrogen mass values are extracted from the databases generated by the ‘filter data’ module and stored in the input file for the URANIE tool.
- A script in the C programming language with instructions for URANIE is automatically created. In that script is specified: what data from the input file, to analyze; what is to be calculated (for example, simple statistics and Pearson correlation coefficients), and how to store the U&S analysis results.
- URANIE tool is run.

- ‘U&S analysis’ module is run.
- Results of the FSTC and URANIE tools are extracted from output files, compared, plots are created.

Here the following is compared:

- The results of simple statistics calculation (minimum, maximum, mean, and standard deviation values) for the mass of the hydrogen produced during the experiment.
- The Pearson correlation coefficient values between chosen output parameter (mass of the hydrogen) and two uncertain input parameters (steam (*stFlow*) and argon (*arFlow*) mass flow rates).

An example of such a comparison is shown in **Figure B-4**. The left part of the figure shows minimum and maximum values of the hydrogen mass. The right part of the figure shows Pearson correlation coefficients between hydrogen mass and two uncertain input parameters – argon (*arFlow*) and steam (*stFlow*) flow rates. The results of simple statistic calculation and Pearson correlation coefficient values produced by the FSTC and URANIE tools are identical, and that confirms correct implementation of functionality for performing U&S analysis in the FSTC tool. In case additional features will be added in FSTC, they can always be validated against other existing and tested tools.

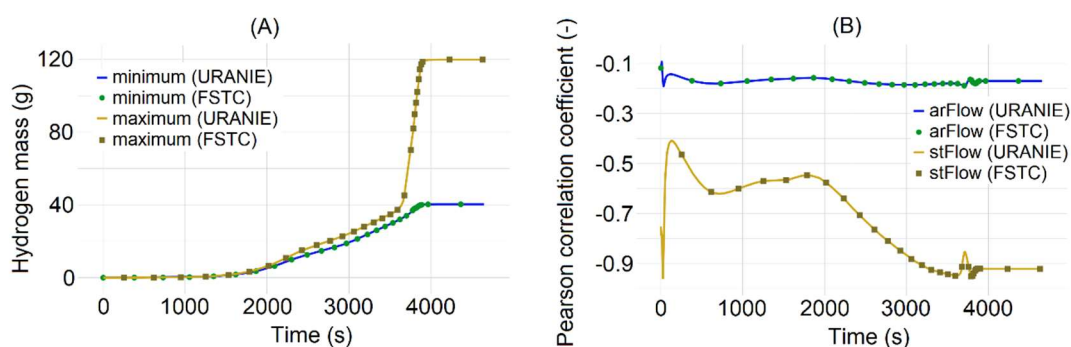


Figure B-4 – Comparison of the ‘U&S analysis’ results performed with the FSTC and URANIE tool using results of the QUENCH-08 experiment simulations. FSTC results presented with dots, URANIE results – with lines. (A): Comparison Minimum and maximum values of the hydrogen mass produced during the experiment. (B): Pearson correlation coefficient values between hydrogen mass and two uncertain input parameters – argon (*arFlow*) and steam (*stFlow*) mass flow rates.

B.5. Validation of the MOCABA algorithm implementation

To check the MOCABA algorithm is correctly implemented in the FSTC tool, a comparison between it and Framatome proprietary code has been made. No original MOCABA source code is available at KIT, but only executable files and mathematical formulation.

To compare the two codes, a set of 200 ASTEC simulations of the QUENCH-08 experiment are used as an input for the ‘prior’ part of the prediction algorithm, and a set of 50 simulations has been considered as ‘experimental’ results. In this example MOCABA predicts the hydrogen

mass (H_2 mass) produced during the experiment ('prediction' parameter) using three different temperatures as 'observable' parameters – cladding temperatures (T_{clad2} and T_{clad3}) of two structures in the ASTEC QUENCH-08 model and temperature of the shroud structure (T_{shroud}). Detailed description of the QUENCH-08 ASTEC model and simulation results is provided in the main text of the thesis. Here, for the purpose of comparison only the similarity of the results provided by the MOCABA algorithm is important.

The comparison procedure step by step looks like:

- 1) Run the 'prior' part of the algorithm implemented in the FSTC tool.
- 2) Run MOCABA executable file for the 'prior' part.
- 3) Pick up one of the samples of the pre-calculated 50 simulations set.
- 4) Extract output data of step 1) and run 'posterior' part of the algorithm implemented in the FSTC tool using the data from 3) as the 'measurements'.
- 5) Extract output data of step 2) and run MOCABA executable file for the 'posterior' part using data from 3) as the 'measurements'.
- 6) Compare results of steps 4) and 5).

An example of such a comparison is provided in **Figure B-5**. Two prediction of how the hydrogen mass produced during the experiment evolve in time are presented. For one prediction 'measured' data up to 165 s are used, for second prediction – up to 3540 s. Results provided by two implementations of the MOCABA algorithm are identical.

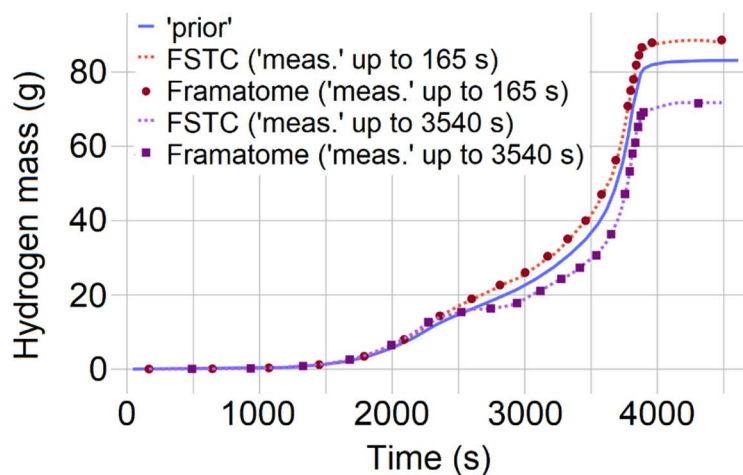


Figure B-5 –MOCABA algorithm implementations validation. Comparison of the results provided by the FSTC tool and the Framatome proprietary code. Hydrogen mass values from the QUENCH-08 simulations results are used. Two predictions – made with using 'measured' data up to 165 s and up to 3540 s – are shown.

Appendix C: Application of the FSTC-tool for the generation of the data base for PWR MBLOCA + SBO SA Scenario

Results of the MBLOCA scenario simulations are presented in the main text of the thesis. Here the results of the MBLOCA+SBO scenario simulations are shown. In [Section C.1](#) results of the U&S analysis are given, and [Section C.2](#) presents the results of applying the prediction algorithm to the MBLOCA+SBO simulation results.

The MBLOCA+SBO scenario starts as MBLOCA with a 440 cm² break in the cold leg. Additionally, the alternating current (AC) power supply is interrupted at the time $t=0$. This initiates a SCRAM is happening, FWPs are shut down and turbine stop valves are closed. It is further assumed that ECCS and EFWS are not available. The occurrence of the major events during MBLOCA+SBO transient simulated with best estimated values of uncertain input parameters are shown in **Table C-1**.

| Event | Time |
|---|--------|
| Break opening. Loss of AC power. MCPs coast down | 0 s |
| SCRAM | 1 s |
| Turbine valves closed. FWPs shut down | 1.5 s |
| Start of FPs release | 554 s |
| First material slump into the LP | 884 s |
| 20 tons of corium relocated into the LP | 944 s |
| 50 tons of corium relocated into the LP | 1334 s |
| Lower head vessel failure | 3151 s |
| End of the corium slump from lower head to the cavity | 3228 s |
| End of simulations | 9151 s |

Table C-1 – Sequence of the events occurring during the MBLOCA+SBO scenario. Results for the reference case.

C.1 Results of U&S analysis

U&S analysis of the MBLOCA+SBO scenario has been performed in a similar manner as described for the MBLOCA scenario. The list of uncertain input parameters and number of samples stay the same, as well as the list of FoMs and major events happening during the accident progression. In case of a station blackout, accident progression evolves much faster. For example, the lower head vessel failure happens in average about ~7 times earlier, than in case of MBLOCA as illustrated in **Figure C-1**.

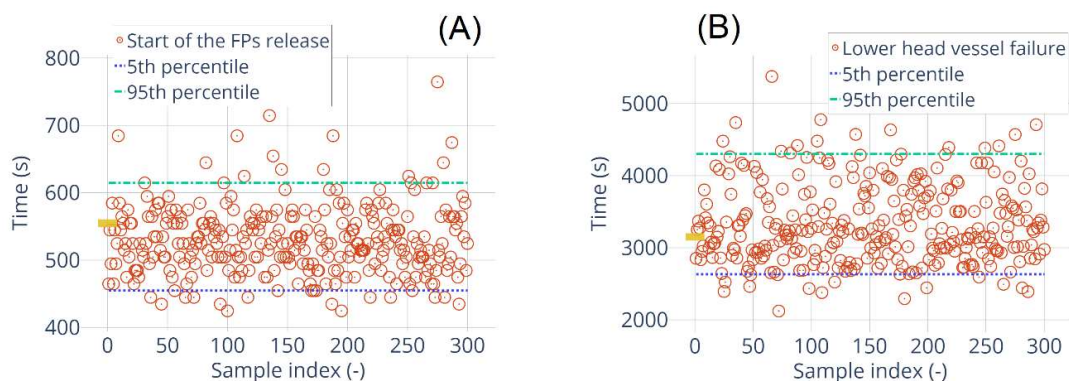


Figure C-1 – Time of the main events for the all non-failed MBLOCA+SBO simulations from the 300 simulations set. (A): time of the start of the FPs release; (B): time of the lower head vessel failure. With orange rectangle the results of the simulation with the best estimated values of the uncertain input parameters are marked.

The selected fission products are the same as in the MBLOCA scenario simulations – Xenon, Iodine, Cesium and Molybdenum. The amount of different FPs (as fraction of initial inventory varying from 0 to 1) released into the environment exhibits a similar behavior in time for this scenario compared to MBLOCA – it increases faster during the first $\sim 1500 - 2000$ s, after that slows down, but continues to increase during the whole transient, as it is shown in **Figure C-2**. Only small amount of FPs reaches the environment, and varies from $\sim 10^{-4}$ for high-volatile elements as Xenon to $\sim 10^{-7}$ for low-volatile elements as Molybdenum. Comparing to the MBLOCA scenario there is no second release into the containment, mainly release happens during the first $\sim 1000 - 2000$ s and reaches the plateau as it is shown in **Figure C-3**. The high-volatile elements like Xenon are fully released into the containment. Around ~ 0.01 of the Iodine and ~ 0.1 of the Cesium initial inventory are released into the containment, the biggest amount of these elements stays in the primary system. The low-volatile elements like Molybdenum mostly stay in the vessel, and only tiny part of initial inventory ~ 0.001 reaches the containment.

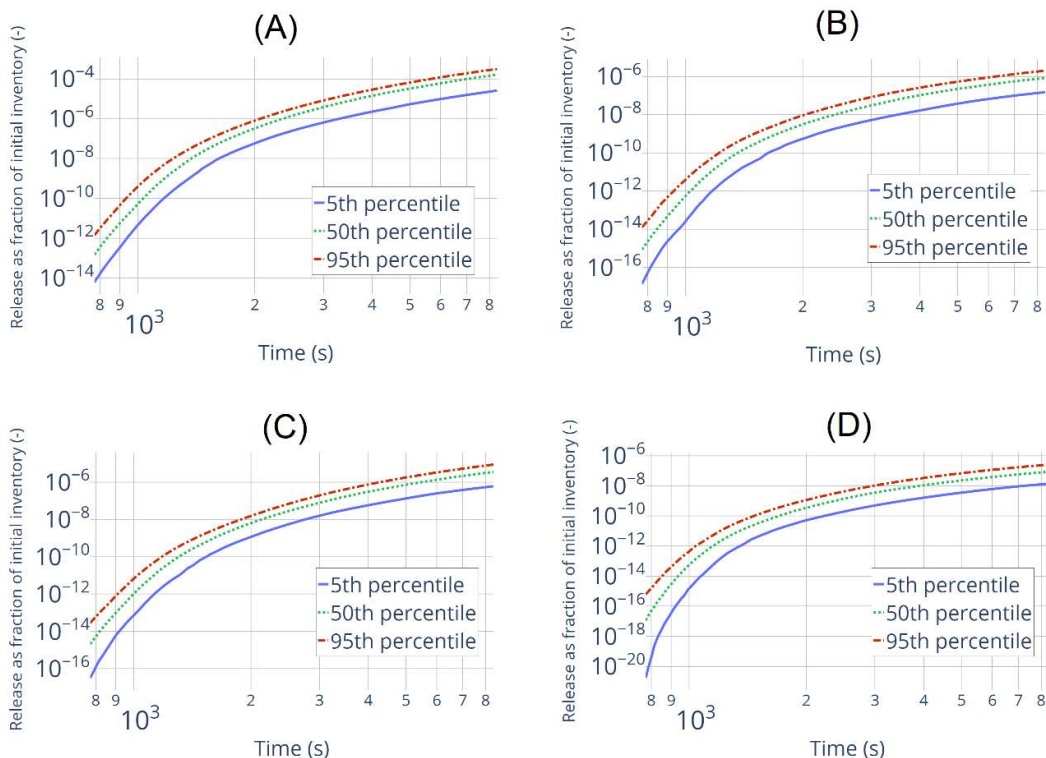


Figure C-2 – Simple statistics for the release into the environment as fraction of initial inventory. (A) – Xenon (Xe); (B) – Iodine (I); (C) – Cesium (Cs); (D) – Molybdenum (Mo).

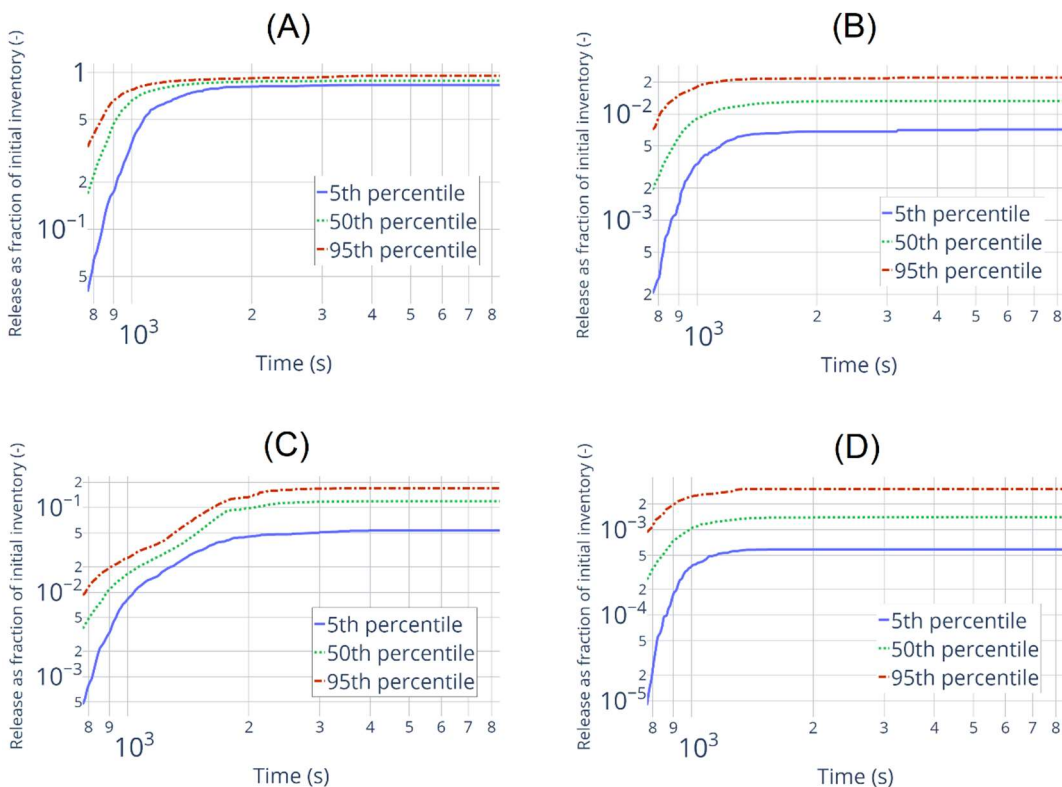


Figure C-3 – Simple statistics for the release into the containment as fraction of initial inventory. (A) – Xenon (Xe); (B) – Iodine (I); (C) – Cesium (Cs); (D) – Molybdenum (Mo).

The release into the environment is mostly affected, as well as for MBLOCA scenario, by two uncertain input parameters – the one governing the leakage between containment and environment and the second one governing the burnup (see Spearman correlation values evolution in time in **Figure C-4**). The Spearman correlation values for the parameter governing the leakage increases fast during the first $\sim 1000 - 2000$ s of the transient and after that reaches plateau or growing very slowly. The Spearman correlation values for the parameter governing the burnup are high during the beginning of the transient, when the FPs release from the fuel pellets is happening, and after that decreases fast reaching the level 0.3 (considering as the boundary between low and moderate correlation) around $\sim 1800 - 2500$ s. The release into the containment is affect only by the parameter governing the burnup, as shown in **Figure C-5**. The Spearman correlation values changes from significant to weak during the first $\sim 1000 - 2000$ s of the transient. The Spearman correlation values for the parameter from ELSA ASTEC model (on the **Figure C-5 (B)** only the parameter related to the correction factor for the surface/volume ratio of the fuel pellets due to roughness is presented, due to other two parameter from the model are correlated with it) are slightly lower, than in case of the MBLOCA scenario. It can happen, that in case of re-running the same simulations due to the re-sampling effect discussed in the main text body the correlation values for this parameter will change. Therefore, the effect from parameters from the ELSA model is not fully clear.

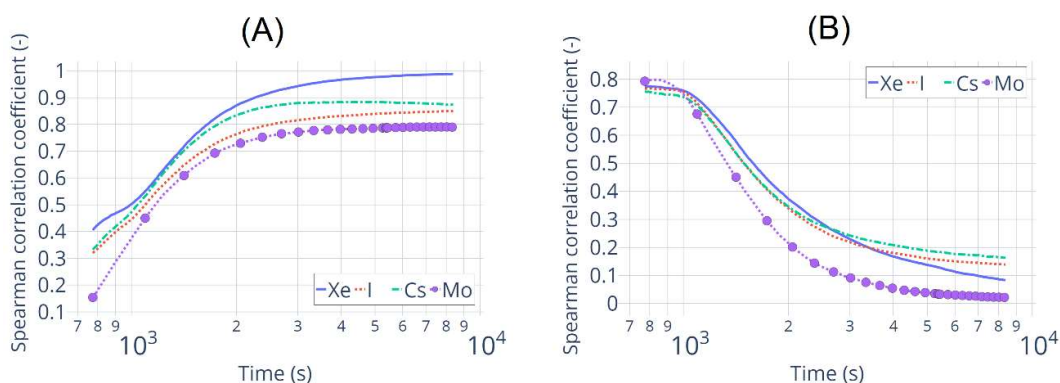


Figure C-4 – Spearman correlation coefficient evolution in time for the amount selected fission product (xenon, iodine, cesium and molybdenum) released into the environment and uncertain input parameter governing (A): the leakage between containment and environment; (B): the burnup.

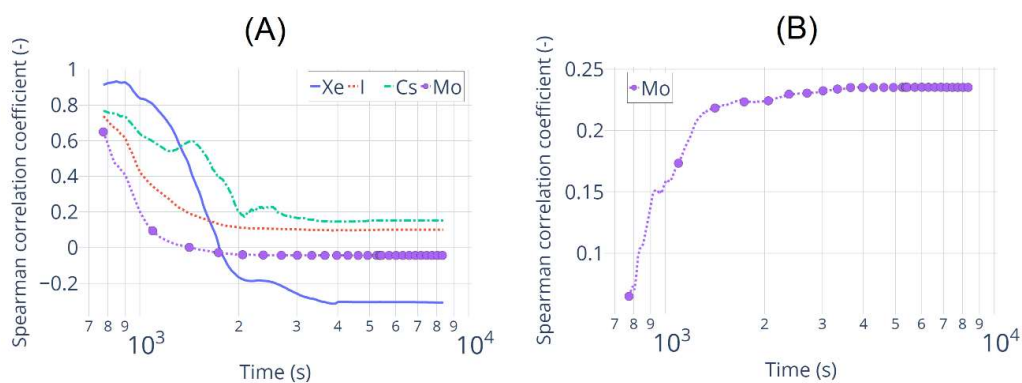


Figure C-5 – Spearman correlation coefficient evolution in time for the amount selected fission product (xenon, iodine, cesium and molybdenum) released into the containment and uncertain input parameter governing (A): the burnup; (B): the correction factor for the surface/volume ratio of the fuel pellets due to roughness.

C.2 Applying the MOCABA algorithm to the MBLOCA+SBO simulations

Applying the MOCABA algorithm to the results of the MBLOCA + SBO scenario simulations has been done in the same manner as for the MBLOCA simulations. As the input data for the ‘prior’ part of the prediction algorithm the results of 300 simulations are used. A prediction has been made on the results of 100 simulations, where each single simulation result is treated as an individual ‘experiment’ realization. Both sets of simulations are made for exactly the same scenario with the same uncertain input parameters. The goal is the same – predict amount of Xenon (as fraction of initial inventory) release into the environment during the transient. The Pearson correlation coefficient values have been checked for two potential ‘observable’ parameters – the total dose rate in the containment and the annulus. As well as for MBLOCA scenario the correlation values between the amount of Xenon released into the environment and the total dose rate in containment has been considered as too low – the correlation value decreases fast at the beginning of the transient and stays around 0 for the rest of the transient (see in **Figure C-6**). Therefore, the total dose rate in containment has been excluded again from potential ‘observables’ parameters, and only total dose rate in the annulus left.

The prediction results are shown here on the two samples from the ‘validation’ set. The values of the Xenon release and the total dose rate in the annulus for these samples are shown in **Figure C-7** with the corresponding ‘prior’ values. For sample №2 the increase for both total dose rate in the annulus and amount of Xenon released into the environment goes faster, than in average. In addition to it, data for sample №2 lie very close to the maximum curves. For sample №17 the time evolution for ‘prediction’ and ‘observable’ parameters goes slower, than in average.

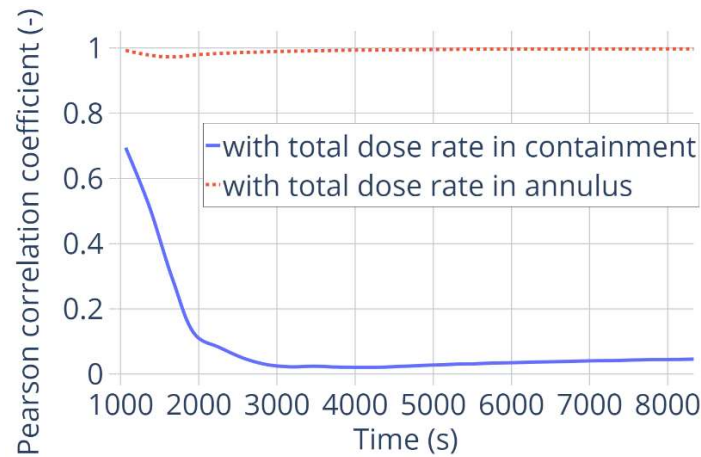


Figure C-6 – Pearson correlation coefficients between ‘prediction’ parameter (amount of Xenon released into the environment) and two initially suggested ‘observable’ parameters (total dose rate in the annulus and total dose rate in containment). MBLOCA+SBO scenario.

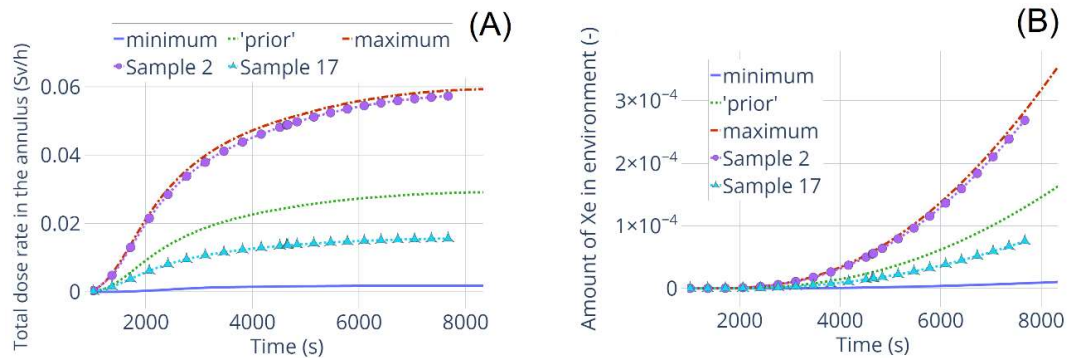


Figure C-7 - Simulated total dose rate in the annulus (A) and amount of Xenon released into the environment (B) evolution in time. Minimum, ‘prior’ and maximum values are from the ‘prior’ set of data. Two samples 2 and 17 are from the ‘validation’ set of data. MBLOCA+SBO scenario.

The AREA metric values showing how the prediction is improving with adding measured data is presented in **Figure C-8**. It is clear from the picture that prediction results are becoming better, when more measurements are used. In addition, comparing to the other results presented in this work, the lowest AREA metric values in that case located at the end of the time scale, which means that the best prediction is constructed, when all ‘measured’ data are used. The reason why it happens only for this case is not yet clear.

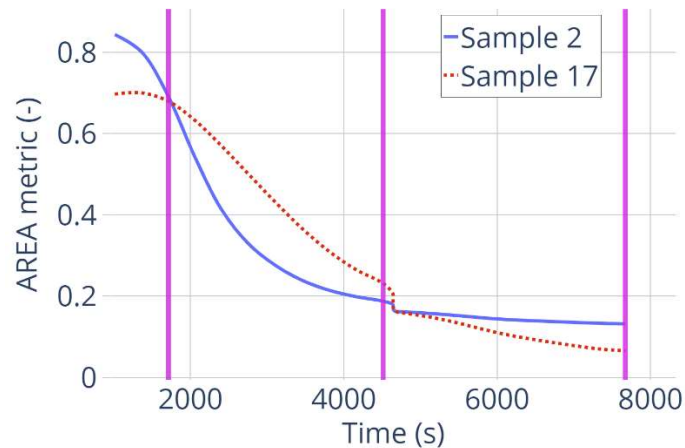


Figure C-8 – AREA metric values for samples №3 and 26 from the 100 samples validation set. Time points up to which the ‘measured’ data are used to construct prediction for the illustration are marked by the vertical lines at 1714 s, 4514 s and 7672 s respectively. MBLOCA+SBO scenario.

The results of the prediction and prediction errors for samples № 2 and 17 are presented at **Figure C-9** and **Figure C-10**. The prediction curves lie closer and closer to the ‘experimental’ one with adding more ‘measured’ data. As for results presented for the MBLOCA scenario, the prediction error is very high at the beginning of the process, no matter how much measured data are used, because the values are too small for correct prediction. The error decreases fast during the first ~2000s. Even though the prediction using more measured data is closer to the ‘experimental’ curve, it doesn’t mean that prediction error is smaller than for the case when less measured data are used – this definitely requires additional investigation.

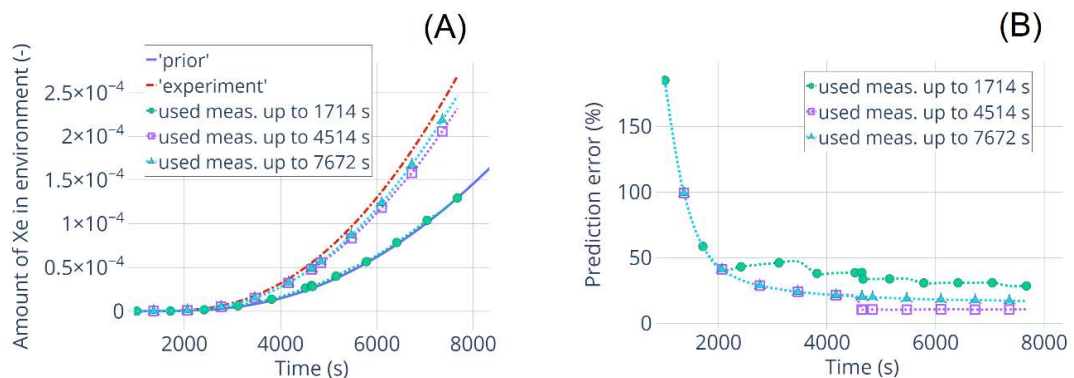


Figure C-9 – Prediction results and errors for the sample №2 from the validation set. Results are presented for the different amount of measured data used for calculating the prediction. MBLOCA+SBO simulations.

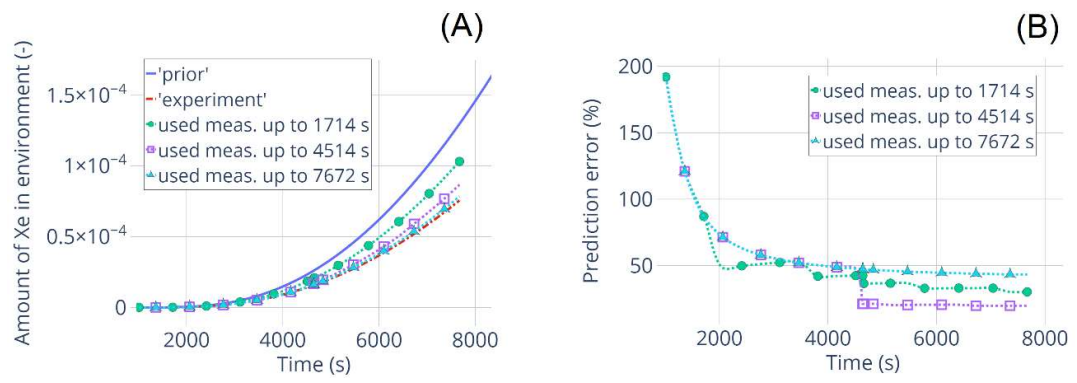


Figure C-10 – Prediction results and errors for the sample №17 from the validation set. Results are presented for the different amount of measured data used for calculating the prediction. MBLOCA+SBO simulations.

Appendix D: Constraints and limitations of the MOCABA algorithm presented on the simple ‘toy’ example

The need to investigate the limitation of the MOCABA algorithm has been mentioned several times during the text. Such investigation seems difficult to perform on actual simulation results of a SA scenario or experiments like QUENCH-08, because these processes are complex and it could be difficult to detect what exactly is influencing prediction results. Therefore, a very simple ‘toy’ example, which gives user full control over the data has been used for this test.

In the ‘toy’ example we want to predict value $Pred_1$ computed using the following function:

$$Pred_1(t) = \frac{Obs_1(t) \cdot Obs_2(t)}{Obs_3(t)}, \quad (D.1)$$

, using three observables Obs_1 , Obs_2 and Obs_3 :

$$Obs_1(t) = 0.8 \cdot t + \alpha_1, \quad (D.2)$$

$$Obs_2(t) = \sin(\alpha_2 \cdot t), \quad (D.3)$$

$$Obs_3 = \alpha_3. \quad (D.4)$$

Both prediction and observables have one argument – t , and three uncertain parameters – α_1 , α_2 , α_3 . Uncertain parameter α_1 is uniformly distributed between minimum value equals 0 and maximum value equals 40. Parameter α_2 is normally distributed with mean value equals 0.5 and sigma value equals 0.2. Parameter α_3 is uniformly distributed between minimum value equals 2 and maximum value equals 8. Note, that there is no specific reason of the function choice, any other function can be chosen in principle to perform the same tests. The number of samples has been set to 100 and values of ‘prediction’ and ‘observables’ parameters have been calculated for time values $t = 1 \dots 40$ with time step equals 1s. Minimum, maximum and ‘prior’ (mean) values for the selected ‘predictions’ and ‘observables’ parameters with plots for all 100 samples are shown in **Figure D-1**.

First seven tests show, how taking into account different observables influence the prediction results. In **Table D-1** is presented, which ‘observable’ parameters have been considered in different tests.

On **Figure D-2** is shown how the Pearson correlation coefficient value between the ‘prediction’ parameter and the given ‘observable’ parameter is changing in time. This value is supposed to influence the prediction quality – the higher the Pearson correlation coefficient the better will be the prediction results constructed using this ‘observable’ parameter. The correlation between ‘prediction’ parameter and ‘observables’ parameters Obs_2 and Obs_3 is significant only at the beginning of the time scale – during the first 5 seconds. For most of the time scale the correlation values for these two parameters lie inside the range $[-0.3; 0.3]$. The correlation

between ‘prediction’ parameter and ‘observable’ parameter Obs_1 lie in the range $[0.8, 1]$ for the most of the time scale. Therefore, it is expected, that taking into account Obs_2 and Obs_3 parameters cannot improve the prediction results significantly.

| <i>Test</i> | <i>Obs₁</i> | <i>Obs₂</i> | <i>Obs₃</i> |
|-------------|------------------------|------------------------|------------------------|
| 1 | Yes | Yes | Yes |
| 2 | Yes | No | No |
| 3 | No | Yes | No |
| 4 | No | No | Yes |
| 5 | Yes | Yes | No |
| 6 | No | Yes | Yes |
| 7 | Yes | No | Yes |

Table D-1 – ‘Observable’ parameters taken into account to construct prediction in first seven tests of the ‘toy’ model.

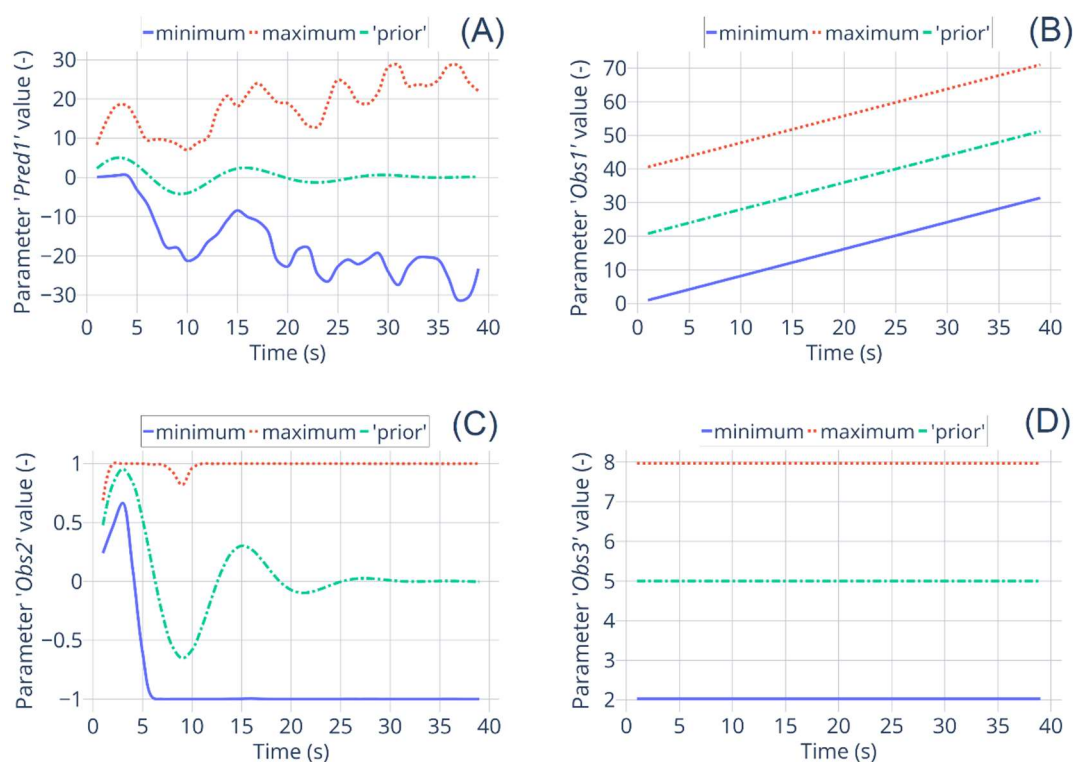


Figure D-1 – Evolution in time of the minimum, maximum and ‘prior’ (mean) values for the selected ‘prediction’ and ‘observable’ parameters. (A): ‘Prediction’ parameter $Pred_1$; (B): ‘Observable’ parameter Obs_1 ; (C): ‘Observable’ parameter Obs_2 ; (D): ‘Observable’ parameter Obs_3 .

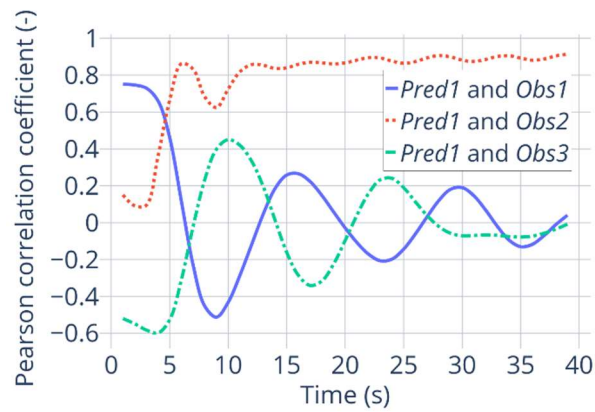


Figure D-2 – Pearson correlation coefficients time evolution between selected ‘predictions’ and ‘observables’ parameters from the ‘toy’ model simulations results. Calculated for the 100 samples ‘prior’ set of data. Selected ‘prediction’ parameter is $Pred_1$. Selected ‘observables’ parameters are: Obs_1 , Obs_2 , Obs_3 .

For the first seven tests to create the ‘measurements’ for the ‘observable’ parameters the values of the uncertain parameters are equal 20, 0.5 and 5, respectively. Therefore, for the Obs_1 and Obs_3 parameters the ‘measurement’ values lie exactly on the ‘prior’ curve – see the ‘prior’ values in **Figure D-1 (B)** and **(D)**. The ‘measurement’ curve for the Obs_2 and the corresponding ‘experiment’ values of the ‘prediction’ parameter $Pred_1$ are shown in **Figure D-3**.

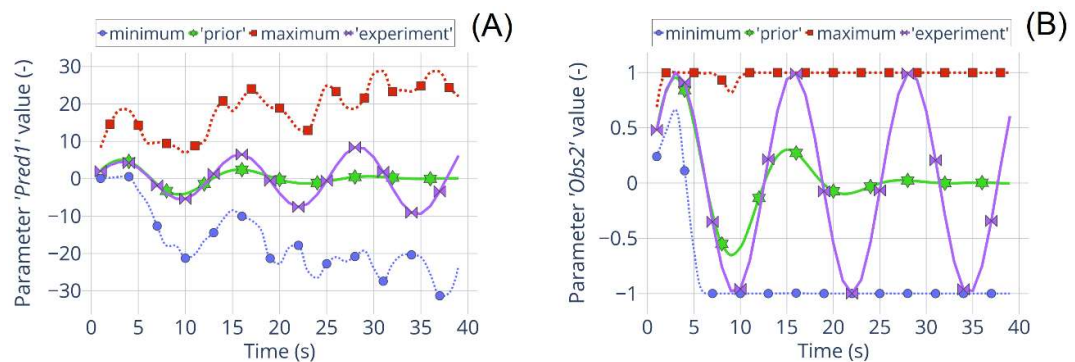


Figure D-3 – Calculated evolution in time of the minimum, maximum, ‘prior’ (mean) and ‘experimental’ values for the selected ‘prediction’ and ‘observable’ parameters. (A): ‘Prediction’ parameter $Pred_1$; (B): ‘Observable’ parameter Obs_2 .

The AREA metric values for the first seven tests are presented in the **Figure D-4**. Initially calculated AREA values have been normalized on the AREA value between the ‘prior’ and ‘experimental’ curve of the ‘prediction’ parameter $Pred_1$. For the tests №2, 4, 7 the prediction quality is really poor (the AREA metric equals 1), because in these tests only Obs_1 and/or Obs_3 ‘observable’ parameters with low Pearson correlation values have been used.

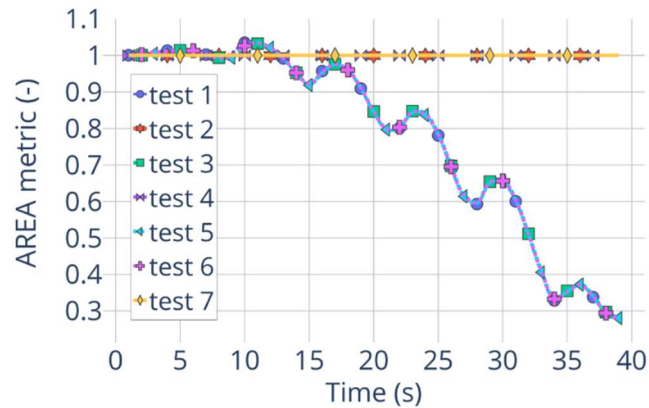


Figure D-4 – AREA metric evolution in time for the first seven tests for the ‘toy’ model.

The results of prediction for these seven tests are presented in **Figure D-5**. Note, that these predictions are constructed using all ‘measured’ data up to the end of the time scale, to these predictions the last AREA values are correspond. The predictions from tests №2, 4 and 7 shown in **Figure D-5 (A)** lie along the ‘prior’ curve, which corresponds the AREA metric values equals 1. The prediction results for tests № 1, 3, 5, 6 are improving with adding more ‘measured’ data, as shown in the **Figure D-4** with the AREA metric evolution in time. The last value of the AREA metric is ~ 0.3 , and corresponding prediction results are shown in **Figure D-5 (B)**. These predictions lie quite close to the ‘experimental’ curve. Also, one can notice that these predictions are identical, therefore using only Obs_2 parameter for prediction as it has been done in test №2 gives good results, it is not necessary to add information about Obs_1 and Obs_3 parameters.

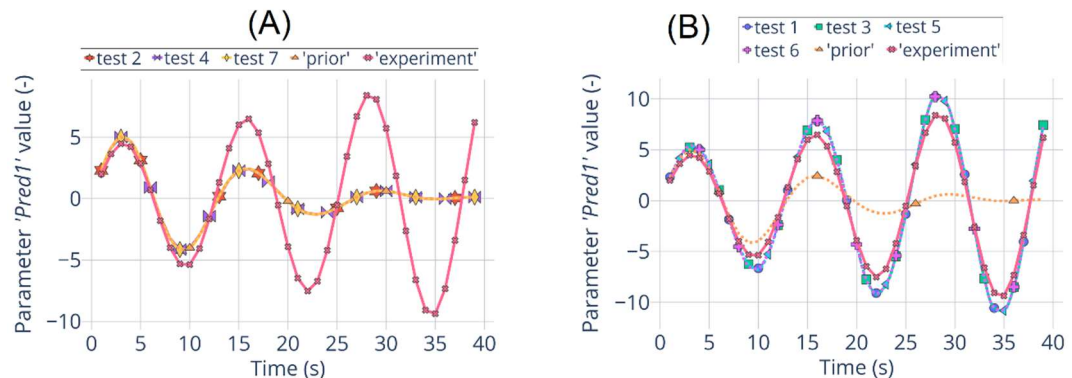


Figure D-5 – Predicted evolution in time of the ‘prediction’ parameter $Pred_1$ for seven tests with the ‘toy’ model. (A): Results of the tests №2, 4 and 7, where Obs_1 and/or Obs_3 have been used; (B): Results of the tests №1, 3, 5 and 7, where Obs_2 alone or along with Obs_1 and/or Obs_3 have been used.

In the next two test № 8 and 9 is explored how the locating ‘experimental’ values of the ‘observable’ parameter Obs_1 outside of the range of the ‘prior’ data will influence the results of predictions, when this ‘observable’ is taken into account or not. The other two ‘observable’ parameters stay the same as in the previous tests №1-7. Results of these two tests are shown in **Figure D-6**. On **Figure D-6 (A)** is shown, how the ‘experimental’ values of the ‘observable’

parameter Obs_1 lie outside of the range of ‘prior’ data. On **Figure D-6 (B)** the corresponding values of the ‘prediction’ parameter $Pred_1$ are presented. These values are still located in the ‘prior’ data range. In the test №8 all ‘observable’ parameters have been taken into account to construct the prediction. As shown in the **Figure D-6 (C) and (D)** the AREA metric value for that test reaches practically the same value ~ 0.3 as for previous successful tests, and the prediction curve lie close to the ‘experimental’ one, at least between 0 and 20 s, after that prediction curve does not repeat the local minimum and maximum values of the ‘experiment’ curve. In the test №9 the same ‘observable’ parameter Obs_1 has not been taken into account at all, and it has significantly worsen prediction results as shown in **Figure D-6 (C) and (D)** – the final AREA metric is ~ 0.5 and the prediction curve does not repeat at all the local extrema of the ‘experimental’ data. It shows that in case if ‘prior’ data does not cover the possible ‘observations’, it is still better to take into account the ‘observable’ parameter with low Pearson correlation value, than does not to consider that parameter at all.

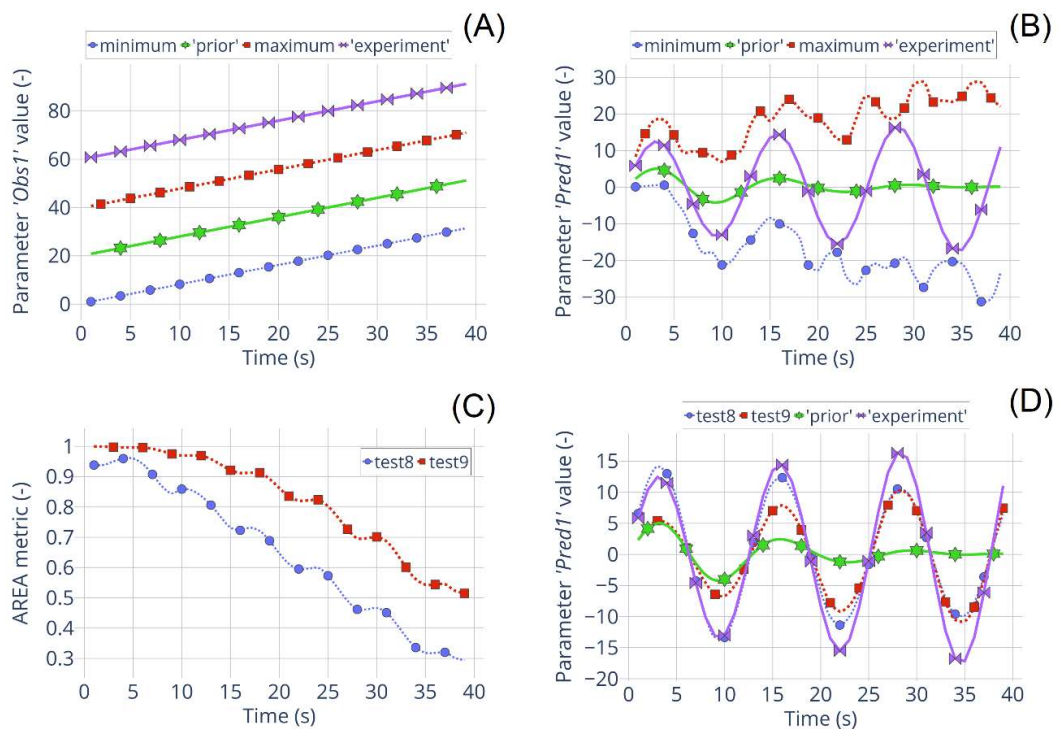


Figure D-6 – Prediction results of the tests №8 and 9 with ‘measured’ values of the ‘observable’ parameter Obs_1 outside of the ‘prior’ data range. (A): Minimum, ‘prior’, maximum and ‘experiment’ values of the parameter Obs_1 ; (B): Minimum, ‘prior’, maximum and ‘experiment’ values of the parameter $Pred_1$; (C): AREA metric values for both tests; (D): ‘Prior’ and ‘experiment’ values of the parameter $Pred_1$ and prediction results for both tests.

To confirm the results presented for tests №8 and 9 two additional tests №10 and 11 have been performed. The idea is the same, but the values of the ‘observable’ parameter Obs_3 lie outside the range of the ‘prior’ data. On **Figure D-7 (A)** is presented how the ‘experiment’ values of the parameter Obs_3 lie higher than the maximum values from the ‘prior’ set of data. The corresponding ‘experiment’ values of the prediction parameter $Pred_1$ are presented in **Figure D-**

7 (B). The AREA metric values for these two new tests are presented in **Figure D-7 (C)**. In test №10 the ‘observable’ parameter Obs_3 has been taken into account to construct prediction, and in tests №11 this parameter has not been considered. As in tests № 8 and 9, to take into account ‘observable’ parameter, which has the low Pearson correlation values and ‘experiment’ values outside of the ‘prior’ data range is better, than does not consider it at all. The prediction results presented in **Figure D-7 (D)** show that in test №10 prediction curve repeats the ‘experimental’ one much better with all its extrema.

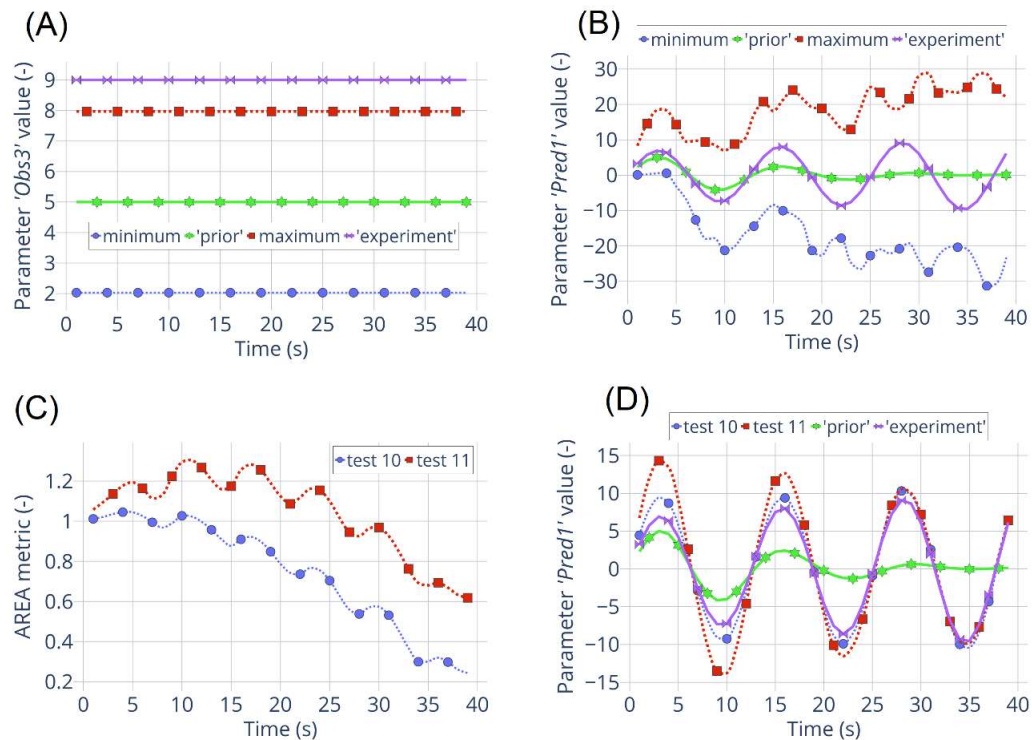


Figure D-7 – Prediction results of the tests №10 and 11 with ‘measured’ values of the ‘observable’ parameter Obs_3 outside of the ‘prior’ data range. (A): Minimum, ‘prior’, maximum and ‘experiment’ values of the parameter Obs_3 ; (B): Minimum, ‘prior’, maximum and ‘experiment’ values of the parameter $Pred_1$; (C): AREA metric values for both tests; (D): ‘Prior’ and ‘experiment’ values of the parameter $Pred_1$ and prediction results for both tests.

In the tests №12, 13 and 14 the values of the parameter Obs_3 lie more and more outside of the ‘prior’ data. All three ‘observable’ parameters are taken into account to construct the prediction. On **Figure D-8** is presented how it affects the prediction results. From **Figure D-8 (B)** it is clear, that the prediction quality is getting worse with Obs_3 ‘experiment’ values lie further from the ‘prior’ data range, which is expected. On **Figure D-8 (C)** and **(D)** is presented how the prediction results lie further from the experimental curve, especially at the local extremums, with increasing distance between maximum and ‘experiment’ values of the Obs_3 parameter. And on **Figure D-8 (E)** the prediction results and ‘experimental’ values at the first 12 second even have the opposite sign.

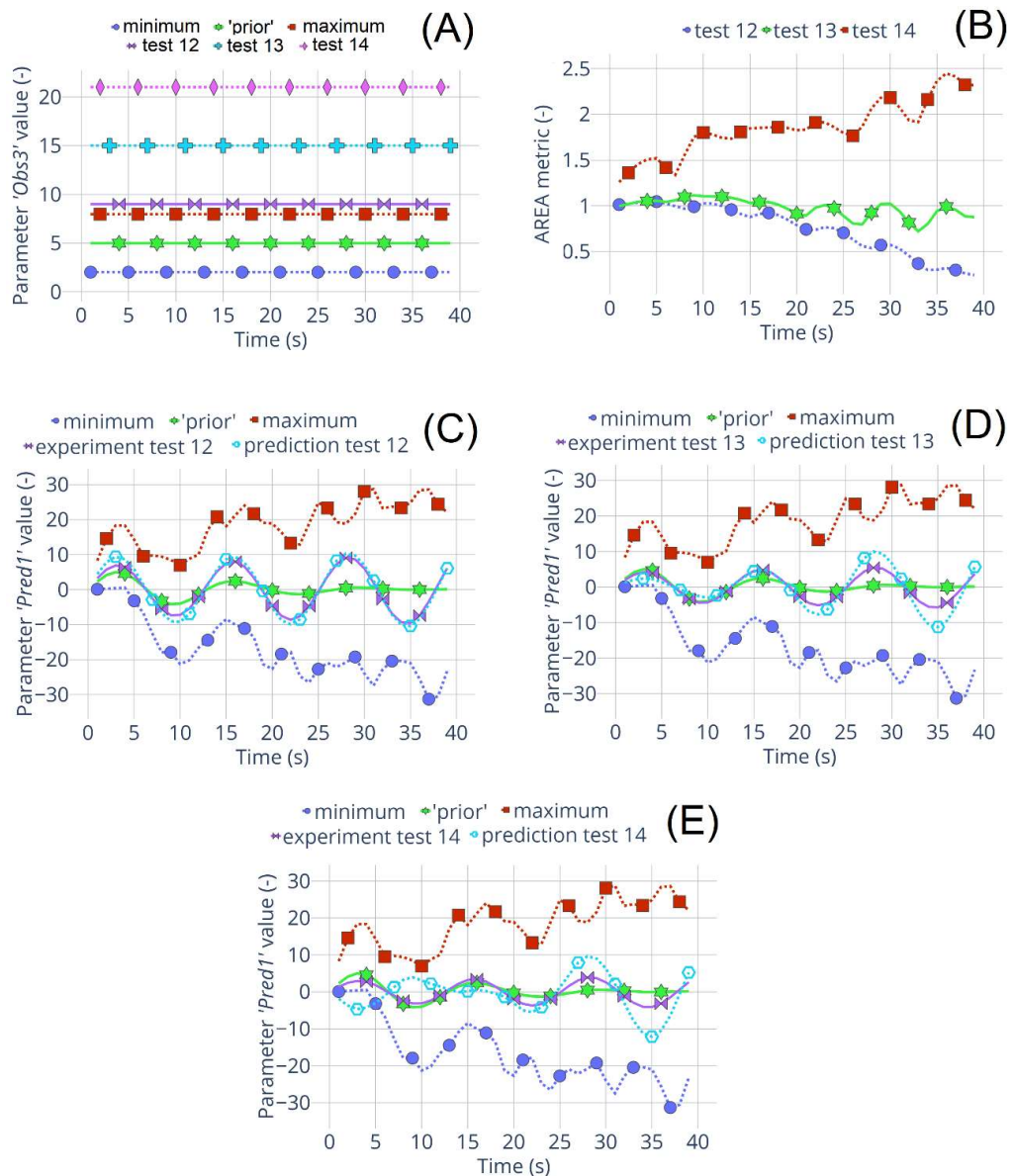


Figure D-8 – Prediction results of the tests №12-14 with ‘measured’ values of the ‘observable’ parameter Obs_3 outside of the ‘prior’ data range. (A): Minimum, ‘prior’, maximum and ‘experiment’ values of the parameter Obs_3 ; (B): AREA metric values for three tests; Minimum, ‘prior’, maximum, ‘experiment’ and prediction values of the parameter $Pred_1$ for (C): test №12; (D): test №13; (E): test №14.

In tests №15 and 16 the attempt to investigate how the shape of the curve of ‘observable’ parameter changing prediction results has been made. As in the tests №12-14 all ‘observable’ parameters are used to calculate the prediction. The results are shown in **Figure D-9**. Unfortunately, it is not clear from these two tests how change in the curve shape influences the results. The initial idea was to make the parabolic curve more and more similar to the straight line (see the **Figure D-9 (A)**). But from the AREA metric values on the **Figure D-9 (B)** the test №16 with more flat Obs_3 curve gives even slightly worse results, than the test №15. Therefore, that question need some further investigation.

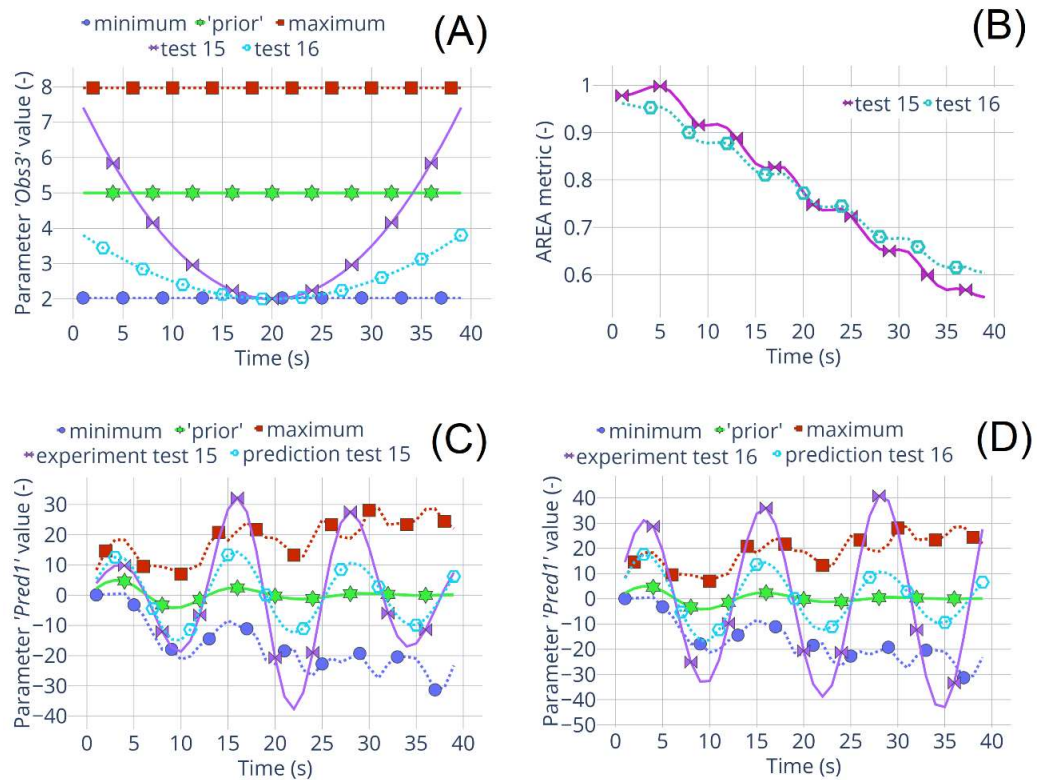


Figure D-9 – Prediction results of the tests №15, 16 with ‘measured’ values of the ‘observable’ parameter Obs_3 forming the curves with different shapes. (A): Minimum, ‘prior’, maximum and ‘experiment’ values of the parameter Obs_3 ; (B): AREA metric values for two tests; Minimum, ‘prior’, maximum, ‘experiment’ and prediction values of the parameter $Pred_1$ for (C): test №15; (D): test №16.

These small example tries to mimic a real application, where:

- The measured values can lie outside of the uncertainty range of the ‘prior’ data (for example, uncertainty ranges of the input parameters are not chosen correctly).
- Not all available ‘observable’ parameters are highly correlated with the ‘prediction’ one.
- The shape of the ‘observable’ parameter experimental curve is not similar to what was expected during the ‘prior’ simulations.

The results presented here are showing that the MOCABA algorithm can be sensitive to:

- Pearson correlation value between selected ‘prediction’ and ‘observables’ parameters.
- Whether the ‘measured’ data lie inside the range of the ‘prior’ data. And if not, whether this ‘observable’ parameter is still included in calculating prediction.
- How far from the ‘prior’ data the experimental values lie.
- Results about the curve shape difference between the ‘prior’ data and experimental values are not clear.

Taking all this into account, a deeper investigation of the algorithm’s limits can be done to make more precise conclusions.

Appendix E: List of publications

1. Sanchez-Espinoza, V. H., Gabrielli, F., Imke, U., Zhang, K., Mercatali, L., Huaccho, G., et. al., KIT reactor safety research for LWRs: Research lines, numerical tools and prospects. *Nuclear engineering and design*, 414, (2023), p. 112573. DOI: <https://doi.org/10.1016/j.nucengdes.2023.112573>
2. Stakhanova, A., Gabrielli, F., Sanchez-Espinoza, V.H., Pauli, E., Hoefler, A., Uncertainty and sensitivity analysis of the ASTEC simulations results of a MBLOCA scenario in a generic KONVOI plant using the FSTC tool. *Annals of Nuclear Energy*, 192, (2023), p.109964. DOI: <https://doi.org/10.1016/j.anucene.2023.109964>
3. Stakhanova, A., Gabrielli, F., Sanchez-Espinoza, V.H., Hoefler, A. and Pauli, E., “Application of the MOCABA algorithm and the FSTC tool for source term predictions during severe accident scenarios”. *Annals of Nuclear Energy*, 184, (2023), p.109703. DOI: <https://doi.org/10.1016/j.anucene.2023.109703>
4. Stakhanova, A., Gabrielli, F., Sanchez-Espinoza, V.H., Hoefler, A. and Pauli, E., “Uncertainty and sensitivity analysis of the QUENCH-08 experiment using the FSTC tool”. *Annals of Nuclear Energy*, 169, (2022), p.108968. DOI: <https://doi.org/10.1016/j.anucene.2022.108968>
5. Stakhanova, A., Gabrielli, F., Sanchez-Espinoza, V.H., Pauli, E., Hoefler, A., “Uncertainty and sensitivity analysis of the ASTEC simulations results of a MBLOCA scenario in a generic KONVOI plant using the FSTC tool”. In *Proceedings of 10th European Review Meeting on Severe Accident Research (ERMSAR-2022)*, 2022, pp.861-872.
6. Pauli, E., Hoefler, A., Gabrielli, F., Stakhanova, A. and Sanchez-Espinoza, V.H., “Prediction of the radiological consequences of a severe accident scenario in a generic KONVOI nuclear power plant”. In *Proceedings of 10th European Review Meeting on Severe Accident Research (ERMSAR-2022)*, 2022, pp. 338-350.
7. Gabrielli, F., Sanchez Espinoza, V.-H., Stakhanova, A., Hoefler, A., Pauli, E.-M., and Feldmann, H. “Impact of Realistic Fuel Inventories on the Radiological Consequences of a Severe Accident Scenario in a Generic Konvoi Plant by Means of the ASTEC Code”. In *the Proceedings of the KERNTECHNIK 2022, Leipzig, Germany, 21-22 June, 2022*.
8. Gabrielli, F., Sanchez-Espinoza V. H., Stakhanova, A., Hoefler, A., and Pauli, E. “Source term evaluation following MBLOCA and SBLOCA scenarios in a generic KONVOI-1300 NPP by means of the ASTEC code”. In *the Proceedings of the EUROSAFE-2021, Paris, France 22-23 November, 2021*.
9. Avvakumov, A.V., Alipchenkov, V.M., Belov, A.A., Bereznev, V.P., Boldyrev, A.V., Grushin, N.A., Khanbikov, I.N., Klimonov, I.A., Kolobaeva, P.V., Koltashev, D.A., Mosunova, N.A., Ozrin, V.D., Rtishchev, N.A., Seleznev, E.F., Semenova, M.M., Stakhanova, A.A., Strizhov, V.F., Tarasov, V.I., Usov, E.V., Veprev, D.P., Veretentsev, V.A., Afremov, D.A., Kudryavtsev, A.V., Semchenkov, A.A., Osipov, S.L., Anfimov, A.M., and Gorbunov, V.S., “Coupled calculations for the fast reactors safety justification with the EUCLID/V1 integrated computer code”. In *the Proceedings of the International Conference on Fast Reactors and Related Fuel Cycles: Next Generation Nuclear Systems for Sustainable Development (FR17)*, IAEA-CN245-184, Yekaterinburg, Russian Federation, 26-29 June, 2017.
10. Koltashev, D.A., Stakhanova, A.A., “Neutronic calculation of fast reactors by the EUCLID/V1 integrated code”, *Journal of Physics: Conference Series*, Vol. 781, No. 1, p. 012003, IOP Publishing, 2017, DOI: 10.1088/1742-6596/781/1/012003.
11. Avvakumov A.V., Bereznev V.P., Vasekin V.N., Veprev D.P., Grushin N.A., Kolobayeva P.V., Koltashev D.A., Seleznev E.F., Semenova M.M., Stahanova A.A., Mosunova N.A., Strizhov V. F., and Hanbikov I. N., “Justification the applicability of new generation integral code EUCLID/V1 for the calculation of BREST-OD-300”, In *the Proceedings of*

the Fourth International Scientific and Technical Conference "Innovative designs and technologies of nuclear power" (ISTC NIKIET-2016), Moscow, Russian Federation, 27-30 September, 2016, (In Russian).

12. Alipchenkov, V.M., Belikov, V.V., Vasekin, V.N., Veprev, D.P., Veretentsev, V.A., Ivanov, E.N., Kolobaeva, P.V., Kudashov, I.G., Mosunova, N.A., Stakhanova, A.A., Strizhov, V.F., Usov E.V., Muratov, A.G., Tyukov V.V., Anfimov, A.M., Gorbunov, V.S., Kuznetsov, D.V., and Osipov S.L., "V&V of EUCLID/V1 universal integrated computer code for the BREST-OD-300 and BN-1200 nuclear power plants", *In the proceedings of the International Scientific and Technical Conference "Innovative designs and technologies of nuclear power" (ISTC NIKIET-2014)*, Moscow, Russian Federation, 7-10 October, 2014, (In Russian).
13. Vasekin, V. N., Mosunova, N. A., Stakhanova, A. A., and Strizhov V. F., "Analysis of operating characteristics of the lead cooled nuclear reactor with EUCLID/V1 code", IAEA TM on Priorities in Modelling and Simulation for Fast Neutron Systems, Vienna, Austria, 14-16 April 2014.
14. Vasekin V. N., Stakhanova A. A., "Neutronic module as a part of the EUCLID integrated code". *In the Abstracts of the Neutronics-2013 conference "Neutron physics questions of nuclear power engineering"*, Obninsk, Russian Federation, 5-8 November, 2013, (In Russian).
15. Belov, A.A., Vasekin, V.N., Veprev, D.P., Veretentsev, V.A., Veshchunov, M.S., Mosunova N.A., Polous, M.A., Stakhanova, A.A., Strizhov V.F., Muratov, A.G., and Tyukov, V.V., "Calculation of steady-state and transient operation of the lead cooled nuclear reactor by the EUCLID/V1 integrated code", *In the Proceedings of the Forth conference "Heavy Liquid-metal Coolants in Nuclear Technologies" (HLMC-2013)*, Obninsk, Russian Federation, 22-27 September, 2013, (In Russian)
16. Stakhanova A. A, Dedov A. V., "Calculation of thermohydraulic characteristics of annular fuel rods". *In the Abstracts of the International Scientific School "Problems of gas dynamics, heat and mass transfer in power technology "*, p. 163-164, 2011, (In Russian).
17. Stakhanova A.A., Varava A.N., Dedov A.V., and Komov A.T., "Studying heat transfer during impulse heating of model fragments of fuel rod claddings", *Thermal Engineering*, Vol. 58, No. 7, pp. 602-609, 2011. DOI: 10.1134/S0040601511070159.
18. Stakhanova A. A, Dedov A. V "Study of heat transfer in the pulse heat emission". In the proceedings of the 5-th Russian National Heat Transfer Conference (RNHTC-5), Vol. 8, pp. 134-137, Moscow, Russian Federation, 2010, (In Russian).